ODESSA ASTRONOMICAL PUBLICATIONS

Volume 22
(2009/2010)

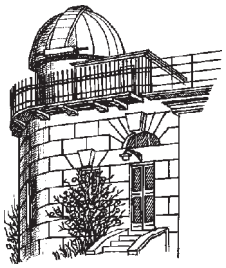

Odessa
«AstroPrint»

FOREWORD

This 22th volume of the "Odessa Astronomical Publications" was mainly intended as an issue that should elucidate the present state of the near-to-Earth's space researches that are carried out in Astronomical Observatory of Odessa National University (11 papers from 14), and some achievemets of the recent years made in this direction.

Space researches in Odessa can be represented by the three main branches: meteor astronomy, observation of the artificial Earth's satellites, and observations of the Solar system small bodies. All these branches are developed in Odessa during more than half a century. Present generation of Odessa astronomers keeps the best scientific traditions and successfully advances these studies using for observations new detectors and new methods. Authors of the papers published in this volume describe these method as well as they discuss their original computer codes elaborated for the data processing.

We hope that this issue of "Odessa Astronomical Publications" will be interesting to those specialists who work in area of the space researches.

S.M. Andrievsky

CONTENTS

DEFINITION OF POLES OF THE LARGE CIRCLES OF METEORIC TRAJECTORIES

Yu.M. Gorbanev, A.V. Golubaev

Astronomical Observatory of I.I.Mechnikov Odessa National University
Odessa, Ukraine
astro@paco.odessa.ua

ABSTRACT. We present the method and software Meteor Pole for calculation of the spherical equatorial coordinates of the meteor points within the images obtained by TV observations. This software is a part of computer package Odessa Meteor which was elaborated for processing of the TV meteor patrol observational material. The results of such processing are the equatorial coordinates of the large circles poles of meteor trajectories on celestial sphere. These data are necessary for determination of the equatorial coordinates of radiants.

We give the description of the method which enables one to estimate accuracy of the equatorial coordinates deternination taking into account specific chatcter of the operation of TV camera WATEC LCL-902 and its modifications.

An analysis of the distribution of the large circles poles based on observations that were carried out in Astronomical Observatory of Odessa National University is given.

We made a conclusion that there is no selected global direction in meteor movement on celestial sphere.

Key words: Meteors: radiant, meteor trajectory, telescopic meteors; meteor observations: TV observations, CCD observations, WATEC, LCL-902K, LCL-902H, meteor patrol

1. Introduction

In the beginning of the XXI century the main principle of the astronomical images recording was cardinally changed. Instead of photoplates and electronic tubes the CCD cameras are widely used now. In particular, the meteor astronomy uses CCD detectors which are working in TV mode.

TV meteor patrol was created in Astronomical observatory of Odessa National University in 2003, and it is in operation until now. There is also expedition of the meteor patrol that was tested several times at the Zmeijny island in Black Sea. As a detector we used TV camera WATEC LCL-902H2, LCL-902H and LCL-902K. Meteor events are recorded with a time resolution of 0.02 second. Such an observing mode was chosen after many years of exploration, while the main aim of this investigation is the possibility of observations in the visual spectral range with a high time and space resolution of the meteor events that are registered only in the radio and visual telescopic modes ($> +6^m$).

Taking above mentioned into account we decided to create new software which is necessary for processing of the observational material. After digitalization of the image we get coordinates of each pixel (X,Y) and its brightness (I). Their exact values give us possibility of using strict mathematical approach, and thus to increase the quality of observational material processing.

The main goal is to obtain accurate photometric and positional characteristics of meteors. In particular, the positional characteristics are the equatorial coordinates of the large circle pole of the meteor trajectory on celestial sphere. If we deal with basis meteor, then we can obtain exact element of its orbit. As a result all these data allow one to identify to which meteor stream a certain meteor belongs, as well as to investigate the fine structure of the meteor stream.

Table 1: Comparative statistics of photographic and TV meteors on major observational projects

Observational project	Period of observations	Number of meteors
Harvard Meteor Project (U.S.)	1936–1959	1245
Prairie Network (U.S.)	1963–1975	2700
MORP (Meteorite Observation and Recovery Project, Canada)	1971–1984	218
Dushanbe, Odessa, Kiev (USSR)	1940–1983	1111
Odessa (Ukraine)	2003–2010	> 3500

In Table 1 we show selective statistics of the photographic and TV meteors registered in the second part of XX century within the different projects. From our experience we can conclude that the number of meteors

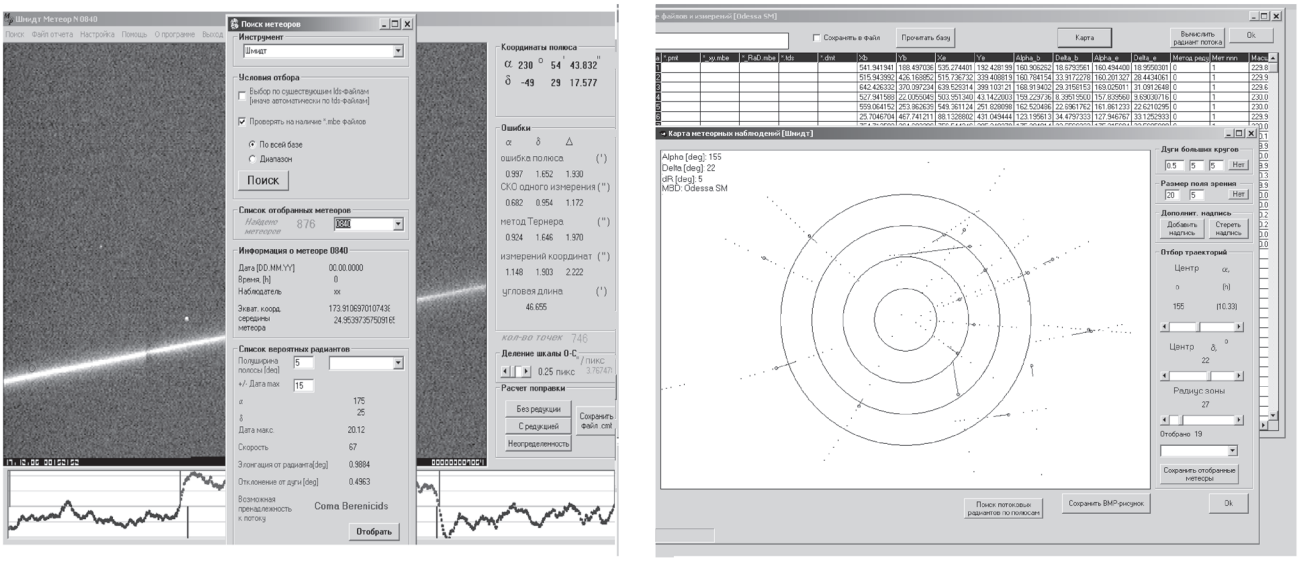

Figure 1: ***Meteor Pole*** interface.

detected by the modern devices increased tenfoldly.

For the sake of comparison, we note that Odessa meteor data-base was supplemented during 2003-2010 by about 3500 registered events (meteors of $+12^m$ and brighter). The number of individual frames for each meteor image often exceeded ten. This statistics testifies about the huge amount of the measuring and calculating work.

The distinguishing feature of the observed material which is collected with the help of CCDs, CMOS-sensor is the numerical representation of the data forming an image, while the further processing of an image is quite similar both for CCD and photographic images. There, of course, exist some factors which are connected to the detector characteristics. We think that the correct account for such factors is very important for precise positional reduction of the observational material, and this point will gain a specific attention in this paper.

2. Software Meteor Pole

In order to understand at which stage and for what one needs to calculate equatorial coordinates of the meteor trajectory large circle poles we give below the short clescription of the scheme of a preliminary processing of the observational material.

Preliminary positional measurements and calculations of the meteor images are carried out as follows:

1. Observational material in the form of video-films recorded in an interlaced mode with 50 video fields (or 25 complete video frames) per sec is cut by AVICutter software into separated images that contain the meteor trace.

2. Using software based on the methods described in (Gorbanev et al., 2006; Gorbanev et al., 2008) the position of the reference stars are found. Equatorial coordinates of these stars are listed in the stellar catalogue (software PSF). The same method is used to find position of the meteor trajectory points in the rectangular system (software PicScan).

3. All measurements are controlled in order to find possible errors. For this the special method and software Meteor Control Data, Meteor Manager were created.

As a result of a preliminary processing, we get the files with rectangular coordinates of each point of the meteor trajectory, rectangular and equatorial coordinates of the reference stars, and calculated coefficients of the Turner method, as well as measurement errors. In addition, the file containing the date and time of the meteor event is created. For the facilities, the software subroutine creates at each stage the corresponding file with calculation results. The Meteor Pole software (Fig. 1) helps to gather all the files containing results of measurements and calculations, and to make the final positional calculations and their analysis.

The practical use of the Meteor Pole software is the following:

1. In "Search" select the observational database that corresponds to a given telescope and detector, and observational place.

2. Push the button "Search" to find the database of the meteor events for which a preliminary processing of the image star field and meteor image was performed.

3. After selection of a given meteor event (certain number), one gets the table with complete positional characteristics: coordinates of the large circle the pole of the meteor trajectory, errors of calculations of this pole position and trajectory. Software also informs about errors of calculations based on the Turner method, angular length of the meteor trajectory that

was adopted for calculation of the pole coordinates and angular scale of the image.

4. Special attention requires an accuracy of calculations of the large circle pole coordinates which is connected to so-called effect of the TV Interlace. Software Meteor Pole affords a possibility to take into account this effect (this is described in details below).

5. Software uses list of radiants of the most known meteor streams, as well as the list of supposed and theoretical radiants. Thus, knowing coordinates of the large circle of a meteor trajectory, coordinates of the observed region and radiant coordinates one can obtain elongation of the meteor from the catalogued radiant value. Then, combining the time of observation of a meteor event with the time of meteor stream operation (catalogue data), one can select the minimum calculated elongation value. Therefore, one can plilimnary estimate to which catalogued meteor stream a certain meteor event belongs. In case the meteor event was registered with a basis method, one can get an individual radiant by calculating equatorial coordinates of the poles of the large circles of meteor trajectories for each observational station.

This is a general description of the positional measurements and calculations based on Meteor Pole software. Below we consider the calculation method enabling one to find equatorial coordinates of the pole of the meteor trajectory large circle.

3. Calculation of the equatorial coordinates of the meteor trajectory large circle pole

For registered meteor trajectory the characteristics are the equatorial coordinates of the large circle pole. These equatorial coordinates can be calculated using Kavrayskiy (Kavrayskiy, 1926) formula:

$$\begin{aligned} \cot\alpha_p &= \frac{\cot\delta_1\sin\alpha_1 - \cot\delta_2\sin\alpha_2}{\cot\delta_1\cos\alpha_1 - \cot\delta_2\cos\alpha_2} \\ \tan\delta_p &= -\cot\delta_1\cos(\alpha_p-\alpha_1) = \\ &= -\cot\delta_2\cos(\alpha_p-\alpha_2) \end{aligned} \qquad (1)$$

Here α_p and δ_p – the equatorial coordinates of the pole of the large circle, α_k and δ_k – equatorial coordinates of the two points on the meteor trajectory ($k = 1, 2$).

After the use of the PicScan software (the meteor image processing) we get more than two points of the meteor trajectory. It should be noted that coordinates of the points are delivered in rectangular system. They should be transformed into spherical equatorial coordinates (Turner method, using the measurement results based on PSF software).

Since the number of points is larger than 2 ($n > 2$), the pole coordinates calculation can be performed

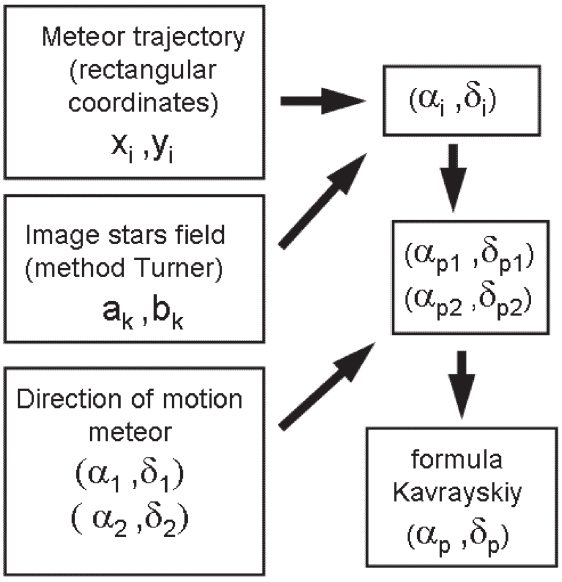

Figure 2: Block-scheme of the meteor trajectory large circle pole coordinates determination.

using the least square method. According to the second equation of the system (1):

$$\begin{aligned} \tan\delta_p &= -\cot\delta_1\cos(\alpha_p-\alpha_1) \\ \tan\delta_p &= -\cot\delta_2\cos(\alpha_p-\alpha_2) \\ &\ldots\ldots\ldots\ldots\ldots\ldots\ldots\ldots \\ \tan\delta_p &= -\cot\delta_n\cos(\alpha_p-\alpha_n) \end{aligned} \qquad (2)$$

Performing a simple transformation and introducing designations:

$$\begin{aligned} \cot\delta_i\cos\alpha_i &= A_i \\ \cot\delta_i\cos\alpha_i &= A_i \\ (i &= 1,2,3,\ldots n) \end{aligned} \qquad (3)$$

we get

$$\begin{aligned} \sec\alpha_1\tan\delta_1 + B_1\tan\alpha_1 &= A_1 \\ \sec\alpha_2\tan\delta_2 + B_2\tan\alpha_2 &= A_2 \\ &\ldots\ldots\ldots\ldots\ldots\ldots\ldots\ldots \\ \sec\alpha_n\tan\delta_n + B_n\tan\alpha_n &= A_n \end{aligned} \qquad (4)$$

This system can be solved by the least square method. In the Gauss we have

$$\begin{aligned} \sec\alpha_1 n\tan\delta_1 + [B]\tan\alpha_1 &= [A] \\ \sec\alpha_1[B]\tan\delta_1 + [B^2]\tan\alpha_1 &= [BA] \end{aligned} \qquad (5)$$

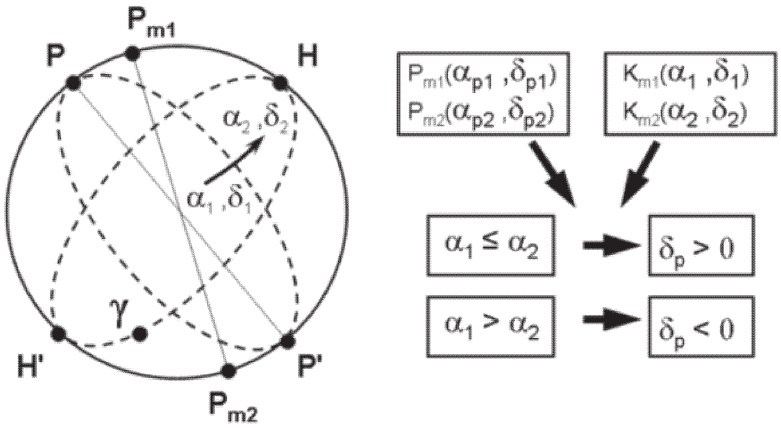

Figure 3: Scheme explaining the selection of one from two solutions for the pole coordinates determination.

where

$$\begin{aligned} [A] &= \sum A_i \\ [B^2] &= \sum {B_i}^2 \\ [B] &= \sum B_i \\ [BA] &= \sum B_i A_i \end{aligned} \tag{6}$$

Using the substitution in (5) we get

$$\begin{aligned} \tan\alpha_p &= \frac{[A][B]-[BA]n}{[B][B]-[B^2]n} \\ \sec\alpha_p \tan\delta_p &= \frac{[A][B^2]-[BA][B]}{n[B^2]-[B][B]} \end{aligned} \tag{7}$$

General block-scheme of the Meteor Pole software is given in Fig. 2.

Solution of (7) gives two sets of the pole coordinates, uniquely defining the arc of a great circle of the meteor trajectory. In order to select one of them, one can use the law which is based on the direction of meteor motion along the arc of the large circle. Fig. 3 represents the scheme which gives an explanation of this procedure. Here P_{m1} and P_{m2} are two pairs of the pole coordinates, K_{m1} and K_{m2} – coordinates of the meteor image ending points. They defines the starting and ending points of the meteor trace on celestial sphere (software Card File). Depending on the right ascension K_{m1} and K_{m2} could be positive or negative.

4. Accuracy of the coordinates determination of the meteor trajectory large circle poles

It is easy to show (Katasev, 1957; Gorbanev et. al., 2008), that accuracy of determination of the coordinates of the meteor trajectory large circle poles depends on accuracy of the trajectory determination and angular length of the meteor. Theoretically such a dependence can be expressed as

$$\sigma_p = \frac{1}{\sqrt{2}} \frac{\sigma_m}{\sin\gamma} \tag{8}$$

were γ – angular length of the meteor image, $\sigma_m = \sqrt{\sigma_T^2 + \sigma_t^2}$ – error of the coordinate determination.

In our case this error is conditioned, first of all, by the accuracy of the Turner method used for the measurements of the stellar images σ_T, secondly, by the accuracy of the measurements of the meteor trajectory image σ_t. Fig. 4a presents dependences of the error value that characterizes determination of the coordinates of the meteor trajectory large circle pole on the angular length of the observed part of the meteor trajectory (both are given in arcmin). Each dependency is calculated for a certain σ_m value (it is showed in arcsec near the corresponding curve). For the short trajectories (shorter than $10'$ the determination accuracy is larger than $20'$, while the trajectory is measured with accuracy of about 4 arsec). Those meteor images that were registered near the TV frame boundaries, and thus they have low angular sizes, are of little avail for the pole coordinates determination.

Each component of error (σ_T and σ_t) can vary within some range forming therefore the error of the of measurement of each meteor image. Fig. 4a shows not only theoretical curves with fixed σ_m values, but also gives the data calculated for the real meteor images based on the random sample of 338 meteors observed with the Schmidt telescope, and 177 meteors observed with astrocamera equipped with objective lens KO-140. With the aim of comparison we also show the small sample of meteors having different angular lengths registered with astrocamera equipped with objective lens KP-35. In this case an accuracy of determination of the meteor trajectory large circle pole is the same as for astrocamera with KO-140 objective lens. It is quite expectable

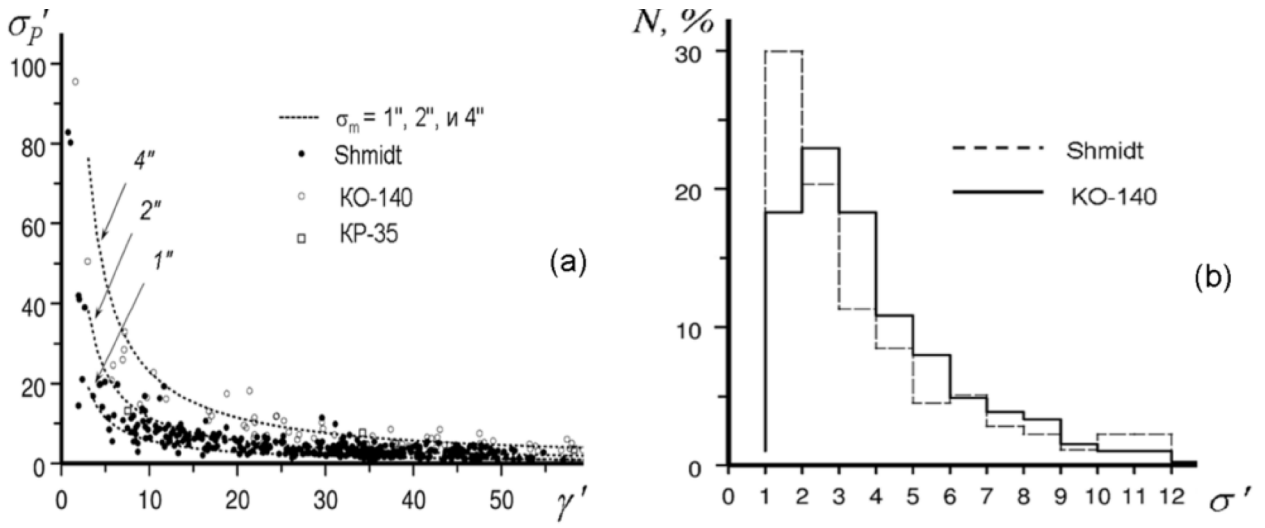

Figure 4: (a) Dependence of the accuracy of the pole coordinates determination on the length of the meteor trajectory for Schmidt telescope and astrocameras with KO-140 and KP-35 objective lenses. (b) Distribution of the accuracy of the pole coordinates determination for our meteor database.

since the optical parameters of both devices do not differ.

Fig. 4b presents the histograms of the error distribution of the large circle pole position determination based on observations with Schmidt telescope and astrocamera equipped with objective lens KO-140. For the firmly measured images the error value of the pole coordinates determination is of about $1'$ and $2'$ respectively, which is limiting value for our meteor patrol.

5. An influence of the Interlace TV effect on the determined coordinates of the meteor trajectory large circle pole.

After the determination of the equatorial coordinates of the meteor trajectory points it is necessary to take into account all the factors connected with detectors work.

The frame scanning of the videomaterials could be progressive scanning (interlinear) or interlaced. In case of progressive scanning, all horizontal lines of image are represented successively. In case of interlace, either all odd, or all even lines are alternately uploaded (together they form the field of frames or semi-frame). At present we carry out the meteor observations in the interlaced mode. This enables one to improve the time resolution of the meteor event registration almost twice. Thus, if the complete frame is combined during 0.04 sec, then each semi-frame (either consisting only of the odd frames, or even frames) will be combined during 0.02 sec. The losses of the permeability for telescope will be insufficient when the interlaced mode is used. The obvious shortcoming of the interlaced mode is some deterioration of resolving power (this is because of the lack in each frame the lines of the opposite parity, and as a consequence the lack of the information about the meteor that might have been obtained from those lines).

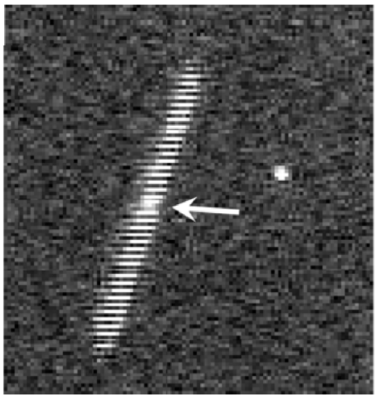

Figure 5: The Interlace effect. The frame composed during 0.04 sec is showed. Effect of the bright dot (discussed in the text) is indicated by the arrow.

The splitting of the vertical boundaries of the horizontally moving objects causes an effect which is called "Interlace" (Fig. 5). When the videofilm with meteor image (or image of the Earth's artificial satellite) is visually examined, then one can note some oscillations of

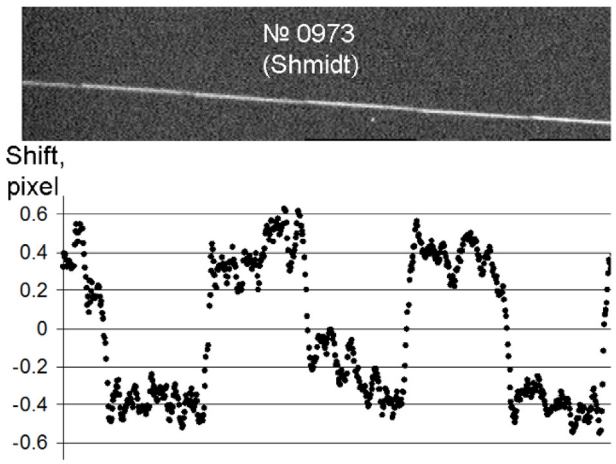

Figure 6: An influence of the Interlace effect on accuracy of the meteor trajectory measurement.

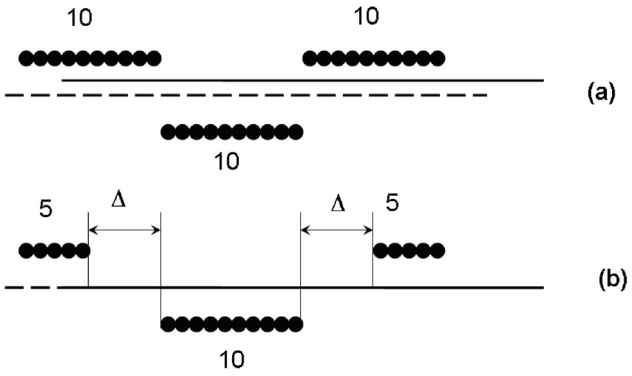

Figure 7: Scheme explaining the correct means of taking into account the equal number of the dots of the meteor image strokes.

the recorded picture of the object relatively the mean line of its motion. Small shifts are seen in case of meteor motion along the frame lines, while for the motion which is transversal to the frame lines such an effect is absent. In positional measurements this effect is developed as periodic shifts of each meteor stroke of the semi-frame relatively the arc of the large circle which is drawn on the combined image based on all the frames of a meteor image (Fig. 6). Since the registered object has its own characteristic size depending on its brightnes, the bright spot is produced in the frame in that region where the odd and even images overlap (Fig. 6, indicated by arrow). The brighter the object, the larger the size of this spot. For the faint objects this effect is weak or absent. This effect can be used for instance for the determination of the length of meteor strokes within each of the semi-frames.

Fig. 6 shows combined image of a meteor composed of the odd and even semi-frames of the videofilm. Below (the same figure) the shown is a plot demonstrating the positions of the measured strokes of a meteor at the semi-frames in pixel (1 pixel in this case corresponds to about 3.85″) relatively to the motion trajectory. The shift of each stroke is about 0.3 - 0.4 pixel (1.2″ - 1.5″).

Thus, when determining the coordinates of the large circle pole it is necessary to take into account correction caused by the effect connected with above described specific character of the meteor image formation by the TV camera.

The size of shift depends upon the object size in the frame and its brightness. As a rule, these parameters change during the meteor event existence. Therefore, in a certain case, an analytic estimate of the correction can be complicated. Nevertheless, for each observational device there is a possibility to determine an averaged dependence of the correction value upon an angle of the meteor trajectory relatively the frame lines basing on the whole observational material. In order to find correction value for a given meteor it is necessary to use this dependence found for a given instruments. For Odessa meteor patrol (Schmidt telescope) in some cases correction can achieve 2″ - 3″.

After the determination of the equatorial coordinates of the meteor trajectory large circle pole, the correction value (in angular measure) should be included in the error of the determination of this pole coordinates.

6. The determination of the large circle pole coordinates with an account of the Interlace effect.

As it was stated above, in the interlace regime the meteor image is separated into two sets of strokes of the odd and even semi-frames. Therefore the second important thing in the determination of the large circle pole coordinates is correct account of the symmetrical number of those strokes of the meteor image relatively an axis of its trajectory.

Let us suppose in the simple case that all strokes have the same length. Let also the number of the strokes from one side of the trajectory axis exceed the same number from another side by one, and consequently the number of the dots that can be used for determination of the large circle arc will be larger (Fig. 7a). It is quite understandable that these dots will shift to their side the large circle arc (the smooth line in Fig. 7a). It will be correct in this case to select equal numbers of the dots from both sides of the trajectory axis. It is important to note that selected dots should be situated at the same distance (Δ, Fig. 7b) relatively to the dots of that stroke which is not used for the length determination. Otherwise, the calculated trajectory will be biased.

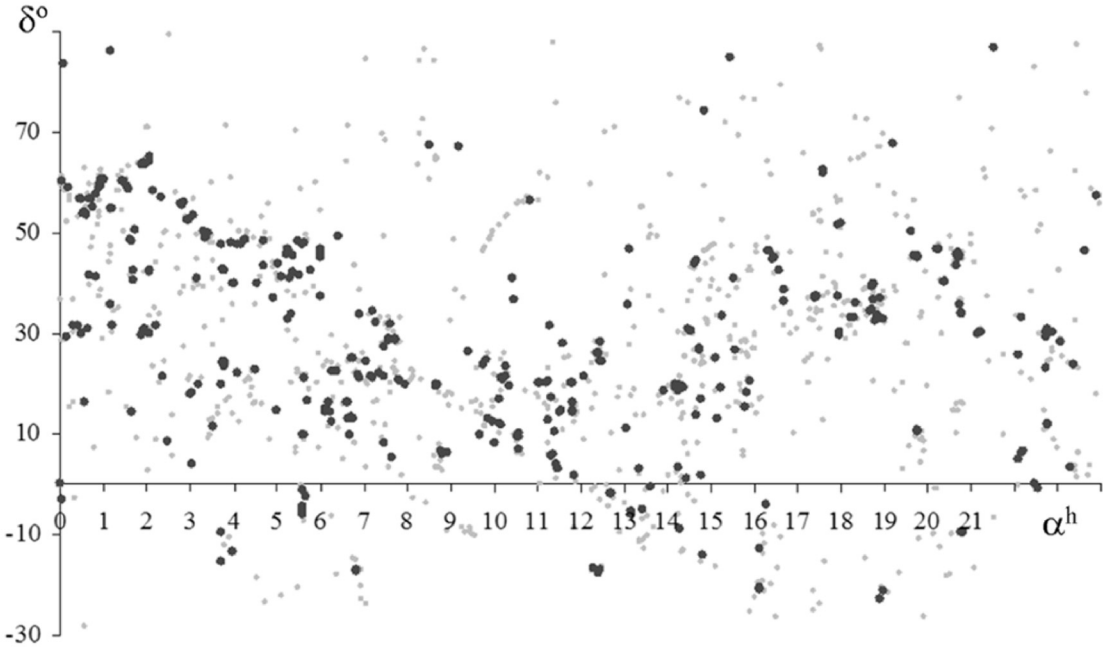

Figure 8: The map of the regions of the meteor patrolling (Schmidt telescope, August 2003 - August 2004)

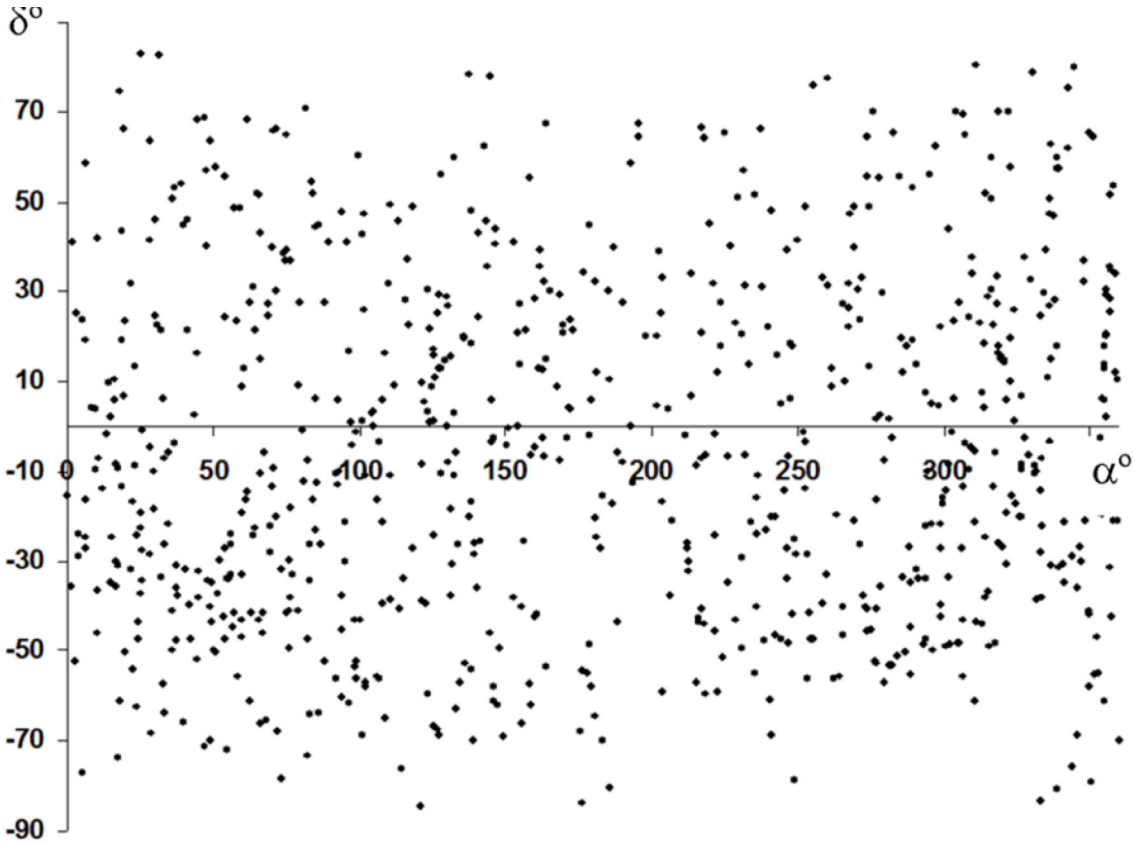

Figure 9: The map showing the distribution of the meteor trajectory large circle poles (Odessa, Schmidt telescope, 2003-2004).

a) In the upper part the total number of the dots which are used for calculation of the large circle arc is 20, while in the lower part this number is 10. Calculated trajectory (smooth line) is shifted towards that side where the number of the dots is larger.

b) The number of the dots on both sides is equal. All selected dots which belong to the upper stroke are at the same distance as the dots of the lower stroke. No trajectory shift is presented.

While determining the arc of the large circle meteor trajectory (software Meteor Pole) the length of the stroke is controlled by user. After that, using the sample of selected dots one can determine equatorial coordinates of the meteor trajectory large circle pole using the approximation method and formulae of the spherical astronomy.

7. Results and analysis.

Software Meteor Pole enables one to integratedly work with astrometric characteristics of meteors.

Fig. 8 shows the map of the region of the meteor observations which are carried out with Schmidt telescope at the Kryzhanovka station. In order to avoid the crowding of the data in Fig. 8, we present here only those observations that were performed during August 2003 - August 2004. Equatorial system is used for presentation. The grey dots represents all observational regions, while black dots show those region where at least one meteor event was registered. As one can see there is a tendency of the meteor activity distribution along a certain line. To some extent it is connected with a concentration of the meteor radiants toward the ecliptic plane (it is a well known fact in meteor astronomy). From the other side, there exist an observational selection, an observer more often carries out observations in those region where the meteor activity is higher.

For the same sample of meteors Fig. 9 displays the distribution of the poles on the celestial sphere. This distribution shows that the large circle poles are distributed uniformly. Since the large circle pole position is determined taking into account the direction of meteor motion, one can make a conclusion that such an uniformity also characterize the meteor motion directions.

Conclusions.

1. Software enabling one to work with meteor images that are registered by means of the TV methods, to calculate equatorial coordinates of the large circle poles of the meteor trajectories, and to estimate an accuracy of these coordinates determination was elaborated in the Department of the Solar system small bodies of Astronomical Observatory of Odessa National University.

2. The precision of the pole coordinates determination for meteor trajectory registered with Scmidt telescope is the same as for astrocamera equipped with KO-140 objective lens (about $1' - 2'$ for the length of the meteor image not less than $10'$).

3. All distortions caused by the TV detector working in the interlace regime are taking into account while calculating coordinates of the meteor trajectory large circle poles.

4. Our analysis of the data shows that there is no preferred direction in the meteor motions on celestial sphere.

Acknowledgements. The authors are thankful to anybody who has read this contribution to the end.

References

Gorbanev Yu.M., Golubaev A.V., Zhukov V.V., Kimakovskaya I.I., Kimakovsky S.R., Knyazkova E.F., Podlesnyak S.V., Sarest L.A., Stogneeva I.A., Shestopalov V.A.: 2006, *Solar System Research* **40**, 5

Gorbanev Yu.M., Golubaev A.V., Zhukov V.V., Kimakovskaya I.I., Kimakovsky S.R., Knyazkova E.F., Podlesnyak S.V., Sarest L.A., Stogneeva I.A., Shestopalov V.A.: 2008, *Solar System Research* **42**, 1

Kavrayskiy V.V.: 1926, *zapiski po gidrografii* **41** 5, (rus. edit.)

Katasev L.A.: 1957, *fotograficheskie metody meteornoy astronomii* (rus. edit.)

POSITIONAL MEASUREMENTS OF THE METEOR TV IMAGES

Yu.M. Gorbanev, S.R. Kimakovsky, E.F. Knyazkova

Astronomical Observatory of I.I.Mechnikov Odessa National University
Odessa, Ukraine
skydust@rambler.ru, keysi@nm.ru, skycomet@te.net.ua

ABSTRACT. We discuss the methods and software which is used for processing of the meteor TV images. Methods are based on the principles of the aperture CCD photometry. Software enables one to make processing of the observational material that was secured using TV methods with telescopic systems (field of view less that 1 angular degree), as well as with astrocameras of the wide field of view (field of view less 2-4 angular degrees, and even more than 50 degrees). We also elaborated method that allows one to identify operatively and to measure automatically rectangular coordinates within the image frame, as well as to calculate equatorial coordinates of the object using the Turner method and compiled stellar catalogues. This method was tested with observational material obtained with the help of TV meteor patrol within the period from 2003 to 2010 at Kryzhanovka station that belongs to Astronomical Observatory of Odessa National University. We performed an analysis of accuracy determination of the stellar images measurements. Software was tested in order to use it for the comet observations.

Key words: meteor, meteor stream, television observations, Terner coordinates reduction.

1. Methods and software

At present the sensitive CCD are commonly used in astronomical observations instead of photographic detectors. This caused the search for the new methods of the image processing and new software creation. In particular, the regular meteor patrol observations showed the necessity of the software creation which is adapted for processing of the observational material obtained via TV method [1, 2]. As a result, we created software ***PSF*** which gives a possibility to operatively identify stellar regions where meteor patrolling is made, automatically determine coordinates of the stellar images within the TV frame, and calculate equatorial coordinates of the object using the Turner method.

Software was created on the base of the licensed version of the Visual Basic 6.0 from Microsoft Visual Studio 6.0. As reference catalogues we used compiled catalogues based on SAO, Tycho-2, USNO A-2 and other catalogues. In more details this question will be considered in Sec.2. Pattern files contain the following parameters of the observational instrumentation: the actual field of view (in arcsec), mirror (telescope) or direct (astrocamera) image, scaling coefficient that corresponds to the instrument focal length. For each image from the database containing images of the registered meteor event, the name of the certain guiding star is assigned. Software makes selection of the reference stars from the indicated catalogue using the necessary for a given image guiding star, then it searches and identifies selected stars within the image. Identifications and measurements are performed in the averaged TV frame which is obtained from 50 individual frames (2 sec).

The method of the preliminary reduction of the observational material is described in details in [2]. This method is based on the differential aperture photometry that is used for determination of the rectangular coordinates, and Turner method, which is used to determine equatorial coordinates.

The Turner method is used for determination of the object position within the frame from the object rectangular coordinates in the frame system relatively the reference stars (for these stars their equatorial coordinates are known from catalogues). The Turner method gives the mathematical relation between the system of ideal coordinates of the reference stars that were previously calculated basing on their known equatorial coordinates, and the system of rectangular coordinates determined within the frame basing on the aperture photometry method.

Relation between the ideal coordinates ξ, η and measured rectangular coordinates x, y of celestial bodies can be written as power series (the system of the reducing Turner equations):

$$\begin{aligned} \xi &= ax + by + c + dx^2 + exy + fy^2 + \dots \\ \eta &= a'x + b'y + c' + d'x^2 + e'xy + f'y^2 + \dots \end{aligned} \qquad (1)$$

Where $a, b, c, \ldots, a', b', c' \ldots$ – are the reducing coefficients which are called "frame constants". They can be found using the least square method and system of the separated Turner equations composed for the series of reference stars. Obtained in such way relations then can be used for transformation of the measured in the frame rectangular coordinates x and y of a given object into the ideal coordinates ξ и η. The latter ones are used to derive equatorial coordinates.

We use some modification of the aperture photometry for determination of the rectangular coordinates of the stellar images. In this case calculations are made for the sum of the pixel intensities inside some region. As a rule the summation is performed inside the circle. In our method the aperture radius is determined for each stellar image depending on the catalogued stellar magnitude of the star. For different instruments we introduce specific correction depending on focal length. If necessary, the aperture radius can be set manually by user itself. After the determination of the aperture radius one can calculate the mean background value for each star outside the aperture. All the points inside aperture with intensity value exceeding the background value by 3 σ belong to the stellar image. The photometric center of image can be calculated using the following formulae:

$$X = \frac{\sum(X_i * I_i)}{\sum I_i} \; ; \; Y = \frac{\sum(Y_i * I_i)}{\sum I_i} \qquad (2)$$

where X_i and Y_i are the rectangular coordinates of the pixels that belong to the stellar image, I_i - signal intensity for the corresponding pixels (in appropriate units). Processing is performed in the following way.

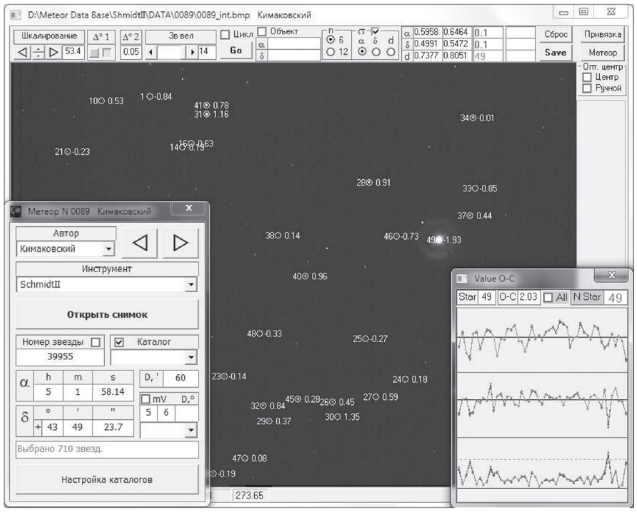

Figure 1: ***PSF*** interface.

After the starting ***PSF*** software user should be authorized. This is necessary to control the measurements which are made by each user. Then user has a possibility to choose the necessary instrumentation from the pattern file. Then after the loading of the added frame, the user indicates the reference catalogue and guiding star. The stars from the reference catalogue are selected (taking into account the size of the effective field for a given instrument) and then dispatched to the main menu window (Fig.1).

Equatorial coordinates of the stars from reference catalogue are recalculated into rectangular coordinates in the image frame system and displayed by the circles of the different diameters. Let us call such images as the measuring diagrams (MD). User manually performs approximate superposition of the MD centers with the reference stars. At this stage the limiting stellar magnitude can be set. In this case an identification and superposition can be performed only for those reference stars whose magnitude does not exceed the limiting one.

After this, the photometric centers are calculated automatically for each star using the Eq. 2, and equatorial coordinates are calculated with the 6 and 12 constants of Turner method. Simultaneously the errors of the coordinates of the measured reference and control stars are calculated. The results of the measurements and calculations are displayed in the corresponding windows (see Fig.1). In particular, in the left lower corner (Fig.1) the resulting plot shows the errors found for control stars along the right ascension, declination, and also total errors. These relations enable one to identify the wrong orientation of the MD images: at the error plot there could be recognized some bias along one of the coordinates. Thus, the user may control the errors in the plot along each coordinate, as well as taking into account the value of the mean errors (α, δ and total) calculated using reference and control stars the user can correct the position of aperture diagrams of the stars with a fixed step on the rotation angle and coordinates, and by this making the accuracy of the calculations much better. By analyzing the value of error along each coordinate and total error (three plots), the user can also exclude the stars showing large errors. Large errors arise, first of all, because of the wrong orientation of the catalogued stars relatively to the stellar images, secondly, the source of the large errors is the distortion of the stellar images in the frame caused by the Earth's atmosphere, thirdly, the errors can arise as a result of the hot pixels of CCD. As a rule, the largest errors are typical for the most faint and most bright stars. For the former ones, the reason is the low number of pixels forming the image, for the latter ones - the flickering effect.

In that case when geometrical center of the effective field of CCD does not coincide with the optical axis of the system, before calculations it is necessary to search for the optical center of an image. This can be done automatically with a fixed step. The optimal position will be found even if the optical center is outside the frame. For this one needs to use the mean errors for

control stars. The optical center position can be also set manually. If optimal values of parameters are selected, then the result will be quite accurate.

Using ***PSF*** one can measure rectangular coordinates of the comet and asteroid images, and then to calculate their equatorial coordinates. During the processing one can also calculate the errors for control stars that are situated in the frame in vicinity of the meteor trace. They are used for calculation of the equatorial coordinates of the large circle pole of the meteor trajectory.

As a result we obtain the file that contains calculated equatorial coordinates and measured rectangular coordinates, coefficients of the Turner method, the errors of determination of the reference and control stars coordinates, as well as other characteristics of the stellar images. File also keeps information about user and applied stellar catalogue that gives a possibility to perform the further analysis of the measurements and calculations made.

PSF enable one to work also with FTP (File Transfer Protocol), and to save measurements at the remote server. In this case, the result of processing immediately becomes available for other users. This afford a possibility to perform processing using remote computers (for example, this is important while performing the preliminary reduction of the observational material at the patrol stations, or if the different remote users are working simultaneously with the same material).

2. Stellar catalogues

Positional measurements and photometric analysis of the meteor images can be made with a highest precision if the reference stellar catalogues containing positions, photometric and spectral characteristics are selected correctly. In our case we used the following catalogues:

1.**SAO** (Smithsonian Astrophysical Observatory Star Catalog) /Publ. of the Smithsonian Institution of Washington, D.C. 4652 (1966)/ This catalogue contains positions of the stars on J2000 epoch, V and B stellar magnitudes, spectral classes and proper motions;

2.**Hipparcos** (Hipparcos Input Catalogue, Version 2) /Bull. Inf. CDS 43, 5 (1993):/This catalogue contains the high-precision positions of the stars, stellar V and B magnitudes (catalogue photometric system), spectral information, proper motions;

3.**Tycho-2** (The Tycho-2 Catalogue) /Astron. Astrophys. 355, L27 (2000)/ - high-precision stellar positions, V and B magnitudes, proper motions;

4.**USNO A2** (The PMM USNO-A2.0 Catalogue) / US Naval Observatory Flagstaff Station (1998)/ contains accurate positions of the stars, R and B stellar magnitudes.

Catalogues AGK3 /Astron. Astrophys. Suppl. Ser. 16, 345 (1974)/ and PPM (Positions and Proper Motions - North & South) / Astron. Astrophys. Suppl. Ser. 74, 449 (1988)/ were excluded from consideration as quite old sources, since the more recent catalogues are based on the more accurate data provided by satellites. The catalogue ACT (The ACT Reference Catalog) and similar ones were also ignored as being based on Tycho-2 catalogue and some ground-based observations that are not more precise than the data from Tycho-2 catalogue.

Selection criteria and analysis of used catalogues were the following. First of all, we need not astrometrical precision of the stellar positions: it is clear that the accuracy of the rectangular coordinates measurements results in equatorial coordinates determination with a precision not better than 1 arcsec. The same requirements are valid for the stellar magnitude accuracy (accuracy of 0.1^m is quite sufficient for our aim). All the above-mentioned catalogues satisfy to these criteria. For the photometry B and V magnitudes of the reference stars should be available. The data in both these filters are present in the most of listed catalogues. For SAO catalogue instead of V magnitude one can use the very close photographic magnitude, and for USNO-A2 catalogue one can change V magnitude to R magnitude. Considering the required for our aim accuracy such a substitution is quite justified. Availability of the spectral information is desirable, of course, but not necessary, since an analysis of the spectral characteristics is needed for some small tasks, but not for the extensive photometric and positional measurements of the meteor images.

In addition to the listed original catalogues we also created two compiled catalogues containing information about equatorial coordinates of the stars and their B and V magnitudes. These catalogues fit to our requirements concerning the positional and photometric characteristics of our measurements. These two compiled catalogues are: Hipparcos + Tycho-2 and Tycho-2 + USNO-A2. This enables one to increase the total number of the reference stars.

We should note that our optical devices do not allow us to register stars fainter than 13.5^m in V-band, therefore we have restricted the data from used catalogues up to 15^m (i.e. with some reserve in order to have a possibility to estimate the qualitative tendency in our analysis).

Very strict requirement is a necessity to have the great number of the faint stars (fainter than 10.5^m in V-band). It is even more important when the data obtained with Schmidt (field of view is about 0.5 square deg.) are reduced. To apply this criterion we have constructed the distribution in the available bands for all catalogues (Fig.2). As one can see the two catalogues Tycho-2 and USNO-A2 (as well as two compiled catalogues based on them) are most abundant

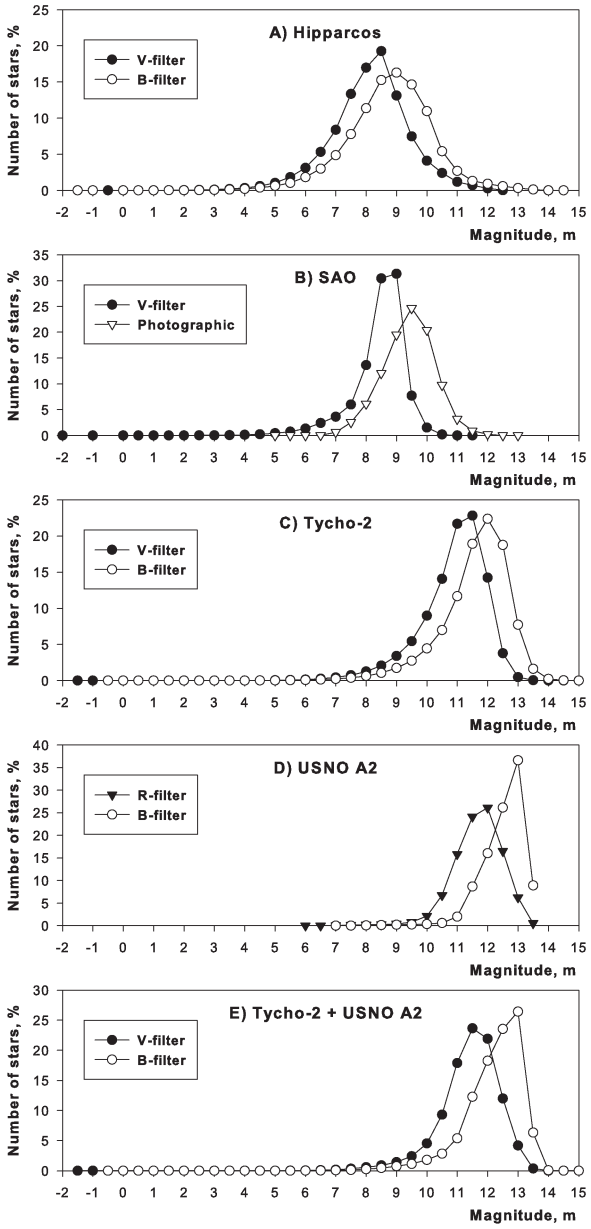

Figure 2: Percentage distribution of the stellar magnitudes in different bands for used catalogues.

in faint stars (plots C and D, and E and F respectively). Thus, having made a preliminary analysis of the plots in Fig.2, one can conclude that for meteor observations performed with Schmidt telescope (Turner method and photometry of the meteor trajectories) it is better to use these above mentioned catalogues. For observations which are performed with the wide-field view (about 2.5 square deg.) cameras with objective lens KO-140 SAO and Hipparcos catalogues can also be used since the very faint stars are not used in this case.

The next requirement is the high density of stars in the square degree. Fig.4 presents the distributions the total number of the stars from all sky with a step of 1 square degree (we call such a distribution as "density map"). In particular, for all catalogues one can note the clear tendency of the density increase along the ecliptic that testifies about the observational selection. We did not show in Fig.4 the density map for Hipparcos catalogue because it qualitatively resembles that of SAO catalogue (plot A), while the density along the ecliptic is even lower. We also do not present the density map for the USNO-A2 catalogue because qualitatively it is the same as for the corresponding compiled catalogue (plot C) where more clearly is seen the density inhomogeneity, in other words some "platform-like" distribution which is caused by the specific way of this catalogue creation by the combining of the space and ground-based observations. In the density map we also show the position of the centers of obtained images in equatorial coordinates. As one can see we often carry out our observations within those regions where the stellar density provided by SAO catalogue (and even more so by Hipparcos catalogue) is clearly insufficient. Table 1 lists the mean values of the stars in the square degree.

Table 1: The mean catalogue values of the star density (in 1 square degree).

Catalogue	Mean value
Hipparcos	2
SAO	4
Tycho2	39
Hipparcos + Tycho-2	40
USNO A2	72
Tycho-2 + USNO A2	112

This value for the compiled catalogues should be decreased by about 50-70% because of the practically the same positions of the stars that are presented in the base catalogues used for the compilation. About 30-50% additional stars can be included from the ground-based surveys (in some cases for our aim it is enough to use such stars that were excluded from the more recent catalogues because of the lower accuracy of their atrometric characteristics). Selection and exclusion of the same stars from compiled catalogues is made by ***PSF*** software at the direct measurements of each image. The semi-automatic regime is also available.

Having analyzed the results of our measurement one can note that we use the following resources of catalogue selected for observational program: about 90% of the all number of available stars if observations are made with Schmidt telescope and up to 40% if astro-camera with objective lens KO-140 is used. Thus, the high density of the stars at the square degree is an important factor which is necessary for the high-quality data reduction.

As to the distribution of the spectral characteristic of the stars presented in our reference catalogues, their per cent ratio is showed in Fig.3.

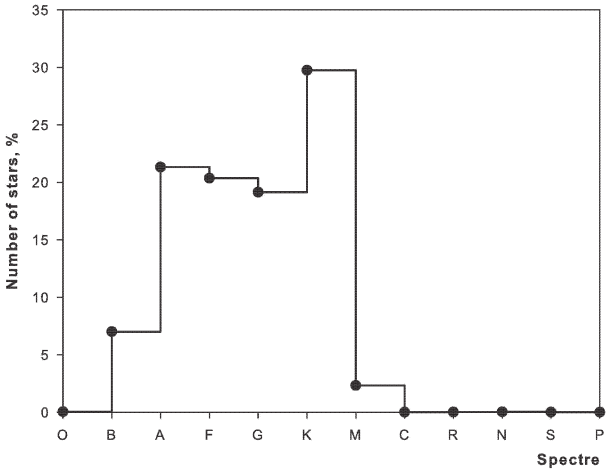

Figure 3: Distribution of the spectral characteristics for the stars from SAO catalogue.

Below we give some technical description of the catalogues used for the data processing. We created catalogues which are based on the primary files that are available (free access) at the web-page VizieR Catalogue Service (http://vizier.u-strasbg.fr/). For the most of the catalogues they are the text files, for the USNO-A2 catalogue they are binary files because of its big size (nowadays this catalogue is completely available at the abovementioned web-page). Using the file descriptions we selected only that information which is necessary for our observation, namely: equatorial coordinates of the stars, proper motions, spectral data, magnitudes of the stars in different band. As we mentioned above, from USNO-A2 catalogue we excluded all information about the stars fainter than 15^m (V-band).

All used catalogues were transformed in uniform format MS Access DBMS which enable one to perform a quick search inside the catalogue using the broad possibilities of SQLanguage. To accelerate the search process we divided the data on hour belts (24 tables inside of each database), and also calculated equatorial coordinates with fractional part. Program part is organized as VB language module with the help of ADO 2.8 technology. This module can be used both independently, and a part of ***PSF***. Used by us the storing format of the reference catalogues allow one to easy perform an analysis of the selected samples.

Let us make the short analysis of the measurements that are obtained using the selected reference catalogues.

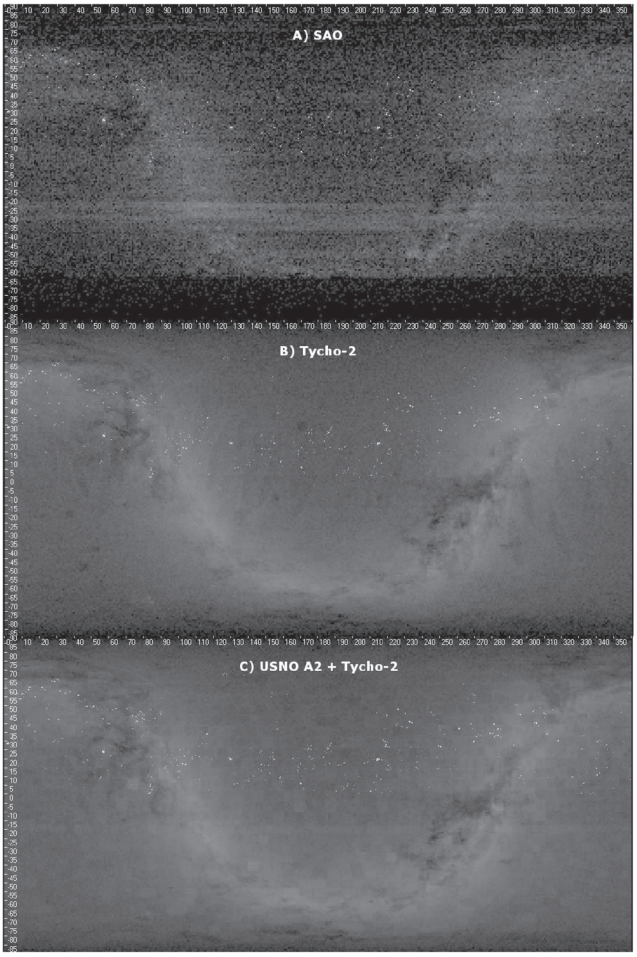

Figure 4: Stellar density as it is represented by the used catalogues. Dots - positions of the centers of the frame regions. Axes - equatorial coordinates.

3. Statistics of observations

Fig.5 shows the mean-square deviations for the reference stars for different catalogues and both observational instruments for more than three thousands meteor images depending on the stellar V-band magnitude. One can immediately note the obvious tendency: a decrease of the mean-square deviation with an increase of the stellar magnitude ("brightness equation"). For the brighter stars error is connected with their larger-scale and structured images. This significantly hampers measurements and worsens the quality of the processing (see Sec.1). For the observations performed with Schmidt telescope (the plots A, B, C) one can conclude that the most appropriate range of the reference stars magnitudes begins with $+6^m$. As to observations obtained with astrocamera (KO-140 objective lens), the plots D, E, F show that there one can trace one more tendency: for the reference stars fainter than $+9^m$ errors suddenly increases. This is caused by that fact that faint stars cannot be registered with this

astrocamera, therefore during the image processing the faint stars are either cannot be measured, or it can be done but with a significant error. Since ***PSF*** enables one to determine the position of the reference stars in semi-automatic regime, for such stars user often selects either bright intensities of the background, or hot pixels (in some cases even defects of the images). Naturally, such stars are then excluded from analysis (because of the large value of mean-square error, or because of the limiting magnitude criterion). The plot gives concrete recommendations to users about the range of the stellar magnitudes of the reference stars that can be used (taking into account the instrumental characteristics applied for observations).

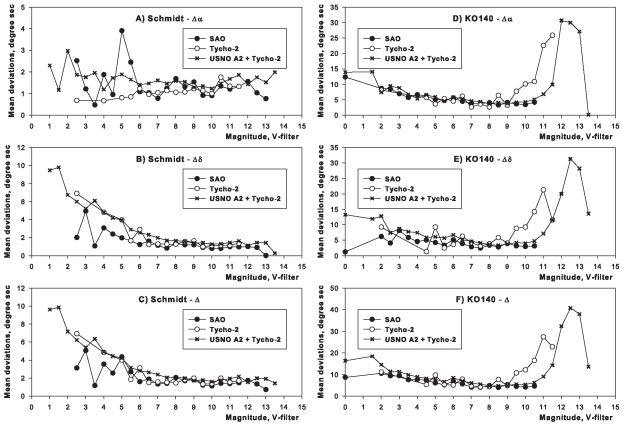

Figure 5: Mean-square deviations of the reference stars as a function of the stellar magnitude in V-band (along the right ascension and declination) for each reference catalogue and each instrument.

In Fig.6 we show maximum mean-square deviations of the reference stars (the same data as in Fig.5). It is clearly seen that for both instruments more bright stars show large deviations. The reason in this case is the same as for mean-square deviations in Fig.5. Similar situation (as for the mean-square deviations for the stars fainter than $+9^m$) also takes place for the data obtained with KO-140 (see plots D, E, F). One can also note that even for observational data obtained with Schmidt telescope the maximum errors attributed to the Tycho-2 and USNO-A2+Tycho-2 catalogues (particularly to the latter one) are larger than deviations resulting from SAO catalogue. Therefore such plots can be used for indirect estimate of the quality of positional data in the reference catalogues, and moreover they can be important for corresponding recommendations about some details of the data reduction process. We recommend using SAO catalogue as a reference one for the processing of the data obtained with KO-140 objective lens (if the number of stars within the field of view is quite enough). This is because the range of the stellar magnitudes covered with KO-140 is the same as that available in SAO catalogue. Images obtained with Schmidt telescope can be reduced only by using USNO-A2+Tycho-2 catalogue (this combination is abundant in faint stars, but it does not guarantee high accuracy of calculated equatorial coordinates).

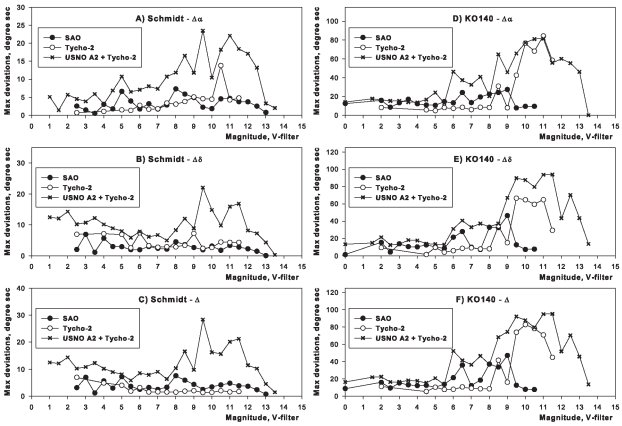

Figure 6: Maximum mean-square deviations as a function of the stellar magnitude in V-band (along the right ascension and declination) for each reference catalogue and each instrument.

Table 2 lists the mean-square deviations for the both instruments and for the three frequently used catalogues. N_m - the number of observed regions containing the meteor images, N_s - the number of the stars, σ_α (right ascension), σ_δ (declination) and σ (total) - the mean-square deviations of the reference star coordinates. The tendency mentioned above is confirmed (see Fig.6): the highest precision can be achieved using SAO as reference catalogue (which has a deficiency of the faint stars).

The content of Fig.7 is the further recommendation of using the SAO catalogue for the photometric analysis of the observations obtained with KO-140, and USNO-A2+Tycho-2 catalogue for the photometric analysis of the data gathered with Schmidt telescope.

In addition we show the distribution of the mean-square deviation across the optical field of our instruments (at the first approximation they can be considered as being uniform). This indicates that we correctly selected the method of the data reduction and testifies that our optical systems have the good quality.

Finally, we show percentage distribution of the module of the mean-square deviation of the reference star equatorial coordinates for different catalogues (Fig.8).

As one can see, the larger the error, the lower the percentage of the stars. For the great majority of the stars observed with Schmidt telescope the error value does not exceed 2-3 arcsec, while for the data obtained with KO-140 - 6-7 arcsec.

To carry out an express analysis of data processing quality depending on the catalogue used we created

Table 2: Statistical results for the meteor images reduction based on the use of different catalogues. Images were obtained with the help of Schmidt telescope and astrocamera KO-140.

	Schmidt					KO-140				
Catalogue	N_m	σ_α	σ_δ	σ	N_s	N_m	σ_α	σ_δ	σ	N_s
SAO	29	1.34	1.20	1.70	588	196	3.93	3.42	4.82	6653
Tycho2	61	1.30	1.41	1.78	1192	10	3.49	2.64	4.23	471
USNO A2 Tycho-2	2102	1.58	1.58	2.01	66260	701	4.51	4.39	5.78	47071

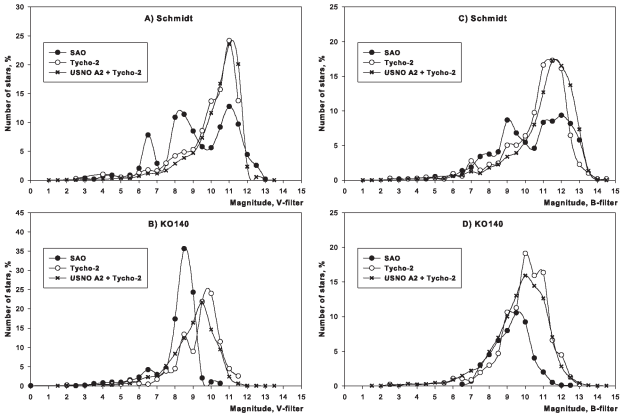

Figure 7: Percentage ratios of the stars in the reference catalogues with different magnitudes in V- and B-bands.

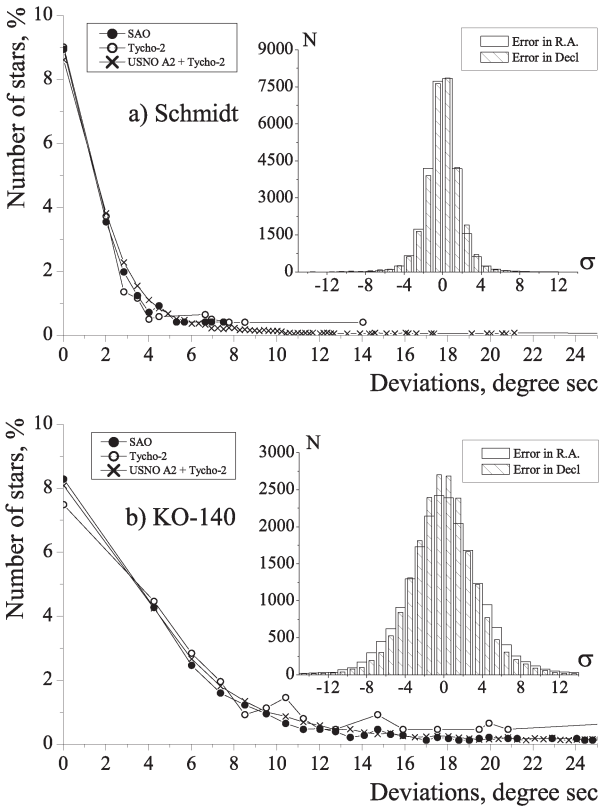

Figure 8: Percentage distribution of the stars from different catalogues depending on mean-square deviation.

software which enables one to get the following characteristics based on the measurements: the mean-square and maximum mean-square deviations (depending on the stellar magnitude), the distributions of the stellar magnitudes of the reference stars (V- and B-bands), the distributions of the mean-square deviations for the reference stars, the mean-square deviations mapped across the field of view. Summarizing, we note that selected catalogues are well appropriate for obtaining positional and photometric data which are necessary to reduce our observations. Both preliminary and subsequent analyses of all the catalogued data together with the results of our measurements allow one to correctly select the necessary catalogues depending on parameters of the telescope and astrocamera.

Fig.9 presents the distributions of the errors in position of the reference stars for Schmidt telescope and astrocamera equipped with KO-140 objective lens. Errors on α, δ and the total errors are presented separately. It is seen that the accuracy of the measurements is higher for the Schmidt telescope images. The ranges of the errors on α and δ are similar, and this indicates that there is no systematical error bias in our measurements. The large interval of the errors (up to 10 arcsec) is caused by that fact that during the meteor patrolling some cases can be met when the number of the reference stars within the field of view is limited (or the atmosphere transparency is bad, and this restricts the limiting magnitude; the same problem can also arise if observations are carried out during the twilight). An internal accuracy is determined by residuals found with reference stars, an external accuracy is found from residuals of the control stars. As the control stars we use that sample of stars that are not used to derive the parameters of the Turner equation. In addition, in order to determine an accuracy of our measurements we also use the precision which is conditioned by the residuals of the control stars just near to the meteor trajectory image.

After ***PSF*** creation we applied several tests to check the quality of the observational material reduction. As one of the tests we used IRIS code (Christian Buil, http: //www.astrosurf.com/buil, free access). Using this software and our ***PSF***, we obtained similar results

(within the standard errors [2]). Another test is the positional observation of comets. As a result of the following comets observations: C/2002 T7 (LINEAR) and C/2006 W3 (Christensen), we sent their calculated equatorial coordinates to IAU Minor Planet Center. The results of the comet image reduction completely satisfied to the Minor Planet Cent requirement, and after that Kryzhanovka observational station was assigned the designation A85 Odessa Astronomical Observatory, Kryzhanovka, and the corresponding coordinated were published in Minor Planet Electronic Circular [3],[4].

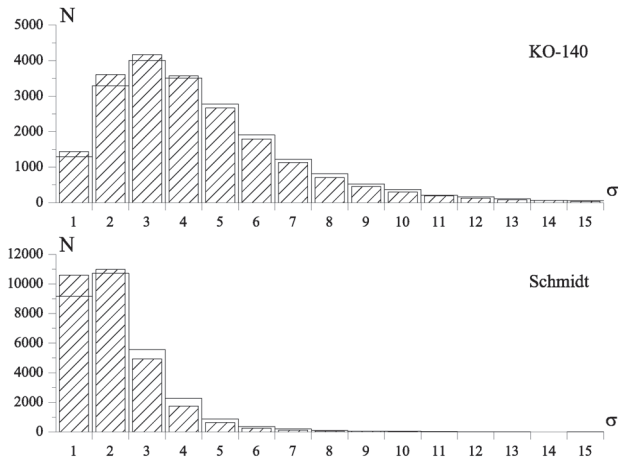

Figure 9: Distribution of the position errors for the reference and control stars.

4. Conclusions

Software ***PSF*** was created in the Department of the Solar system small bodies (Astronomical Observatory of I.I. Mechnikov Odessa National University). Using this software one can calculate equatorial coordinates of the celestial objects using the images of the reference stars obtained via TV method. This software was adapted for various optical systems and it was tested during the meteor and comet observations. For the star-like objects an error of the positional measurements is about 1.0-1.5 arcsec (for Schmidt telescope having focal length 50 cm). For the astrocameras equipped with Pentzval lens (focal length 14 cm) this error achieves 3-5 arcsec.

References

1. Gorbanev Yu.M., Golubaev A.V., Zhukov V.V., Kimakovskaya I.I., Kimakovsky S.R., Knyazkova E.F., Podlesnyak S.V., Sarest L.A., Stogneeva I.A., Shestopalov V.A.: 2006, *Solar System Research*, **40**, 5.
2. Gorbanev Yu.M., Golubaev A.V., Zhukov V.V., Kimakovskaya I.I., Kimakovsky S.R., Knyazkova E.F., Podlesnyak S.V., Sarest L.A., Stogneeva I.A., Shestopalov V.A.: 2008, *Solar System Research*, **42**, 1.
3. A.V.Golubaev, S.R.Kimakovsky, I.I.Kimakovskaya, L.A.Sarest, V.A.Shestopalov: Comet Observations [A85 Odessa Astronomical Observatory, Kryzhanovka] //Minor Planet Circular 53902, 49 (2005).
4. A.V.Golubaev, S.R.Kimakovsky, I.I.Kimakovskaya, L.A.Sarest, V.A.Shestopalov: Comet Observations [A85 Odessa Astronomical Observatory, Kryzhanovka]//Minor Planet Circular 66408, 33 (2009).

U.D.C. 521.95, 521.97

MONITORING THE ACCURACY OF OBSERVATIONS OF PASSIVE OBJECTS ON THE BASIS OF THE INTERNATIONAL LASER RANGING SERVICE (ILRS) DATA

I.V.Kara

Astronomical Observatory of I.I.Mechnikov Odessa National University
Odessa, Ukraine

ABSTRACT. Today, the problem of pollution of the near-Earth space environment is becoming more acute. In view of that, a larger number of stations for observation and tracking of artificial earth satellites (AES) and space debris objects have been set up. The accuracy of the ephemerides of such objects depends on the quality of the observations obtained. Therefore, the possibility of efficient quality control and monitoring the accuracy of the gathered observations is extremely essential. The suggested method allows of promptly conducting a check on the correctness of the data obtained. The coordinate data of the International Laser Ranging Service (ILRS) are assumed as a basis of the method mentioned above. The developed mathematical software (MS) enables observers to analyze their observations efficiently and without assistance in order to reveal and solve arisen instrumental problems opportunely.

Introduction

At the present stage of development of space science and technology, the mankind has already faced the problem of pollution of the near-Earth space environment. The pollution occurs due to spent rocket stages abandoned in orbit and AES on-orbit explosions generating numerous uncontrolled objects. Such explosions can be caused by collisions between AES or by AES collision with space debris objects. Collisions between AES are still a rare case. That problem of AES explosions has just been worsening year by year. The number of AES launches has been augmenting, and the probability of collisions in space has been increasing simultaneously. That is why more and more observatories allot observation instruments tasked for observation, cataloging and tracking of space debris objects and AES. The creating of catalogues of potentially hazardous objects in the near-Earth space will enable to predict collisions and to preserve expensive satellites, and not to increase the number of perilous objects. When generating such catalogues, it is necessary to regularly monitor the quality of the observations gathered. The accuracy of the obtained ephemerides straightly depends on the quality and correctness of the data. Such monitoring can be conducted either by an observer independently or with assistance of specialists from other observatories. The second alternative lowers manifold the efficiency of detection and solution to an observation accuracy problem if there is any. In this case, the ability of an observer to independently check up the accuracy of observations before their passing to the customer is of great value.

Proceeding from the grand necessity of such monitoring the accuracy of observations, the task to discover a method of observers' independent monitoring the quality of the observations obtained by them was set. The mathematical software (MS), developed on the basis of the discovered method, should enable an observer to promptly conduct a check on the correctness of observations. By using the MS, it will be possible to calibrate either new observation instruments or upgraded available ones in order to increase the accuracy of observations.

Using the ILRS data to monitor the observations obtained

The direct comparison of actual observations with reliably correct reference observations of the same objects is the most reasonable method of checking on the accuracy of observations. The AES Cartesian coordinates from the website of the International Laser Ranging Service (ILRS) [1] can be taken for such reference standard AES observations. The ILRS provides AES and lunar laser tracking data and related products to support geodetic and geophysical research activities. The website of the indicated service offers free access to the files with geocentric Cartesian coordinates expressed in the International Terrestrial Reference System (ITRS) for a certain list of AES [2]. The detailed information on satellites and their orbital elements is given at the ILRS website [3]. Information on the positions is given at the website in separate files for each satellite. Each laid up file contains geocentric Cartesian X, Y, Z coordinates of a particular AES for the current day when the file was created and the ephemerides for several subsequent days. Those coordinates are generated from the orbits obtained by a high-precision model of motion of AES (the Earth's gravitational field, air resistance (drag), solar radiation pressure, etc.). That is exactly why such Cartesian coordinates of AES can be used as reference standard ones. An example of the header of such a file is given in Fig. 1. More detailed information on the structure and format of the prediction file can be found at the website [4].

```
H1 CPF  1  HTS 2009  9 16 12  7591 ajisai           NONE
H2  8606101 1500    16908 2009 09 16  0  0  0 2009 09 21  0  0  0   240 1 1  0 0 0
H5  1.0100
H9
10 0 55089  85200.00000  0    5104060.378    4599246.690    3810782.560
10 0 55089  85440.00000  0    4666026.698    5712020.846    2715644.558
10 0 55089  85680.00000  0    4044116.477    6575900.301    1492264.912
10 0 55089  85920.00000  0    3258286.721    7156768.810     198465.511
10 0 55089  86160.00000  0    2335175.372    7433074.936   -1104701.959
10 0 55090      0.00000  0    1307254.820    7396585.330   -2355883.381
10 0 55090    240.00000  0     211730.692    7052513.897   -3496338.783
```

Figure 1. The header of a part of the prediction file from the ILRS website.

The accuracy of the ephemerides in prediction files depends on the type of AES orbit. Taking into consideration the fact that prediction files contain ephemerides for several days, it is possible to determine the inherent accuracy of the ephemerides by comparing the files. Satellite Ajisay (altitude of about 1500 km) is taken as an example. The analysis of accuracy found that the inherent accuracy of positions in the file is about several meters for four days (Fig. 2). Such accuracy ensures an error in topocentric angular coordinates of about 0.5 arcsecond for the fourth day. Therefore, when using positions from the file only for the current day, it is possible to consider an error in coordinates themselves as negligible. It is evident that if the accuracy of observations themselves is less than 1 arcsecond, such an error should not be neglected. At the same time, it is not reasonable to consider that other satellites from the ILRS list have approximately the same accuracy. In that list, there are also satellites, orbits of which are regularly adjusted. The error curve for such satellites is to be more abrupt as the prediction files, generated before and after such an adjustment of orbit, are not comparable. For example, the ephemeris error for the Envisat satellite (altitude of about 700 km) is analyzed. The analysis showed that the ephemeris accuracy is admissible only for the current day when the file was generated. For the subsequent day the prediction accuracy is sharply worsening (Fig. 3).

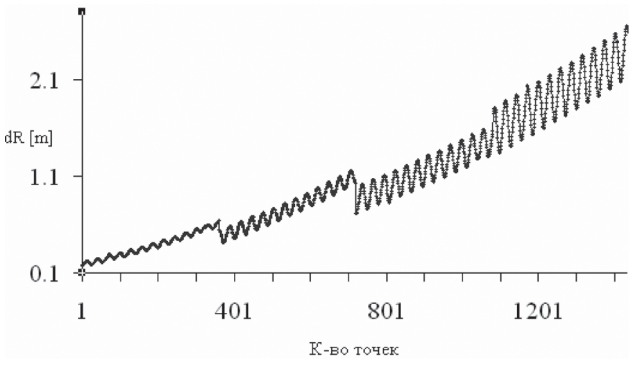

Figure 2. Inherent accuracy of the prediction files for Ajisay

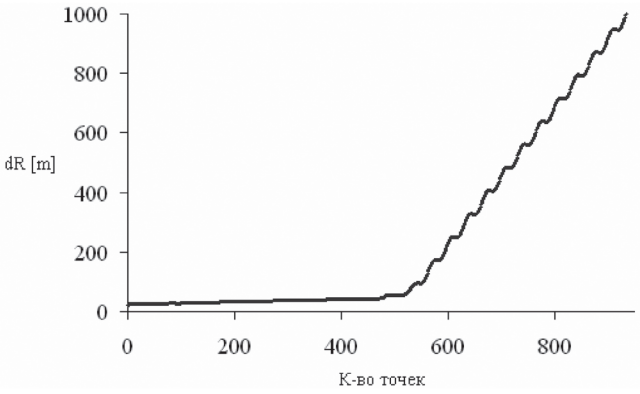

Figure 3. Inherent accuracy of the prediction files for Envisat

Stages of conversion of the ILRS positions to monitor the accuracy of observations

To be able to compare actual observations with reference standard ones, it is necessary to conduct a step-by-step conversion of both the ILRS positions and actual observations. It is indispensable as actual angular coordinates of objects turn out to be topocentric in the International Celestial Reference System (ICRS) for epoch J2000.0 as well. To get correct comparison, it is needed to convert the ILRS positions to the ICRS for epoch J2000.0.

Stage 1. As the Cartesian coordinates in the files are expressed in the ITRS, it is necessary to transform coordinates to the ICRS for epoch J2000.0. To do that, standard formulae for conversion of reference systems (1) can be used:

$$\begin{pmatrix} x \\ y \\ z \end{pmatrix}_{ICRS} = P' \cdot N' \cdot R_3(-S_\oplus) \cdot R_1(y_p) \cdot R_2(x_p) \cdot \begin{pmatrix} x' \\ y' \\ z' \end{pmatrix}_{ITRS} \quad (1),$$

with P' – the precession matrix; N' – the nutation matrix; $R_3(-S_\oplus)$ – the Earth rotation matrix; $R_1(y_p)$ – the matrix for clockwise rotation about the x-axis by empirical pole coordinate y_p; $R_2(x_p)$ – the matrix for clockwise rotation about y-axis by empirical pole coordinate x_p.

The time argument for the precession and nutation matrices is time referred to the Barycentric Dynamical Time (TDB) scale. The Earth rotation matrix represents the rotation about z-axis by angle equaled to the apparent sidereal time $S_{\oplus}$. The apparent sidereal time is a function of Universal Time $UT1$. Universal Time is obtained by adding the time correction ΔUT to UTC. It is recommended to use the algorithm for computing precession, nutation and rotation matrices for the apparent sidereal time as per formula (1) presented in the IERS Conventions (2003) [5. pp. 33-52]. The obtained AES position vector referred to the ICRS is used then to compute topocentric coordinates of the AES.

Stage 2. To compute the AES topocentric coordinates as per formula (2), the geocentric position of the observation station should be known:

$$\vec{r} = \vec{R} + \vec{\rho} \qquad (2),$$

with $\vec{r}$ – the geocentric position vector of the AES; $\vec{R}$ – the geocentric position vector of the observation station; $\vec{\rho}$ – the topocentric position vector of the AES. It is possible to compute the observation station coordinates in the ITRS on having known its accurate latitude, longitude and elevation above sea level. When the station coordinates expressed in ITRS is known, they should be converted to the ICRS using the same formula (1). Then, using the obtained vector $\vec{\rho}$, it is possible to compute topocentric angular coordinates of AES by spherical trigonometry formulae.

Stage 3. Actual observations are usually obtained by image processing on video frames. There are many methods for processing of such data and extraction of the angular coordinates of the observed objects, for example [6]. Each frame is processed as a photographic plate. Referring to the coordinate system of a frame, the angular coordinates of the necessary object relative to reference stars in the frame are determined by the Turner's method. The peculiarity of such method of determination of the object's angular coordinates is that positions of the reference stars, caught in the frames, are taken from publicly-accessible high-precision star catalogues, such as Tycho and USNO catalogues. Those catalogues give the stars positions for epoch J2000.0 in the celestial coordinate system. Therefore, the objects angular coordinates, obtained by the method indicated above, are also turn out to refer to epoch J2000.0. However, as those observations are carried out from the Earth revolving around the Sun, the coordinates are distorted by annual and diurnal aberrations as well. To apply corrections for those aberrations, it is possible to use formula (3) to compute diurnal aberration and formula (4) to compute the annual one [7].

$$\begin{aligned} \Delta\alpha\cos(\delta) &= 0^{s}.0213\cos(\varphi)\cos(t) \\ \Delta\delta &= 0''.320\cos(\varphi)\sin(\delta)\sin(t) \end{aligned} \qquad (3),$$

where φ - the astronomical latitude of the observation site; t – the hour angle.

$$\begin{aligned} \Delta\alpha\cos(\delta) &= \frac{1}{c}\left[-\dot{X}\sin(\alpha)+\dot{Y}\cos(\alpha)\right] \\ \Delta\delta &= \frac{1}{c}\left[\dot{Z}\cos(\delta)-\dot{X}\sin(\delta)\cos(\alpha)-\dot{Y}\sin(\delta)\sin(\alpha)\right] \end{aligned} \qquad (4),$$

where c – the speed of light; $\dot{X}\ \dot{Y}\ \dot{Z}$ – components of the Earth Barycentric velocity in the Cartesian coordinate system; $(\alpha;\delta)$ – the object's equatorial coordinates in the ICRS.

As per description of the consolidated format of the ILRS files, the coordinates are given with no aberration corrections applied. Thus, to make a correct comparison, it is needed to apply corrections for annual and diurnal aberrations to the coordinates of actual observations.

Stage 4. Besides annual and diurnal aberrations, actual observations are distorted by planetary aberration as well. Moments of time, corresponding to the angular observations, should be corrected for planetary aberration. The value of aberration can be computed from the ILRS positions if the distance to the object and the speed of light are known.

Stage 5. As in the ILRS files of predictions all positions are given with a fixed step size of units of minutes, it is necessary to use the Lagrange interpolation method in order to obtain the ILRS coordinates for a certain instant of time from actual observations [8]. That method of interpolation is recommended for usage in the ILRS prediction format description [4]. It should be kept in mind that when interpolating coordinates at a certain instant of time from actual observations it is necessary to take into account the delay due to planetary aberration for that instant.

Testing the efficiency of the suggested method of monitoring the accuracy

The method of comparison of actual observations with the ILRS coordinate data has been implemented in the form of mathematical software. Using that, the analysis of the accuracy of the obtained actual observations of AES was conducted. To make such an analysis, the observation data for satellite Ajisay, obtained with telescope KT-50, are provided by Odessa Astronomical Observatory. The observations are in the equatorial coordinate system in arrays of points $(MJD;\alpha;\delta)_i$. The number of observation nights and points used for comparing with the ILRS coordinates are indicated in Table 1.

Table 1. Data on the observations analyzed

Observation date	Number of points
16.09.2010 – one pass	627
16.09.2010 – two passes	387
17.09.2010 – one pass	323
17.09.2010 – two passes	146
21.09.2010	353
23.09.2010	267

The error curves are output in the orbital coordinate system to make easier perception of graphs of difference between the observed and the computed positions (O-C). Therefore, on the (O-C) graphs, the satellite along-track error dL is displayed instead of right ascension error and the cross-track error dH – instead of declination error. The along-track error dL is given both in the angular measures and in the time scale, obtained using the satellite orbital velocity. On the following graphs, the x-axis shows the index numbers of points in the file containing actual observations. The (O-C) graph for the comparison of the first night observations is shown in Fig. 4.

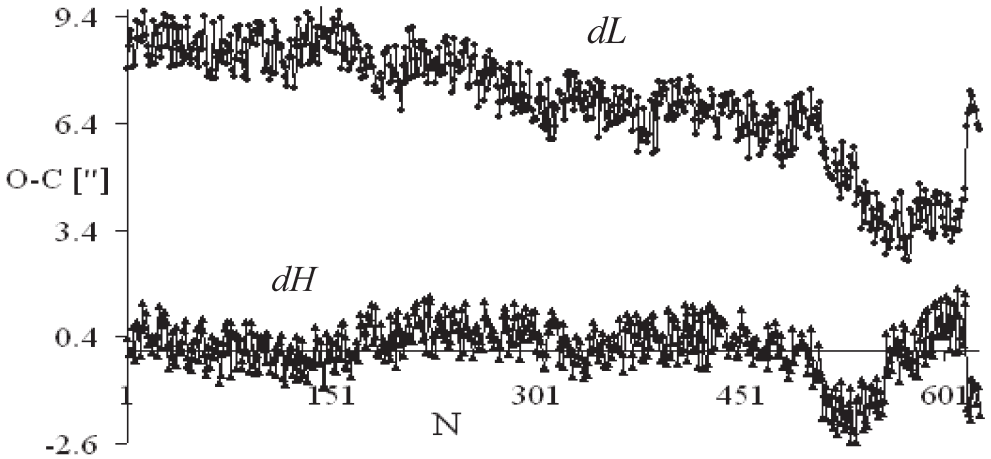

Figure 4. (O-C) observations on 16.09.2010 – one pass

As is evident from Fig. 4, the error curves are irregular due to the instruments operation when recording the observations. It is also clear that the error curve lies above the x-axis. That means that there is some problem in recording instants of time. Fig. 5 shows the along-track error dL in the time scale. On the average, the delay is about 10 ms. When that delay is considered in the instants of time of actual observations, then, as it is shown in Fig. 6, the (O-C) graphs are located along the x-axis as it should be. The analysis of the other observation nights demonstrated the same type of dH and dL error curves. That means that the problem of delay in recording instants of time is of general type. The analysis of such a delay led to a conclusion that the delay value defines the CCD-matrix operating speed, used to obtain observations. A value of 10 ms is equal to a quarter of the frame, which is formed by a CCD-matrix with a frame frequency of 25 fps. Thus, by comparing actual angular coordinates with the ILRS positions, using the method indicated above, we succeeded in measuring and applying the CCD-matrix response time when forming the observations themselves. That allows of increasing the accuracy and quality of the observations obtained.

Conclusion

The described method of monitoring the accuracy of observations using the ILRS coordinate data is relatively simple and enables to promptly conduct a check of the AES observations obtained. As the regularly-updated daily positions are provided for the satellites from the ILRS list, those are recommended to be used as reference standard ones to calibrate and monitor operation of observation instruments. Implementation of the suggested method enabled to determine for the first time the re-

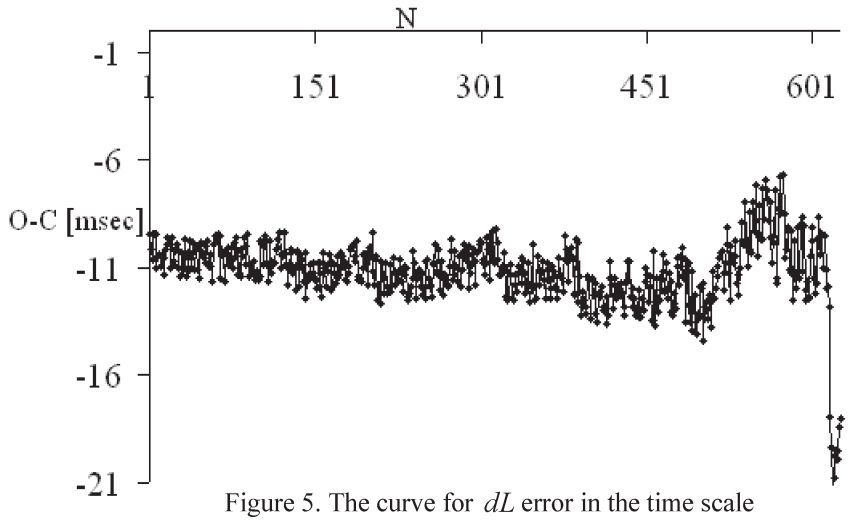

Figure 5. The curve for dL error in the time scale

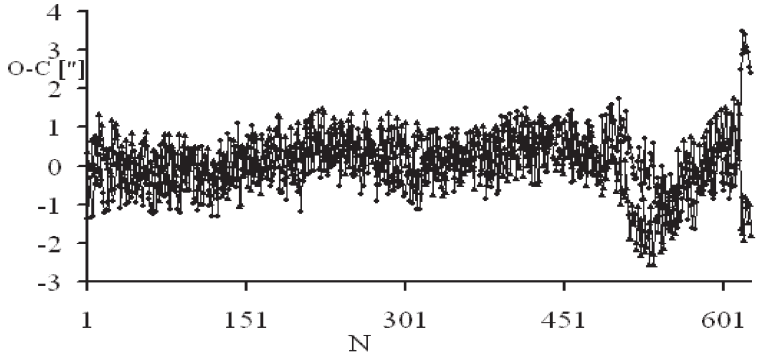

Figure 6. The curves for dH and dL track errors after adjustment of 10 ms

sponse time of CCD-matrices, used to obtain observations, and to apply that value when processing the observations of Odessa Astronomical Observatory. Moreover, the comparison with the ILRS data allowed of making the methods of processing the observations of Nikolaev Astronomical Observatory more precise [9] and of increasing the accuracy of their observations gathered. The leaders of both observatories made a decision to carry out regular observations of AES from the ILRS list in order to continuously monitor the observations obtained.

References

http://ilrs.gsfc.nasa.gov/ - the International Laser Ranging Service official website

ftp://cddis.gsfc.nasa.gov/slr/cpf_predicts/

http://ilrs.gsfc.nasa.gov/satellite_missions/list_of_satellites/

http://ilrs.gsfc.nasa.gov/docs/cpf_1.01.pdf - Consolidated Laser Ranging Prediction Format, Version 1.01

IERS Conventions, 2003: 2004, *IERS Technical Note* № **32** // U.S. Naval Observatory.

Козырев Е.С. Сибирякова Е.С. Шульга А.В.: 2008, *Сборник трудов конференции «Околоземная астрономия 2007»*, Нальчик, 288-292.

Жаров В.Е. *Сферическая астрономия*: М., 2002.

Калиткин Н.Н. *Численные методы*: М., Наука, 1978.

Козырев Е.С., Сибирякова Е.С., Шульга А.В.: 2010, *Космічна наука і технологія*, **16**, №5, 71-76.

U.D.C. 521.6

THE CONDITIONS OF AN ACTIVE EQUATORIAL GSS ENTERING THE EARTH'S SHADOW

G.F.Karpenko[1], B.A.Murnikov[2], P.P.Suhov[1]

[1] Astronomical Observatory of I.I.Mechnikov Odessa National University
[2] Department of Astronomy of I.I.Mechnikov Odessa National University
Odessa, Ukraine
sppete@rambler.ru

ABSTRACT. In this article we describe the conditions of an active GSS entry and exit from the Earth's shadow relative to the plane of the Earth's equator with a small inclination of the orbit to the equator.

Geostationary satellites is the agreed definition for geosynchronous satellites with periods of rotation around the Earth's centre of mass from 22^h to 26^h, the eccentricity of not more than 0.3 and the inclination of the orbital plane to the equator of up to 15°. Therefore any GSS is to immerse repeatedly into the Earth's shadow for different time in during a year.

The active GSS that orbit along the plane of the Earth's equator have an orbital inclination to the equator close to 0^0. The mentioned GSS are to enter and exit from the Earth's shadow close to the vernal and autumnal equinoxes on the conditions provided below (see formula (1)). Besides the conditions of formula (1), the time of immersing, emerging and passing into the shadow for passive GSS depend on the inclination of the GSS orbital plane to the equator, the direction of the GSS motion relative to the shadow: towards or away from the shadow.

It is often mentioned [1, 2, 3, 4], that the photometric observations of GSS on entry and exit from the shadow arouse a special interest as they allow to improve the temporal resolution of photometrical observations and hence to make more precise the detailing of the field structure of reflective surface of satellites. Therefore it is necessary to calculate the time of the observed satellite entry and exit from the Earth's shadow.

The Sun's declination changes from $+\varepsilon$ ($+23^0\,26'$) to $-\varepsilon$ ($-23^0\,26'$) throughout a year between the summer and winter solstices. And during a year the Earth's shadow moves correspondingly relative to the plane of geostationary orbit that is located along the plane of the Earth's equator (see Fig.1).

The shadow of the equatorial region passes through a GSS for the dates when the Sun is close to the vernal and autumnal equinoxes, so the GSS is passing into the shadow for the longest period - for about 70 minutes. The shadow of the Earth's polar regions passes through a satellite before and after the equinox, so the duration of its passing into the shadow shortens to several minutes.

The following two conditions must be met for a GSS entering the Earth's shadow:

$$|\delta_s - \delta_t| < \rho_s, \text{ и } |\alpha_s - \alpha_t| < r_t, \qquad (1)$$

with δ_s – the satellite declination , δ_t – the shadow axis declination, α_s, and α_t – the right ascension of the satellite and shadow axis correspondingly.

The length of the chord along which the satellite traversed the shadow is

$$r_t = \rho_s \sqrt{1 - \left(\frac{\delta_s - \delta_t}{\rho_s}\right)^2} \text{ [radians]}, \qquad (2)$$

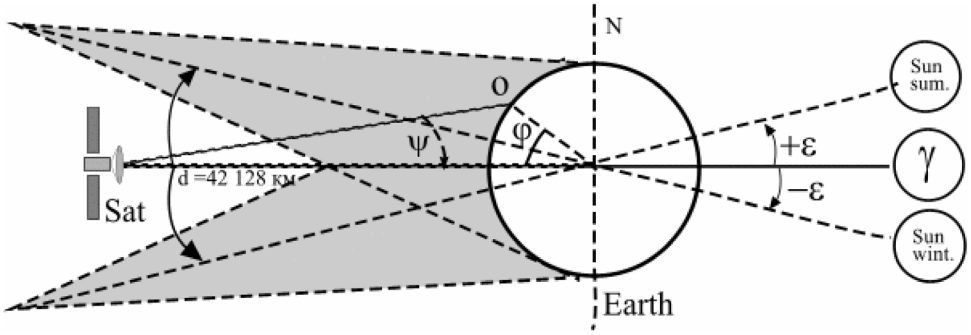

Figure 1. The Earth's shadow motion on the geostationary orbit during a year. The signs are described in the text below.

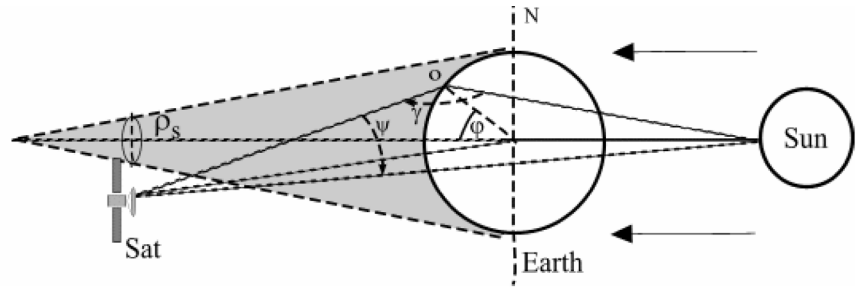

Fig. 2. The equatorial GSS location before its entering the Earth's shadow close to the equinox.

with $\delta_t = -\delta_\odot$, $\alpha_t = \alpha_\odot - 12^h$, ρ_s – the shadow cone diameter, $\rho_S = \dfrac{R_\oplus + d\cos\gamma tg\vartheta}{d\cos\gamma} = 08°25' = 6235.6$ [km], where $d = 42\,128$ km – the geostationary orbit radius, ϑ – the angle between the shadow axis and its generatrix for the cone-shaped shadow ($tg\vartheta = R_s/R_{SE}$, $R_s = R_\odot - R_\oplus = 696000$ km; $R_\odot$ – the Sun's radius, $R_\oplus$ – the Earth's radius, $R_{SE} = 1.49597\cdot10^8$ km – the Earth-Sun average distance), $\cos\gamma = (\mathbf{u}_\odot \cdot \mathbf{u}_s)$, γ – the Sun-satellite-observer angle, with $\mathbf{u}_\odot$ and $\mathbf{u}_s$ – unit vectors in corresponding directions, $\mathbf{u}_\odot = [\cos\alpha_\odot\cos\delta_\odot, \sin\alpha_\odot\cos\delta_\odot, \sin\delta_\odot]$, $\mathbf{u}_s = [\cos\alpha_s\cos\delta_s, \sin\alpha_s\cos\delta_s, \sin\delta_s]$.

The curves for the variation of duration of the GSS passing into the Earth's shadow and the phase angle variation on entering the shadow for different dates close to the autumnal equinox are defined with formula (2) and shown on the Fig. 3 and Fig. 4.

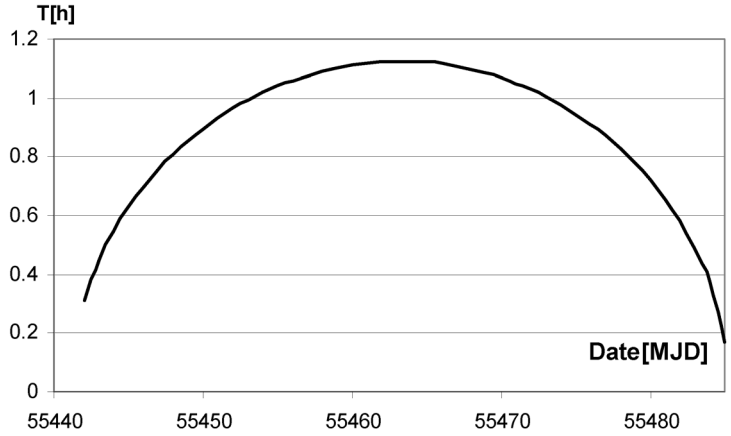

Fig.3. The duration of the GSS passing into the shadow. The X-axis shows the modified Julian date. The entering starts on 02.09.2010 = 55442[MJD], the maxima corresponds to 23.09.2010.The last date of entering the shadow is 16.10.2010.

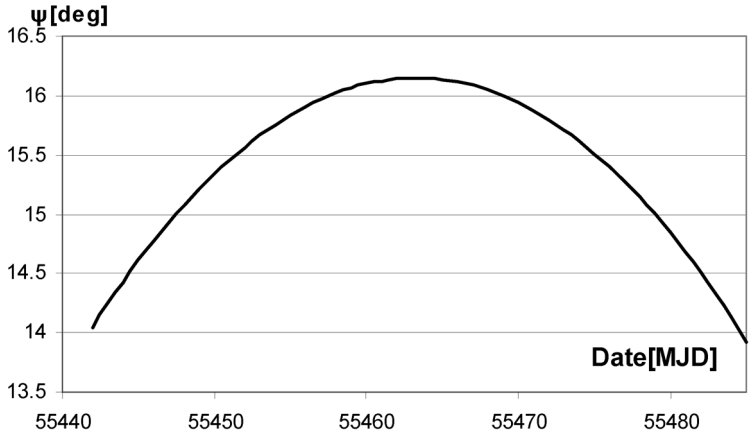

Fig. 4. The phase angle ψ variation on entering the shadow for different dates.

The calculations are made for the geostationary coordinate system, the equatorial GSS declination is 0^0. The cone-shaped Earth's shadow is assumed as a basis. For other shadow shape that heeds the presence of penumbra, the blurriness of the umbra-penumbra boundary and refraction, the time of the GSS entry and exit from the Earth's shadow as well as the phase angles are to be slightly different from those given on the Fig.3 and Fig.4. And the actual observed boundary dates for the equatorial GSS entry and exit from the Earth's shadow are shifted relative to the equinox (the 23rd of September) to the 30th of August and the 23rd of October accordingly. The observer located on the equator is to observe the satellite entry the shadow at the same time as the observer not located on the equator.

However it must be noted that on carrying out observations it is impossible to register accurately either the moments of total immersion or the moment of the exit start from the shadow. Such limits in observations caused mainly by the optical characteristics of telescopes, the atmosphere properties and the light detector sensitivity.

References

1. Диденко А.В., Усольцева Л.А.: 2002, *Космические исследования в Казахстане*, Алматы, КазГосИНТИ, 355-373.
2. Диденко А.В., Усольцева Л.А.: 2005, *Первые Фесенковские чтения «Современная астрофизика: традиции и перспективы»*, Алматы, 2005, 75-76.
3. Багров А.В. *Диссертация на соискание ученой степени доктора физико-математических наук*: М., 44.
4. P.P. Sukhov, G.F. Karpenko: presented in this issue, 55.

OBSERVATIONS OF THE MUTUAL PHENOMENA OF THE GALILEAN MOONS IN 2009

N.Koshkin[1], E.Korobeynikova[1], L.Shakun[1], N.Dorokhov[1], D.L.Doan[2], T.N.Manh[2], T.N.Minh[2], S.Udovichenko[1], Y.Bondarenko[1], V.Kashuba[1], A.Klabukova[1]

[1] Astronomical Observatory of I.I.Mechnikov Odessa National University, Odessa, Ukraine
[2] Astronomical Observatory of Vietnam National University, Hanoi, Vietnam

ABSTRACT. The instrumental and ephemeris preparation for the photometric observations of the mutual phenomena in the system of planetary satellites was conducted within the PHEMU09 project. Several reliable light curves and more than two tens of preparatory photometric observations of various mutual phenomena in the Jovian system were obtained. The observation data were processed, and the moments of the greatest phases of the phenomena were defined. The difference of moments of the observed greatest phases of the phenomena and the ephemerides, computed by the theory of V. Lainey, is about 0.02÷0.5 minutes. To construct an improved theory of motion of the Jovian moons, the observations are to be used for the concluding processing in the IMCCE (Institute de Mécanique et de calcul des éphémérides, France) that coordinates the PHEMU09 campaign.

Introduction

The Galilean satellites (moons), known since 1610, induced numerous observations and theoretical researches. The motion of these quickly rotating moons is perturbed by the Sun, Jupiter's flattening, interaction between them, and also by the adjacent planet Saturn. The Galilean moons can be reckoned as a small model of the Solar system where weak gravitational and nongravitational effects, as well as problems related to resonances and not yet considered in other cases, are studied.

In 2009, the PHEMU09 campaign for observations of the mutual phenomena (eclipses and occultations) of the Galilean satellites was launched on the initiative of the IMCCE (Institute de Mécanique et de calcul des éphémérides, France, http://www.imcce.fr/phemu09/). These phenomena occur only once per six years when the Earth and the Sun cross the orbital planes of the Galilean moons, and are especially valuable for the astrometry of natural satellites system. Since the mentioned moons became a target of space missions, they have aroused keener practical interest. The studies, made by Pioneer, Voyager and then Galileo probes, advanced our knowledge of the Jovian system greatly. In 1968, to prepare the mentioned missions, a specific research was commenced, and photographic observations from the Earth were carried out using long-focus instruments. The above, together with the early photographic observations and photometric observations of eclipses by the planet, permitted to construct a theory of motion of the Galilean moons, describing their position to within 400 km (or 0.1" of geocentric arc). Unfortunately, those observations have some systematic errors, and therefore, it is extremely important to develop various types of observations on an up-to-date level of accuracy standards.

Large number of accurate observations, from the one hand, and a progress in mathematical formulation of dynamic model, from the other hand, are necessary to improve the theory of motion of the Galilean moons. Such a progress can be ensured by especially precise photometric observations of the mutual phenomena in the satellites system. In 1973 and 1979 some data of observations of those phenomena were obtained, and that made possible to estimate their potentials. In 1985, 1991, 1997 and 2003, several international campaigns of coordinated observations took place. In 2009 ephemerides of more than 50 phenomena were computed for different locations [3].

Mutual phenomena can occur when the orbits of the Galilean moons are visible edgewise, and when in so doing the Sun passes through their orbital planes. Practically, it means that two moons are aligned with the Sun or the Earth, and that causes either a mutual eclipse or a mutual occultation. As it can be seen by a terrestrial observer, in the first case, a satellite enters the shadow produced by another satellite; in the second case, a satellite passes behind another satellite. When a mutual occultation occurs, it is possible to observe the approaching of the involved satellites when two images merge into one spot. The brightness is to reduce rapidly, reach the minimum and return to its initial value as the satellites part again. Throughout a mutual eclipse, only a decrease in the satellite brightness is observed, and in so doing the involved satellites can be observed separately.

The duration of such brightness variations is from several minutes to one hour or longer. The amplitude of variations depends on the relative positions of the satellites and on their radii; partial, annular or total phenomena can be observed.

The observation of brightness variations provides extensive information. The shape of the light curve and the moment of brightness minimum that conforms to the minimum distance between the satellites are the most valuable data for astrometry. Those moments are pre-computed by the theory and depend on relative positions and shapes of those gravitating bodies. The difference between the predicted and the observed moments is used to correct the theoretical model of the system of natural satellites [6].

Types and methods of observation of the Galilean moons

Observations of positions of the satellites. The photographic observations of the Galilean moons started in 1880-1890. Only short-focus refractors were used at that time. During 1920-1930, the abstract researches on the theory of motion of the Galilean moons, as well as their observations, were interrupted as it seemed very hard to improve the ephemerides. However, when electronic calculators appeared in 1960s, the study of the dynamics of the Galilean moons recommenced. The photographic observations were carried out all over again, but this time with long-focus telescopes and better photographic emulsions.

The appearance of CCD detectors with the improved sensitivity, comparing to emulsions, made the photographic plates useless. The only problem was the small size of CCD detectors, providing too small field of view. But that was solved when new star catalogues appeared, making possible to calibrate any field, even a very small one. Such calibration allows of using of any instrument, so there is no more requirement of either the field of view of high quality or the stability of the sky during the nighttime. The excessive brightness of the Galilean moons, complicating the simultaneous presence of satellites and comparison stars in a frame, still remains the only problem for their observation.

The resultant accuracy of the measured positions of the Jovian satellites for different types of observations is shown in Table 1. It is obvious that the photometry of mutual phenomena yields the best results in determining the geocentric position of the satellites with a minimum error, even under the city sky conditions.

Time scale for the observations. Since the observations are carried out to be used in the dynamic models of motion directly, all data should be referred to a certain time scale to link all observations together. Note, for example, the moon Io has an orbital velocity of 17.2 km/s; thus, an error of 0.1 second of time corresponds to an error of about 17.2 km/s in space. As the intrinsic accuracy of the theory of motion of the satellites is about one kilometer, it is evident that a timing accuracy better than 0.1 second is necessary. That means that each photometric measurement compiling a light curve should be dated in the UTC time scale with an error less than 0.1 second.

As a rule, the ephemerides of phenomena in the Solar system are computed in the Terrestrial Time (TT) scale. The most stable time standard is the International Atomic Time (TAI); the Terrestrial Time is offset from TAI by a constant value: TT=TAI+32.184 s. The Universal Time Coordinated (UTC) scale, which we use every day, has been adjusted relative to TAI and TT constantly, but irregularly. Since 1972, such an adjustment has been realizing by inserting a leap second on either December 31st or June 30th of another year. Therefore, UTS is a discontinuous time scale. The correlation between TAI, TT and UTC is shown in Fig.1. It is evident that UTS is offset from TT by more than one minute of time in 2009 (TT-UTC=66.184 s). The last positive leap second was added on December 31st, 2008, and the difference between TAI and UTC as per now is 34 seconds (http://hpiers.obspm.fr/eop-pc/). Since the observations are generally planned and dated in the UTC scale, it is indispensable to take into account the scale difference indicated above.

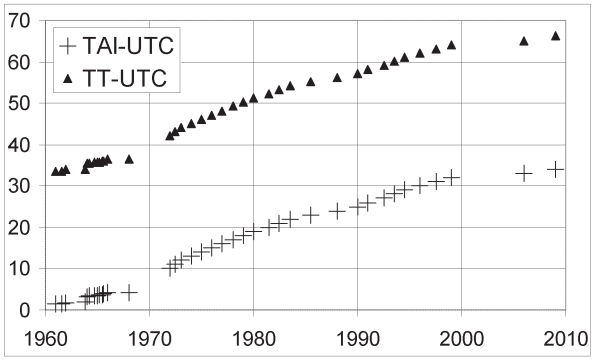

Figure 1. The difference of the null points of the TAI, TT and UTC time scales in seconds.

Photometry of the satellites with a CCD detector. The photometry with a CCD detector is efficient even for the phenomena very close to the planet. For the mentioned phenomena, to reduce the light of Jupiter, it is possible to use interference filters, such as CH4. By using a small telescope, it is possible to observe without any filter in the wavelength of the detector's sensitivity in order to gather more light. The spectral band with less light pollution is preferable for the observations carried out in a city polluted with light.

Table 1. Astrometric accuracy of observations of the Galilean satellites [2, 4]

Observations	Type	Telescope		Individual geocentric error	
				(")	km
Astrograph	Photographic	f=3,4 m	d<40 cm	0,190	760
Eclipses	Photoelectric photometry		d<60 cm	0,150	600
Mutual phenomena	Visual (medium quality sky)		d<40 cm	0,055	220
Astrograph	Photographic digital	f=10 m	d<60 cm	0,040	160
Mutual phenomena	Digital image (city sky)	f=20 m	d=1 m	0,015	60
Mutual phenomena	CCD photometry (city sky)		d=40 cm	0,012	48
Mutual phenomena	CCD photometry (high quality sky)		d=1 m	0,002	8

The Galilean moons are very bright and can saturate the detector. To avoid over-exposure of the image, it is necessary to decrease the telescope aperture or to use neutral density filters. To increase the number of illuminated pixels of the detector, it is possible also to defocus the image slightly.

The solar-type stars can be used for calibration. But usually, it is a satellite not involved in the phenomenon that is used as a photometric reference. It is necessary to measure the luminous flux emitted by the satellites before and after the phenomenon.

The photometric calibration. To eliminate the problem of non-uniform quantum yield for different pixels, it is necessary to have a map of the detector's sensitivity. To do that, it needs to illuminate the CCD with calibrated light; then, to divide each pixel of the image by the respective flat-filed (FF) image pixel and to multiply by its mean value. Usually, to make the above, the sky image $\mathbf{I}_{FF}(x,y)$ (several images would be better) should be obtained in the twilight at an altitude of 45^o at antisolar azimuth so that the average brightness corresponds to the middle of the detector's dynamic range. Further, the dark image should be obtained for the same temperature and time of accumulation $\mathbf{I}_{tt}(x,y)$. The accounting of the flat filed (FF) and spurious counts for the image $\mathbf{I}(x,y)$ is the following:

$$\mathbf{I}^*(x,y) = (\mathbf{I}(x,y) - \mathbf{I}_{tt}(x,y)) \times \mathbf{I}_{FF\ average} / \mathbf{I}_{FF}(x,y)$$

Calculation of the luminous flux emitted by the object. It is necessary to properly take into account the brightness of the sky background. If the local background near the satellite is homogeneous (for example, when the satellite is far from Jupiter), it takes only to calculate the sum of counts of pixels, located within the window centered on satellite Sat1 (the window can be either square or round). Let us denote the mentioned sum as S1 and the number of pixels within the window as N1. The same calculation is made for the bigger window. We are to get new values S2 and N2 respectively. Then, the sky background is Fon = (S2 - S1) / (N2 - N1), and the averaged flux emitted by the satellite is F = S1/N1 – Fon.

We use a comparison object for the relative photometry. If comparison object Sat2 is in the filed of the CCD camera, we can calculate its average flux F2 for each image using the same method. Then, the relative luminous flux emitted by the eclipsed or the occulted satellite Sat1 is FR = (F/F2) * FM2, where FM2 – the time-averaged flux emitted by comparison object Sat2. Such methods enable to observe mutual phenomena under difficult conditions: by closeness of Jupiter (the background by two satellites can be quite different), with variations of the sky transparency or passage of light clouds (in the process F/F2 is still constant), by observation in the twilight (the sky background changes considerably, but it is subtracted from each image).

The observations carried out using CCD television camera are processed by the similar scheme. But even stable observations, performed using such a camera and recorded on the computer, require the measurement reduction to be made. The problem is the detector's strong nonlinearity. It should be taken into account by building a calibration function with solar-type stars. Then, that function is used for the brightness reduction to restore the true light curve of the phenomenon with actual drop of the apparent magnitude.

Observations of mutual phenomena in 2009

In 2009, in Odessa, 49 various mutual phenomena of the Galilean moons in the Jovian system could be observed from May 7^{th} to December 25^{th} under conditions when the Sun was not less than 5^0 below the horizon (the twilight), and Jupiter was 10^0 above the horizon at the moment of phenomenon occurrence. The fragment of the phenomena ephemerides for the dates of observations carried out in Odessa is given in Table 2.

Table 2. Ephemerides (TT) and conditions of observations of the mutual phenomena in the Jovian satellites system in 2009.

Year	Month	Day	Hour	Minute	Second	Phenomena	Flux drop	Duration, s	Distance to Jupiter, RJ	Impact factor	RA, h	m	sec	Declination, degrees	'	"	Azimuth, degrees	Altitude, degrees	The Sun's altitude, degrees
2009	8	15	23	54	9	1 ECL 3	0,282	359	5,5	0,556	21	38	32,8	-15	13	51,9	149,3	22,9	-24,6
2009	8	17	21	17	9	1 ECL 2	0,525	601	5,7	0,384	21	37	35	-15	18	51,1	188,7	27,8	-29,6
2009	8	17	21	5	53	1 OCC 2	0,42	762	5,8	0,109	21	37	35,2	-15	18	49,8	191,7	27,4	-29,1
2009	8	24	23	32	43	1 OCC 2	0,425	947	5,7	0,003	21	34	0,41	-15	36	59,7	145	20,8	-29
2009	8	25	0	15	49	1 ECL 2	0,468	831	5,3	0,429	21	33	59,5	-15	37	4,1	135,3	16,1	-25,1
2009	9	1	21	5	16	1 ECL 2	0,349	460	6,3	0,516	21	30	14,7	-15	55	32,4	173,9	27,4	-34,3
2009	9	1	20	3	22	1 OCC 2	0,192	713	5,9	0,573	21	30	15,9	-15	55	26,7	190,6	27	-29,9
2009	9	8	23	44	2	1 ECL 2	0,561	449	6,5	0,344	21	27	11,2	-16	10	10	128,4	11,2	-32,8
2009	9	8	22	27	33	1 OCC 2	0,195	599	5,9	0,562	21	27	12,5	-16	10	4	145,1	20,3	-37,6
2009	11	16	15	14	29	2 OCC 1	0,426	234	2,6	0,015	21	27	20,6	-16	2	51,3	187,2	27,2	-9

Table 3. List of observations of the mutual phenomena in the Jovian satellites system obtained in Odessa in 2009.

Year	Date	Time of phenomena	Observation sites (points)	Observer
2009	August 15th	23h54m UTC	p. Mayaki	S. N. Udovichenko
2009	August 17th	21h06m UTC	p. Odessa	N. I. Koshkin
2009	August 17th	21h17m UTC	p. Odessa	N. I. Koshkin
2009	August 24th	23h32m UTC	p. Mayaki	S. N. Udovichenko
2009	August 25th	00h 16m UTC	p. Mayaki	A.V. Klabukova, V. Kashuba, Y. Bondarenko
2009	September 1st	20h03m UTC	p. Odessa	N.I. Koshkin, S.M. Melikyants, S.S. Terpan
2009	September 1st	21h05m UTC	p. Odessa	N.I. Koshkin, S.M. Melikyants, S.S. Terpan
2009	September 1st	21h05m UTC	p. Mayaki	A.V. Klabukova, I. Shepelenko
2009	September 8th	22h27m UTC	p. Mayaki	A.V. Klabukova, N.I. Dorokhov
2009	September 8th	23h44m UTC	p. Mayaki	A.V. Klabukova, N.I. Dorokhov, Y. Bondarenko
2009	November 16th	15h14m UTC	p. Odessa	N.I. Koshkin, S.M. Melikyants, S.S. Terpan

Altogether, 14 observations of phenomena in the Jovian satellites system were carried out at Odessa observatory in 2009 (Table 3).

Within this project, in addition, trial photometric observations were obtained with the participation of the authors with AZT-8 at the Hissar observatory at Sanglok Mountain on October 10th, 2009, from 7h56m33s to 18h03m09s (UT); in Hanoi, Vietnam on October 28th, 2009, from 22h06m06s to 23h02m27s (UT); and with 80-sm telescope of OAO at the Mechnikov ONU on Terskol peak.

Observation point in Odessa with KT-50. The observations were carried out with telescope KT-50 with video camera. The geodesic coordinates of the observation point are the following: the longitude 30.75565E; latitude 46.47780N; altitude 86 m; X=3781186, Y=2250073, Z=4602039 in WGS84 system. KT-50 is the Maksutov telescope with the primary mirror diameter of 0.5 m and the equivalent focus length of 1.50 m [1]. To reduce the luminous flux emitted by the satellites and by Jupiter itself, the entrance pupil is diaphragmed to 0.22 m. CCD television camera WAT-902H2 Sup with Sony detector operates in the TV standard of 25 frames per second (or interlaced 50 fields per second). The camera's filed of view with the indicated focal length is 25x20 arcminutes in the sky that scales to about 2" per a pixel for the frame of 768x576 pixels. The reference to the UTC time scale is provided by receiving of GPS signals by ACE III GPS module and then by entering the pulse-per-second output straight to the video frame. The accuracy of time reference should be of 0.1 ms. The observations were performed without any filters. Under operating conditions, a 12-bit digitized frame occupies a lot of disc space so that the frame recording rate is reduced to 6.25 frames per second for the same filed exposure time of 0.02 s for the long lasting (longer than 10 minutes) observations (in fact, one frame, composed of two fields, is recorded; then, three frames are skipped, etc.).

The results of the observation of the occultation and the subsequent eclipse of satellite J2 by satellite J1 occurred on August 17th, 2009, that was carried out in Odessa are presented in Fig. 2 and 4.

Figure 3 shows the brightness variation for satellite J3 that was observed simultaneously along with the phenomena and used as a comparison object for the photometry.

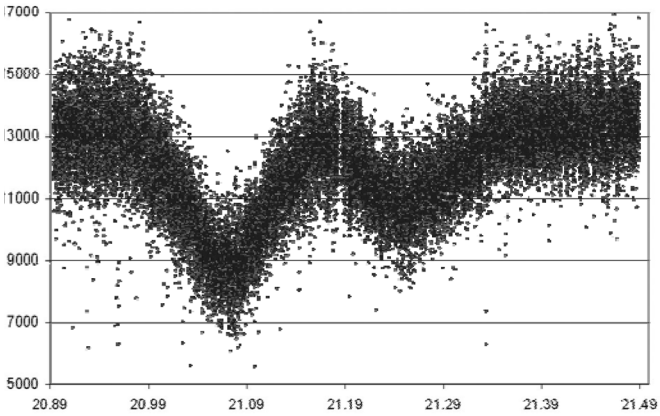

Figure 2. The light curve for the occultation and the eclipse of satellite J2 by satellite J1 on 17.08.2009. The X-axis shows time in hours (UTC). The Y-axis shows the total luminous flux emitted by two satellites in the instrumental scale.

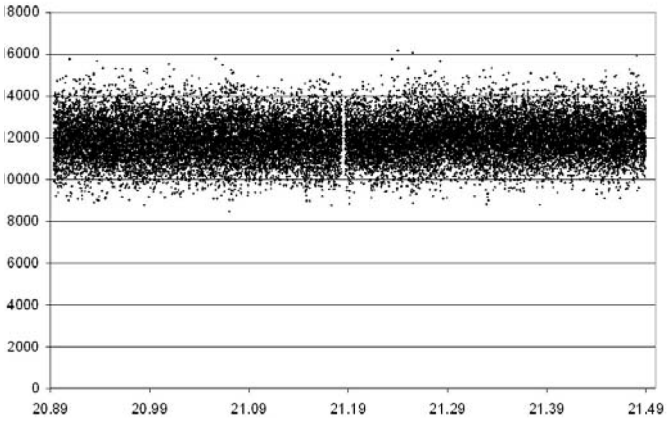

Figure 3. The light curve for comparison satellite J3 on 17.08.09. The axes are similar to Fig. 2.

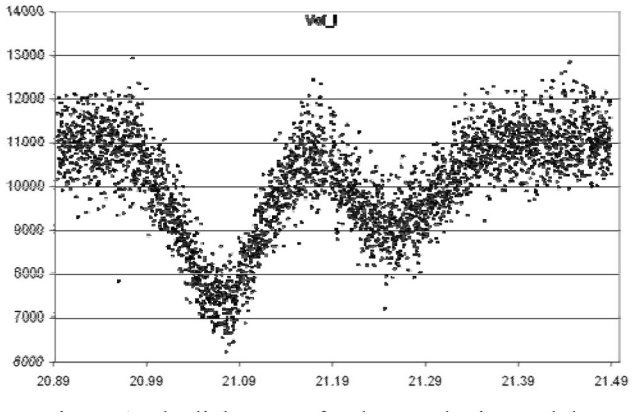

Figure 4. The light curve for the occultation and the eclipse of satellite J2 by satellite J1 on 17.08.09 on having the total luminous flux (J1+J2) pointwisely divided by flux J3 and averaged in eight counts.
The axes are similar to Fig.2.

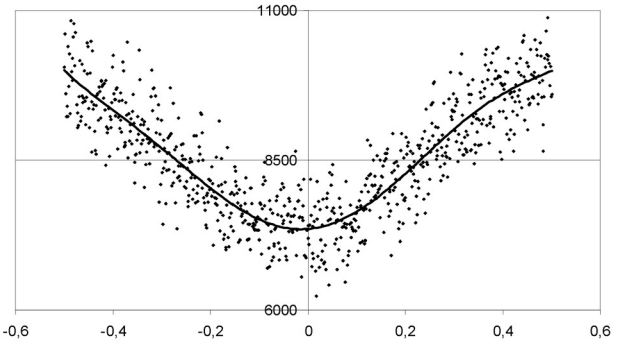

Figure 5. The part of the light curve corresponding to the maximum phase of the occultation on 17.80.2009.
The X-axis shows time normalized within the range of -0.5 – +0.5.
The curve shows the 6th degree polynomial approximation of the brightness variation.

The smoothing polynomial approximation of the light curve as it is shown in Fig. 5 for the occultation allows of determining of the moments of maximum phases of the phenomena observed:

- The occultation (J1 occ J2) 17.08.2009 at 21h04m14.5s ($21.^h07068$) ±0.5 s.
- The eclipse (J1 ecl J2) 17.08.2009 at 21h15m01.4s ($21.^h25038$) ±0.5 s.

The relative light curve as a result of the occultation observation (in instrumental scale) is shown in Fig. 6; the initial light curve for the eclipse of satellite J2 by satellite J1 that occurred an hour later is shown in Fig. 7. Both curves are compiled on September 1st, 2009, in Odessa.

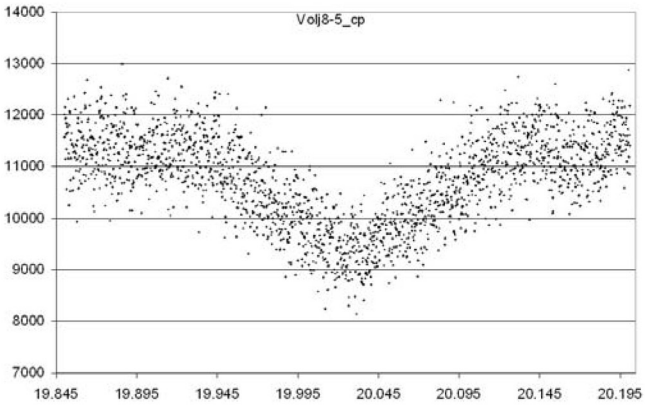

Figure 6. The relative light curve averaged in eight points for the occultation of satellite J2 by satellite J1 on 01.09.2009. The X-axis shows time in hours (UTC). The Y-axis shows the total luminous flux emitted by two satellites.

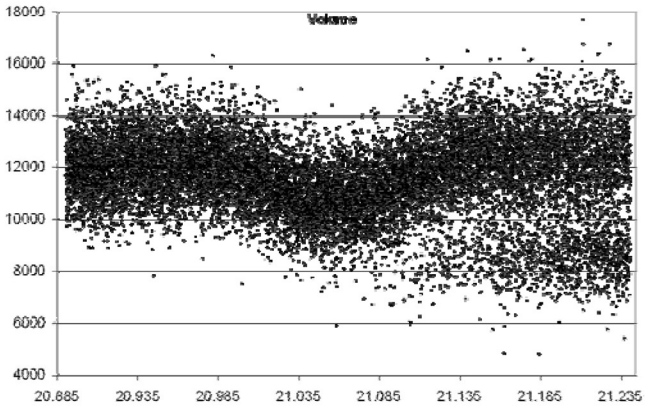

Figure 7. The light curve for the eclipse of satellite J2 by satellite J1 on 01.09.2009.
The axes are similar to Fig.6.

It should be noted that some part of the light curve is imperfect due to a wide dispersion of the points on the plot after the eclipse occurred on 01.09.2009. It can be caused by the phenomenon of eclipse itself, as well as by the processing method used. Since during this phenomenon the directions to satellites J1 and J2 are rather close at the beginning of the eclipse, their images merge into one spot in the frame, and then, by processing, they are automatically placed to the common diaphragm as a single object. But, as a result of the satellites moving away from each other with the lapse of time, their images periodically part and then merge again into one spot due to atmospheric distortions, so the program record them alternately as two objects at one moment, and as a single object at another. That leads to recurring loss of a portion of the total luminous flux and distorts the light curve for the eclipse.

The 6th degree polynomial approximation of two parts of the light curve corresponding to the minimum enables to obtain the following moments of the observed maximum phases:

Table 4. The theoretically predicted moments of the maximum phases for the gathered observations of the mutual phenomena and the respective values (O-C).

The moment of the maximum phase of the phenomenon	Theory of					
	V. Lainey V2.0|V1.1, 2004a, A&A, v. 420, p. 1171; 2004b, A&A, v. 427, p. 371.		J.-E. Arlot G-5. 1982, A&A, v.107, p.305.		D. Lieske E-5, 1998, A&AS, v.129, p.205.	
Occultation (J1 occ J2) 17.08.2009	21h04m13.5s	+ 1.0 s	21h04m48s	– 33.5 s	21h04m50s	– 35.5 s
Eclipse (J1 ecl J2) 17.08.2009	21h15m40s	– 38.5 s	21h16m00s	– 58.5 s	21h16m10s	– 68.5 s
Occultation (J1 occ J2) 01.09.2009	20h01m46s	+ 1.0 s	20h02m15s	– 28 s	20h02m22s	– 35 s
Eclipse (J1 ecl J2) 01.09.2009	21h03m40s	– 19 s	21h04m08s	– 47 s	21h04m14s	– 53 s

- The occultation (J1 occ J2) 01.09.2009 at 20h01m47.0s (20.^{h}02972) ±0.5 s.
- The eclipse (J1 ecl J2) 01.09.2009 at 21h03m20.7s (21.^{h}05574) ±0.5 s.

To preliminary define the observed moments, we compare them with the predictions of motion and approaching of the satellites, made on the basis of different theories presented in Table 4 (*http://lnfm1.sai.msu.ru/neb/nss/nssoc5hr.htm*).

The difference of moments predicted by different theories gives an idea of the characteristic value of inaccuracy that is inherent in modern theories of motion of the Galilean moons of Jupiter. The obtained discrepancy between the observed and the predicted moments is also from units to tens of seconds of time.

Observation point at Mayaki station (*46.39679°N, 30.27274°E., 27 m).* Telescope AZT-3 with the mirror diameter of 0.5 m is equipped with a classical astronomical CCD camera with optical photometer Sony ICX429ALL that operates in the charge storage mode with the following readout of the frame to the computer.

The light curve for the total brightness for the occultation of satellite J2 by satellite J1 on 24.08.2009 at 23.5h (UTC) is shown in Fig. 8.

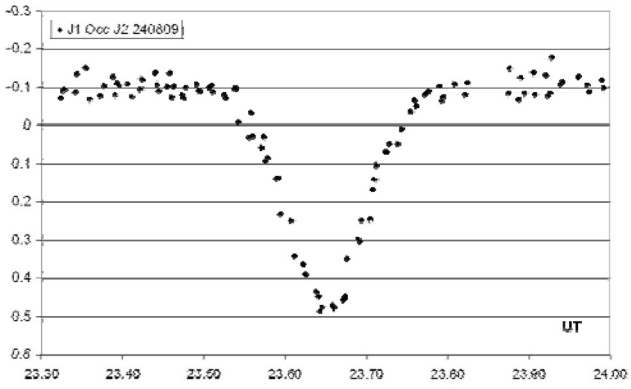

Figure 8. The light curve for the total brightness for the occultation of satellite J2 by satellite J1 on 24.08.2009. The brightness is in relative magnitude m(J1+ J2)–m(J3). The X-axis shows time in hours (UTC_hel).

The 4th degree polynomial approximation of the part of the light curve dated 24.08.2009 allows of determining of the moment of maximum phases of the phenomena observed:

24.08.2009 J1 occults J2 at 23h39m04.6s (23.^{h}65128) ±0.5 s (UTC heliocentric) or

J1 occults J2 at 23h30m49.5s (23.^{h}51376) ±0.5 s (UTC).

The prediction (by the theory of V. Lainey V2.0|V1.1) is 23h30m58.5s, and (O-C) = -9 s.

The observations of the mutual phenomena were conducted at Mayaki astronomical station using several telescopes simultaneously. In particular, with 60-sm telescope of Ricci-Chrétien type with CCD camera FLI IMG1001E, 1024x1024 pixels in 24 microns (the filed of view is 22'x22'):

2009-08-25 (J1 eclipses J2); observation start at Tstart = 0h05m42s and end at Tend = 0h28m35s. About 120 measurements are made with the time of exposure of 0.1 s and the time interval between observations dT of about 7 s.

2009-09-01 (J1 eclipses J2); observation start at Tstart = 20h58m54s and end at Tend = 21h15m22s. About 130 measurements are made with the time of exposure of 0.5 s and dT of about 7.5 s.

2009-09-08 (J1 occults and then eclipses J2); observation start at Tstart = 22h06m59s and end at Tend = 23h53m15s. About 344 measurements are made with the time interval dT of 7.2 s, but with different time of exposure: 0.3 s or 0.5 s.

At the same time, numerous image records of the Jovian satellites system were obtained and subsequently undergone the photometric processing using 40-sm telescope with a video camera.

The observations conducted with all three telescopes at Mayaki station are encumbered with a number of shortcomings. First of all, it applies to the lack of calibrated reference to the UTC time scale with a sufficient accuracy for some telescopes. The measurements made with a CCD camera in the television mode are not reduced to the magnitude scale. The closeness of bright Jupiter with a narrow field of view, poor operation of mount RC-60 and, as a sequence, nonhomogeneity and fluctuations of the sky background brightness impeded the photometry and

background brightness impeded the photometry and caused corruption of useful signal by a considerable noise. Nevertheless, those observations can be of use to analyze the fact of occurrence itself and the type of the observed phenomenon (appreciably less qualitative observations were processed during the previous campaign [5]).

Several examples of images of the Jovian satellites system obtained with CCD detectors of different telescopes to subsequently undergo the photometric processing are given in Fig. 9.

Mayaki, 40-cm, 09.09.2009

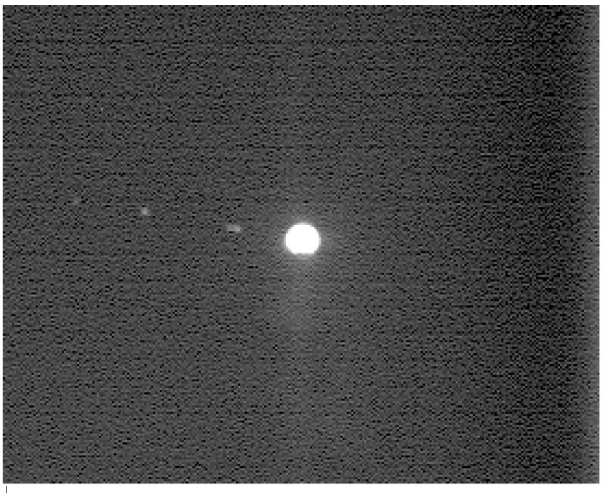

Mayaki, 60-cm, 08.09.2009

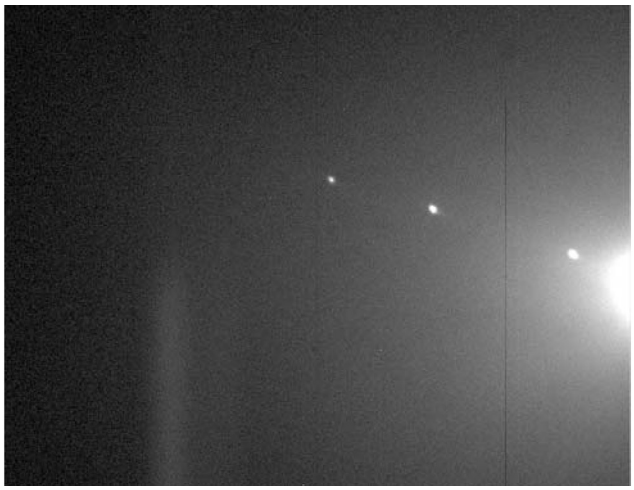

Gissar, 80-cm, 09.10.2009

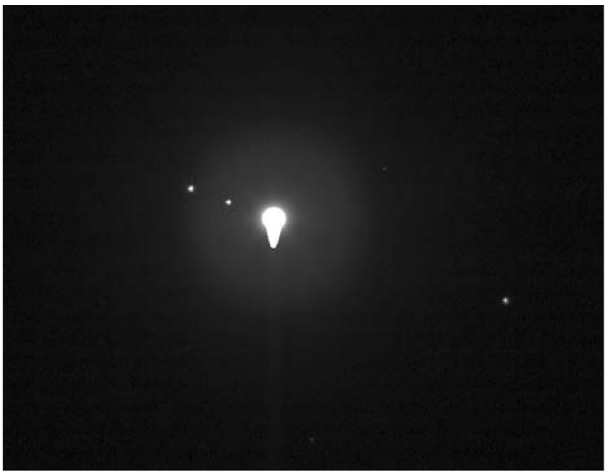

Hanoi, 30-cm, 29.10.2009

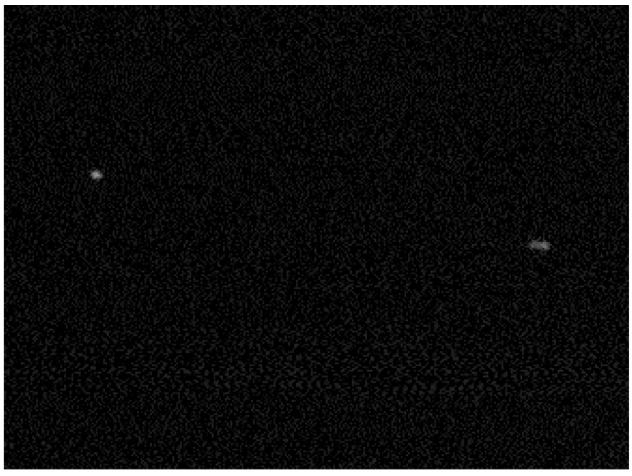

Figure 9. The examples of images of the Jovian satellites system obtained with CCD detectors of different telescopes.

Conclusion

The methodological, instrumental and ephemeris preparation for the photometric observations of the mutual phenomena in the system of the Jovian satellites was conducted at the Astronomical Observatory of the I. I. Mechnikov Odessa National University and at the Astronomical Observatory of Vietnam National University, Hanoi.

Five reliable light curves and more than twenty preliminary photometric observations of different mutual phenomena in the Jovian system were compiled.

The observation sites are the following: observatory in Odessa, observation station in Mayaki village, observatory in Hanoi (Vietnam), observatory on Terskol peak (Russia) and the Hissar observatory at Sanglok Mountain (Central Asia).

The observations were processed and the moments of the maximum phases of the phenomena were obtained.

The comparison of the moments of the maximum phases of the phenomena, obtained as a result of the observations, with the ephemerides computed by the theory of V. Lainey and other authors shows a significant discrepancy (of about 0.5-1 minute of time).

To construct an improved dynamical theory of motion of the Jovian moons, the results of the observations were submitted for the concluding processing to the IMCCE (Institute de Mécanique et de calcul des éphémérides, France) that coordinates the PHEMU09 campaign (*http://www.imcce.fr/phemu09*).

References

1. Бурлак Н., Драгомирецкий В., Кошкин Н., Рябов А., Шакун Л.: 2007, *Межд. конф. "Наблюдение околоземного космического пространства"*, Звенигород, Россия (http://lfvn.astronomer.ru/report/0000018/Od/index1.htm).
2. Arlot J.-E. *Presentation of the Galilean Satellites of Jupiter and of their mutual phenomena*, IMCCE/CNRS, Technical Note N **1**, 2008 (www.imcce.fr/fr/presentation/equipes/GAP/travaux/phemu09/note01-en.htm).
3. *Tables of predictions of the events of the Galilean satellites (2009-2010)*. (ftp://ftp.imcce.fr/pub/ephem/satel/phemu09;http://lnfm1.sai.msu.ru/neb/nss/nsso-c5hr.htm).
4. *French-chinese Spring School on Astrometry, occultations and Mutual events held in Beijing, China*, on April 7-11, 2008.
5. Arlot J.-E., W. Thuillot, T.N.Dorokhova, N.I.Dorokhov et al.: 2009, *A&A*, **493**, 1171–1182.
6. Emelyanov N.V.: 2009, *M.N.R.A.S.*, **394**, 1037-1044.

DETERMINATION OF THE ROTATION PARAMETERS OF REFERENCE ARTIFICIAL SATELLITE AJISAI AND SYNCHRONIZATION OF THE PHOTOMETRIC CHANNELS

N.I.Koshkin[1], E.A.Korobeinikova[1], S.L.Strakhova[1], L.S.Shakun[1], V.V.Lopachenko[2]

[1] Astronomical Observatory of I.I.Mechnikov Odessa National University, Odessa, Ukraine
[2] National Center of Control and Tests of Space Objects, SSAU, Evpatory, Ukraine

ABSTRACT. The aim of the present study is to obtain the adjusted current coordinates of the rotation pole of artificial satellite Ajisai and the up-to-date sidereal period of its rotation. To do that, the light curves obtained in Odessa during 2009-2010 are considered. Using both the Ajisai pole's coordinates and the reduced null point of the hardware-based time scale, has made it possible to improve the timing of the observed flashes of its brightness. By the accurate timing of the simultaneous photometric observations of Ajisai satellite the photometric channels synchronization at the stations in Odessa and Eupatoria is accomplished. The further photometric observations of that satellite are necessary to construct a theory of its rotation about the centre of mass; that will allow of its using as a reference source of the time-calibrated optical signals for any ground-based observatories.

Introduction

Japanese experimental geodetic artificial satellite Ajisai was launched in 1986 to the almost circular orbit at altitude about 1500 km with the inclination of 50^0 to the equator. The satellite is manufactured from fiberglass strengthened plastic; it is of the spherical shape with the diameter of 2.15 m; 318 reflecting flat mirrors and 120 laser retro-reflectors are placed on its outer surface [1] (see Fig.1) The mirrors are made of an aluminium alloy and, when reflecting the sunlight by the rotating satellites, they emit short light pulses the duration of which is relative to the rotational velocity. Initially, they were intended to control the orientation and variation of the rotational velocity of the satellite under the influence of cosmic factors. The laser retro-reflectors consist of prisms that, being irradiated by the terraneous laser pulse, reflect the light signal accurately backwards to the radar telescope. That enables to determine the precise distance to the artificial satellite.

Both types of the reflectors are almost uniformly distributed by the designers on the surface of the spherical satellite. It was attained by the placement of the flat mirrors and retro-reflectors in 15 latitudinal rows (rings). The planes of the mirrors additionally inclined with different angles to the mean latitude of the given ring. As a result, the normals to the mirrors are rather evenly distributed in space (like the hedgehog's prickles) and, when the satellite is spinning around its axis, there are always some of them that can reflect the light towards the observer.

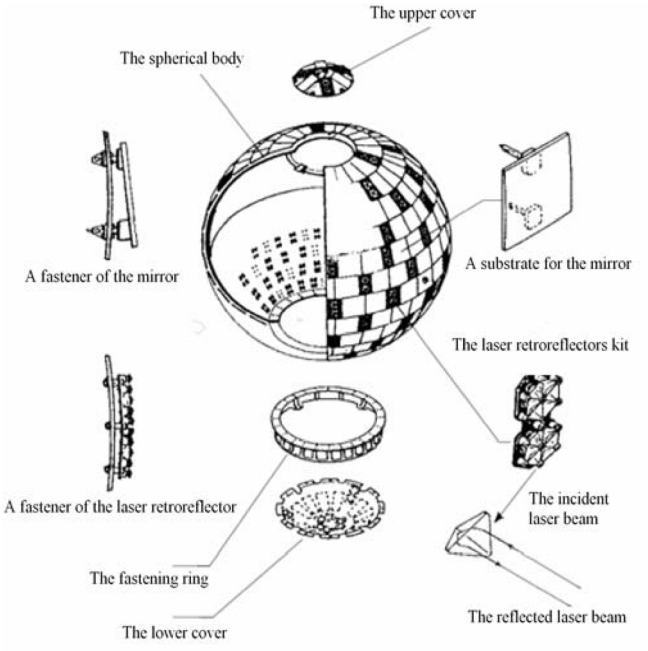

Figure 1. The design of Ajisai satellite [1].

When launching into the orbit, Ajisai artificial satellite was spun with the velocity 40 revolutions per minute around the axis parallel to the Earth rotation axis. And the satellite rotation axis coincides with the symmetry axes of the rings at that. The regular observations of Japanese researchers showed that after the launch the spin velocity of the satellite monotonously decreased from 0.67 Hz (revolutions per second) at the launch to 0.57 Hz in 1988, i.e. 12 years later. According to the results of the high-frequency laser measurements [2], it was determined that the rotation axis in the Ajisai's body is deflected from the symmetry axis by 5.5°.

Objectives of the work

Our goal is to specify more precise the position of the rotation axis of artificial satellite Ajisai in space, and then to use it as the standard source of the optical pulses. When being observed, the satellite demonstrates numerous momentary flashes of brightness with the period of reiteration of the flashes series of about 2.02 sec (i.e. the rotational velocity was already 0.495 Hz in 2010). The light curve is regular during the time span of about several seconds only, and then it is rapidly transformed. It is explained by the fact that when the satellite is moving along the orbit, and a terrestrial observer is tracking it, the local area of the specular reflection is quickly moving on the spherical surface, and its latitude is also altered relative to the rotation axis inside the satellite's body. The set of mirrors reflecting the light towards the observer take turns at each spin of Ajisai at that. (The local area, for which the normals form a small angle with the phase angle bisector – of the order of the angular dimensions of the source of light – is called a "plash of sunlight" on the specular surface; the phase angle is the plane angle between the directions from the satellite towards the Sun and the observer).

Taking into account that the observer is located not in the centre of Earth and relative to that the angular velocity of the artificial satellite in the sky is very uneven, the visible rotation of the satellite turns to be also non constant. That is the result of the parallactic change of the direction towards the satellite and the composition of the angular velocities of the artificial satellite and its orbital movement. That unevenness is slightly contributed by the Earth's rotation along with the observer. When registering the periodicity of the reiteration of the flashes of brightness, the observer can measure only the synodic period of the rotation of Ajisai. The sidereal period of rotation (the period of spinning of the body relative to the inertial coordinate system) can be computed only if the precise orientation of the rotation axis of the satellite in space is known.

When observing the series of the momentary flashes of brightness, the inverse problem can be solved, i.e. it is possible to determine the true spatial orientation of the Ajisai rotation axis and the value of the sidereal period of its rotation.

The duration of the optical flash is determined by the angular dimensions of the light source; in the present case – the Sun; and it does not depend on the dimensions of the mirror. The smooth plane mirror of Ajisai, spinning with the period $P \approx 2$ sec, emits a flash with the minimum duration of $\Delta t = d/360^\circ \cdot P/2 \approx 0.0014$ sec, where d – the angular diameter of the Sun. But if the mirror is a bit rough (matt), then the brightness, shape and duration of the flare will depend on the width of the indicatrix of light reflection by such a "mirror" and on the minimum angle between the normal to it and the vector-bisectrix of the phase angle.

The determination of the polar orientation and the sidereal period of rotation

When considering the specular reflection of the light by the elements of the satellite surface, we will constantly use such terms as "the phase angle bisector" and "normal" to the reflecting area. In consequence of the satellite movement along the orbit, the direction "satellite-observer" is regularly altered, thus, as well as the vector-bisectrix of the phase angle. At the same time, as a result of the satellite rotation around the centre of mass, the normals to the plane mirrors form cones in space, and their traces on the celestial sphere describe concentric small circles. When at any moment the normal approaches to the phase angle bisector (or, vice versa) by the angle less than the width of the specular indicatrix of the plane mirror, then we will observe the "specular" increase of the artificial satellite brightness – a flash of brightness. Such picture is observed also when the specular reflection of the light by the conical or other developable surface of the satellite occurs.

The rotation pole. When the artificial satellite is passing above the observation point, the phase angle bisector forms a certain variable angle $\rho \approx \pi/2 - \delta_B$ with the rotation axis of Ajisai as its rotation axis in space is close to the Pole. Therefore, the declination of bisector δ_B (in the equatorial coordinate system) defines the angle between the rotation axis and the bisector. And the flashes of the specular reflection are produced by those mirrors, which are mounted on the satellite close to the latitude of $\pi/2 - \rho$ at that. The quantity of the mirrors that are to produce the flashes of brightness per one rotation, the intervals and the brightness magnitude of those flashes depend on their distribution on that ring and on the actual positions of their normals. If the angle between the rotation axis and the bisector is to achieve the same value twice per passing of Ajisai, then, at those moments, the similar series of the flashes per that period are to be observed. On having assumed that the satellite rotation axis has not altered appreciably its position. That fact permits to determine the actual orientation of the Ajisai rotation axis in space by considering the corresponding pairs of segments of the light curve.

The course of changes of the declination of the phase angle bisector (in radians) are shown on the left of Fig. 2; two segments of the light curve close to moments t_1 and t_2, when the bisector declination took the identical values, are shown on the right of Fig. 2. The light curve was obtained 09.06.2010 in Odessa with telescope KT-50 with the time resolution of 0.02 sec [4]. The appearance of the two light curve segments in this case is different! However, the segment of the light curve *next* to the second one of the above mentioned pair (with the time lag of ~ +11 sec) almost duplicates the series of flashes on the first segment (see Fig. 3). That means that actually the light rotation pole does not coincide exactly with the celestial pole.

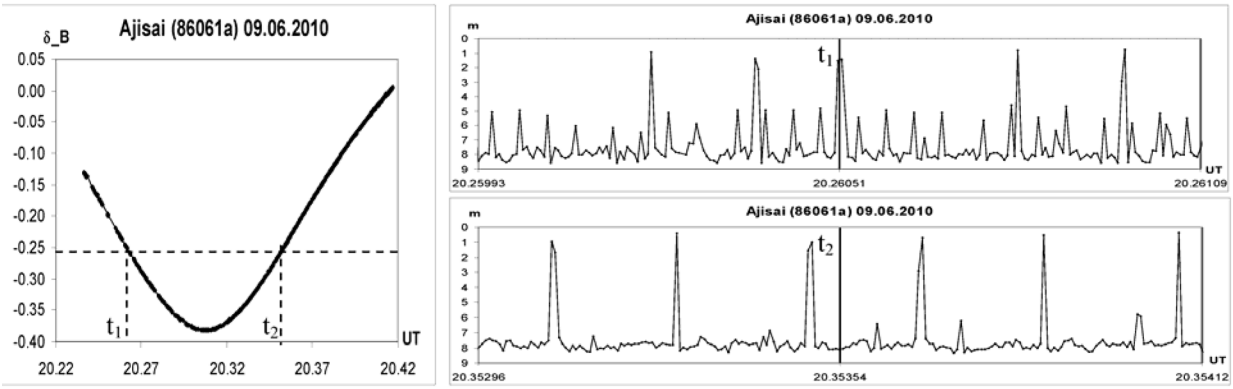

Figure 2. Changes of the declination of the phase angle bisector (on the left) and two segments of the Ajisai light curve close to moments t_1 and t_2 (on the right).

Let us name the pairs of mean time points close to which a series of flashes is repeated, and their associated bisector vectors as "conjugated". Two more pairs of segments of the light curve on 09.06.2010 where the series of flashes is also repeated in pairs are shown in Fig. 4 (a, b). It should be noticed that there are some gaps and other photometric defects on the light curve; that is why the repetition of the segment of the light curve within the interval of two revolutions is achieved only "in whole".

The difference of the values of the bisector actual declination during two "conjugated" moments defines the deflection of the Ajisai rotation axis from the Pole. The analysis of those observation data allows of making more precise the true position of the Ajisai rotation axis within the indicated time span.

Fig. 5 graphically demonstrates more precise definition of the rotation pole position using the positions of three pairs of the "conjugated" phase angle bisectors.

To determine the rotation pole, it is necessary to find the pole of the small circle. It can be computed if there are at least *three* points, lying on that circle, available; or it is possible to use *two* points, lying on the small circle, and *two* more points, lying on the second small circle that is concentric to the first one. Let a point on the sphere is actually the unit vector r(x, y, z). Let us consider the pairs of differences of the corresponding coordinates and to introduce the following designations:

$$a_x \equiv \Delta y_1 \cdot \Delta z_2 - \Delta y_2 \cdot \Delta z_1,$$
$$a_y \equiv \Delta z_1 \cdot \Delta x_2 - \Delta z_2 \cdot \Delta x_1,$$
$$a_z \equiv \Delta x_1 \cdot \Delta y_2 - \Delta x_2 \cdot \Delta y_1,$$
$$D \equiv a_x^2 + a_y^2 + a_z^2,$$

where indexes 1 and 2 correspond to different independent pairs of points, lying on the same circle. Then the pole's direction cosines are equal to:

$$x = a_x/D,\ y = a_y/D,\ z = a_z/D.$$

The radius of the small circle ρ is determined from the equality: $\cos \rho_i = x \cdot x_i = y \cdot y_i = z \cdot z_i$.

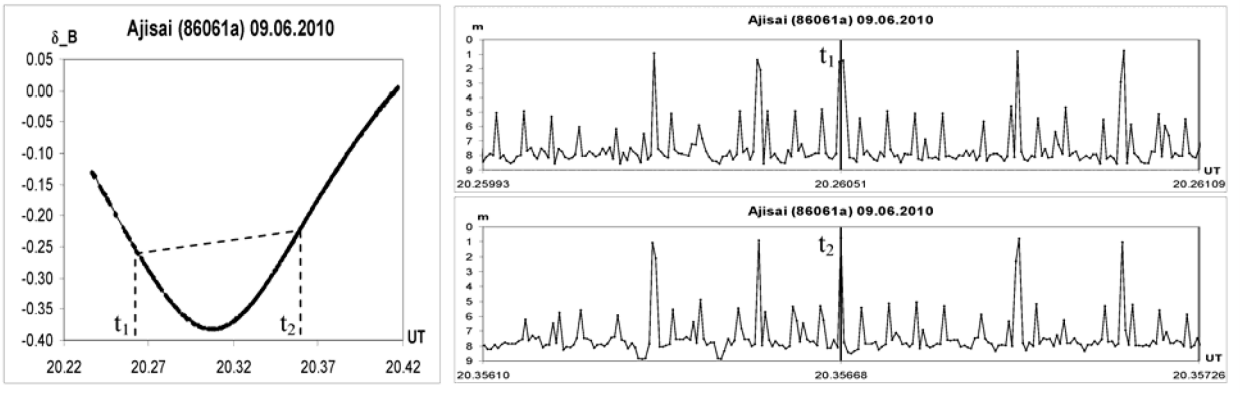

Figure 3. The same as in Fig. 2 but for another moment t_2.

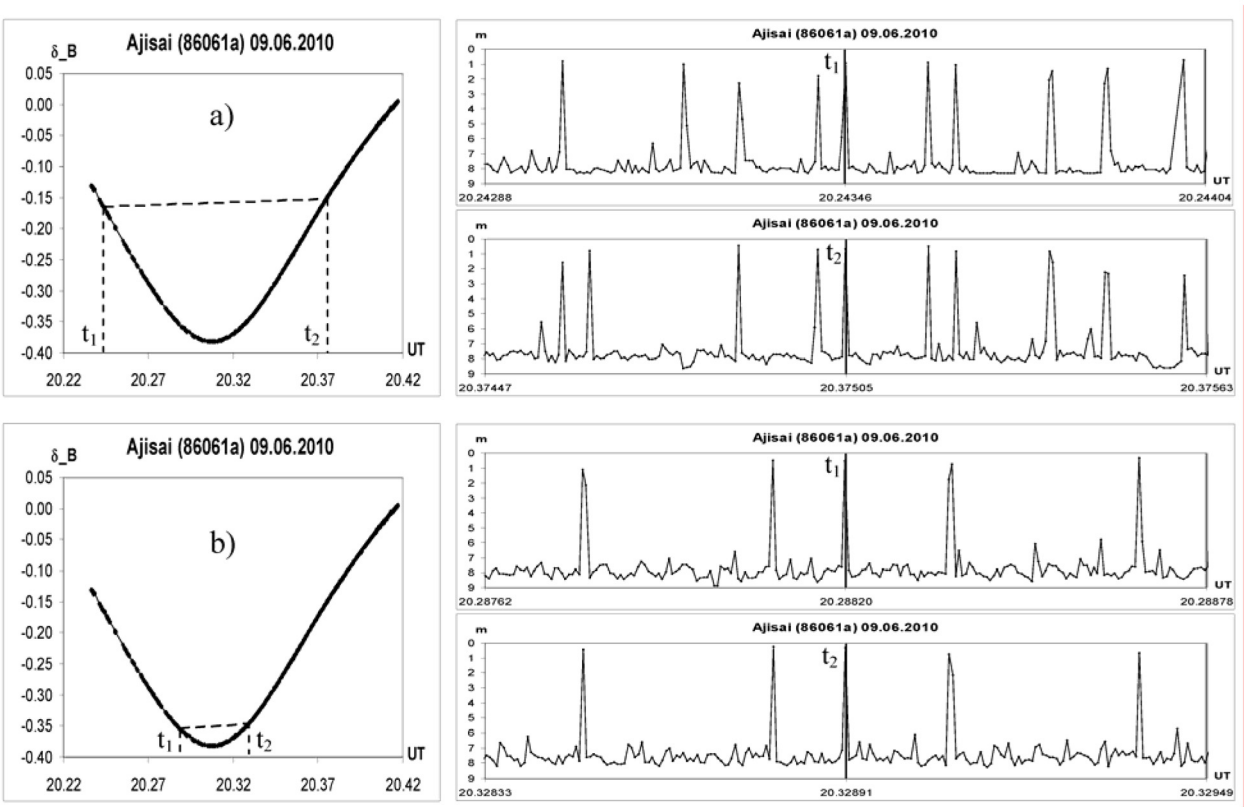

Figure 4. The same as in Fig. 2 but for two other pairs of moments t1 and t2 (their choice is shown on the links).

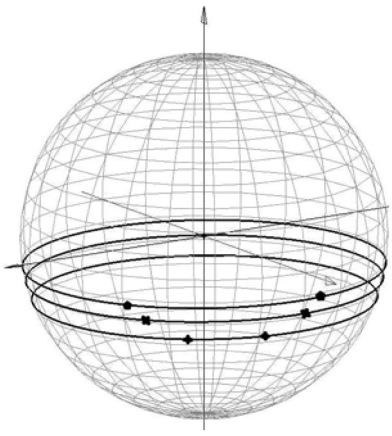

Figure 5. The positions of three pairs of the "conjugated" phase angle bisectors for the Ajisai passing above Odessa (on the base of observations on September 08, 2009).

The comparison of the segments of the Ajisai light curve, analogous to the above indicated, was made for three more dates – 08.09.2009, 16.09.2009 and 21.09.2009. The coordinates (the right ascension and the declination) of the bisectors for the data of artificial satellite Ajisai passings at the middle of intervals where the type of the light curve is repeated on the local segment, as well as the corresponding orientation of the rotation axis (α_{pole}, δ_{pole}) and the true polar distance of the reflecting normals (ρ_{pole}) are presented in Table 1.

The preliminary analysis of the obtained results permit to draw a conclusion on the slow precession of the Ajisai rotation axis near the celestial pole (the deviation is 1÷2°). With the data available, it is possible to assume the clockwise precession direction with the period of about one year.

The rotation period. When the position of the artificial satellite rotation pole in space is known, the possibility to compute the sidereal period of its rotation appears. As it was already mentioned above, only the synodic (observed) period, that depends on the direction and the angular velocity of the satellite's move, can be determined from the observations. As a result of that movement, the coordinates of the bisector of the phase angle change in the lapse of time according to some law. Let us to resolve the angular velocity of the bisector movement into two components – along the artificial satellite rotation axis and along the axis perpendicular to that one. Hence, the first component of the bisector angular velocity will be added to the angular velocity of its rotation. That allows of directly taking into account the movement of the artificial satellite along its orbit when the sidereal period of rotation is computed. The second component of the angular orbital movement, that equal to the rate of change of the angle between the rotation axis and the bisector, will determine the rate of transformation of the kind of the satellite light curve. For Ajisai such change cause the latitudinal shift of the "plash of sunlight" of the specular reflection and change of the mirrors reflecting the light towards the observer and contribute to the total light curve.

Table 1. The bisector positions for the pairs of the "conjugated" moments and the corresponding coordinates of the rotation axis of artificial satellite Ajisai (in degrees).

t_1	α_b	δ_b	t_2	α_b	δ_b	α_{pole}	δ_{pole}	ρ_{pole}
08.09.2009								
19.71249708	151.78	-13.35	19.81522774	191.71	-14.73	254.97	88.0	103.82
19.72628634	158.59	-15.64	19.79048817	185.07	-16.56	254.97	88.0	105.94
19.74561467	167.88	-17.53	19.76428741	176.30	-17.76	254.97	88.0	107.43
16.09.2009								
20.59230258	147.52	-30.68	20.62497658	166.53	-31.32	253.82	88.0	121.18
20.60111395	151.87	-31.45	20.61861935	162.53	-31.76	253.82	88.0	121.75
21.09.2009								
18.08324636	128.85	-31.43	18.15210336	167.80	-32.74	253.82	88.0	122.61
18.09675229	135.48	-34.13	18.13934789	159.93	-34.94	253.82	88.0	125.08
09.06.2010								
20.24345260	31.40	-9.43	20.37504481	96.58	-8.68	338.05	89.3	99.06
20.25279180	34.49	-11.92	20.36549450	93.73	-11.11			
20.26050600	37.39	-14.08	20.35668300	90.62	-13.40	338.05	89.3	103.79
20.26684650	40.08	-15.67	20.35003800	87.90	-15.12			
20.28819800	51.15	-20.27	20.32891000	77.08	-19.88	338.05	89.3	110.15

The synodic period between two specular flashes produced by the same mirror is $P_{syn} = (t_2-t_1)/2\pi \cdot n$. If the rotation pole is known, then the sidereal period P_{sid} can be determined by the formula: $P_{sid} = (t_2-t_1)/(2\pi n \pm \Delta\alpha')$, where t_1 and t_2 – the recorded moments of the maximum brightness; n – the number of complete revolutions of the artificial satellite relative the fixed coordinate system during the time span t_2-t_1; $\Delta\alpha'$ – the angle between two projections of normal's vectors on the plane perpendicular to the rotation axis.

If **r**(x, y, z) is a vector that defines the normal' position in the equatorial coordinate system, and α_Ω, δ_Ω are coordinates of the rotation pole in that coordinate system, then the conversion of the normal' vector to the coordinate system, related to the rotation axis, is carried out by multiplying by matrix $R = R_z(0) \cdot R_x(\pi/2 - \delta_\Omega) \cdot R_z(\alpha_\Omega + \pi/2)$. The index defines the axis, around which the rotation is made at the angle that is the argument. As a result we obtain the vector **r**'(x',y',z'), for which we find its "longitude" α' in this new coordinate system. The sign before $\Delta\alpha'$ determines the direction of rotation.

From the correlation of the observed course of the synodic period with satellite's velocity variation by right ascension, the conclusion can be drawn that Ajisai has the reverse direction of rotation. Analysis of the six light curves obtained in Odessa on 21-23 September 2009 gives the value of the sidereal period error is equal to 0.0000003 sec. On the interval 21-22.09 – mean rotation period is equal to 2.1026397, and on the interval 22-23.09 – 2.1026461 sec.

The synchronization of the photometric observations

Relating various measurements to the world time scale is done nowadays by receiving and registering second-long impulses in the UTC scale from the specialized satellite grouping, for instance, GPS satellites. This binding of the local time storage system to the UTC scale can be performed with sufficiently high accuracy of 10^{-4}-10^{-6} sec. However, any equipment for measurement registration introduces "hardware delay" which is difficult to measure inside an observation complex when the outer time-calibrated signal is not available. While carrying out photometry using CCD receivers (e.g. television CCD cameras), the moments (intervals, to be exact) of matrix exposition by the light of a signal source are, as a rule, separated in time from the image registration in the computer. Relating the image to the UTC scale is performed at the registration stage, so there occurs some uncertainty as to the "hardware delay" value, as well as the question: which instant of time does the obtained image refer to?

Artificial satellite Ajisai can be a convenient source of the optical signals to synchronize the photometric observations, obtained at the separated points, as far its pole position and rotational velocity are known with rather high accuracy. The availability of an independent and globally accessible source of calibrated optical impulses makes it possible either to determine the "hardware delay" value itself in timing of photometric measurements, or to find the "hardware delay" difference of two observation stations.

Figure 6 demonstrates two fragments of the light curves of artificial satellite Ajisai obtained simultaneously (!) in Odessa and Eupatoria, that are referred to the "conjugated" time spans when the bisectors of the corresponding phase angle had the same declination in the coordinate system related to the rotation axis of the satellite. In that case, both Odessa and Eupatoria observers watched the brightness flashes produced by the same mirrors of Ajisai. That is confirmed by the similar shape of the recorded light curves during that time span.

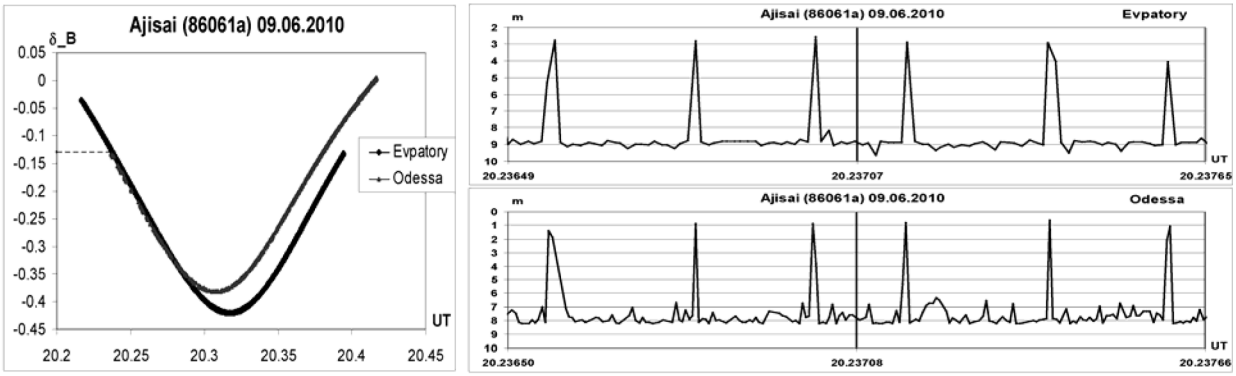

Figure 6. The synchronous change of declination of the phase angle bisector for two observation points (on the left) and the Ajisai light curves segments close to the "conjugated" moments $t_1 \approx t_2$.

However, between the moments of the corresponding flashes, recorded at different observation points, there should exist a delay equaled to the difference of the longitudes of the points in the coordinate system related to the current rotation axis of the satellite. Such a delay is easily computed and taken into account. The residual difference between the fixed flash moments at two observation points represents the "hardware delay" difference of time registration in making photometric observations. It allows the two systems of time registration to be synchronized. The necessity of such synchronization is extremely important when the basic photometric observations are conducted with the goal to jointly process those data to obtain the rotation parameters of any other artificial satellite (for instance, in case of emergency).

The error of determining this synchronizing correction is equal to the sum of uncertainty values of an optical event's time registration moments at two observation stations. This uncertainty is conditioned by finite time of image exposition: we don't know when exactly the flash of brightness within the exposition interval occurred.

The uncertainty of the measurement registration time moment is of the order $T_{exp}/2$. Thus, it is possible to synchronize time scales by the photometric method with the same accuracy as the observations themselves are obtained. Changing to shorter expositions in satellite's photometry is only possible in applying high-speed CCD cameras.

The hardware delay. The technology of observation of an artificial satellite with the panoramic receivers, such as a CCD camera, enables to record its picture against the starry sky background. The artificial satellite coordinates relative to the stars and the brightness of all images in the frame, including the satellite, are measured simultaneously at that. Such simultaneous measurement of the coordinates and brightness of the artificial satellite results in the unified time binding of the proper hardware time scale to the UTC scale. The advantage of that technique is that the corrections of the null point of the time scale can be found by the comparing of the obtained momentary coordinates of the artificial satellite with the coordinate-time measurements, received by different high-precision observational networks. One such high-precision network can be the International Laser Ranging Service (ILRS) [4], which everyday publishes in the Internet forecasts of the positions of the reference geodesic artificial satellites on the basis of the modern high-precision theories of perturbed motion. Using the "normal" coordinates of artificial satellite Ajisai in the International Terrestrial Reference System (ITRS) on the basis of the ILRS ephemerides, I.Kara [5] has converted them to the precision ephemerides of that artificial satellite for the observation point in Odessa in the stars catalogue system for epoch J2000,0. The comparison of the ephemerides of a number of reference artificial satellites with the actual measurements of their coordinates in the same system demonstrated the presence of the "hardware delay" and the necessity to correct the null point of the time scale by about –0.011 sec.

Despite the correction value is great, it is rather expected as the CCD camera operates in the "interlaced mode" and the exposing of the next half-frame takes place during the transmission and recording the previous one [3]. The discrepancies of the measured coordinates of artificial satellite Ajisai relative to the ILRS ephemerides before and after correcting the null point of the time scale are shown in Fig. 7.

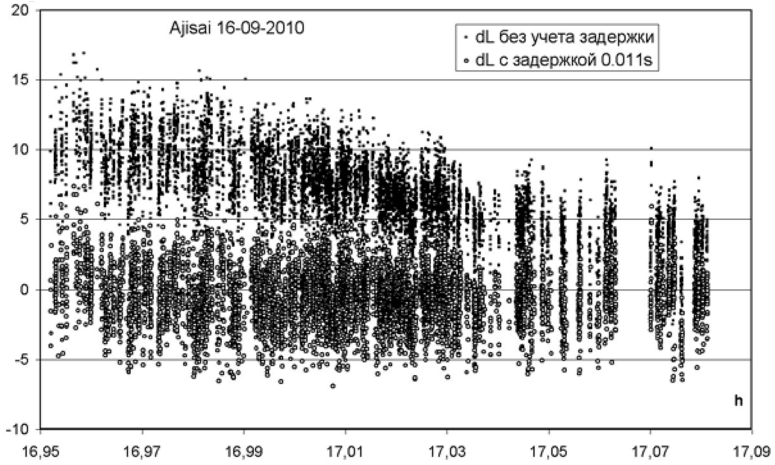

Figure 7. The discrepancies dL (in arc seconds) along the visible trajectory of the artificial satellite between the observed and computed with the ILRS ephemerides positions [4, 5].

Conclusion

As a result of obtaining the adjusted current coordinates of the rotation pole of artificial satellite Ajisai together with the reduction of the null point of the hardware-based time scale and application of the present value of the sidereal rotation period, timing of the observed light flashes of this satellite has been improved. That allowed of realizing the synchronization of the photometric channels at the stations in Odessa and Eupatoria by carrying out the simultaneous photometric observations of the reference artificial satellite Ajisay. The further photometric observations of that satellite will enable to construct a theory of its rotation around the centre of mass and to use it as a reference source of the time-calibrated optical signals by any ground-based observatory.

References

1. Sasaki M., Hashimoto H.: 1987, *Launch and Observation Program of the Experimental Geodetic Satellite of Japan, IEEE Transactions on Geoscience and Remote Sensing*, **GE-25**, No. 5.
2. Hausleitner W., Kirchner G., Cristea E.: 2006, *Proc. XXIX Annual Seminar, Apatity*, 88-91.
3. Burlak N., Dragomiretskiy V., Koshkin N. et al.: 2007, Zvenigorod *(/http://lfvn.astronomer.ru/report/0000018/Od/index1.htm)*.
4. *http://ilrs.gsfc.nasa.gov/*
5. Kara I.V.: 2009, *Odessa Astron. Publ.*, **22**, 20-24.

SURFACE OZONE IN KIEV

A.V.Shavrina[1], I.A.Mikulskaya[2], S.I.Kiforenko[3], O.B.Blum[4], V.A.Sheminova[5], A.A.Veles[6]

[1] Main Astronomical Observatory of National Academy of Sciences of Ukraine, Kiev, Ukraine, *shavrina@mao.kiev.ua*
[2] MNUTS IT and C, National Academy of Scinces and Ministry of Education and Science of Ukraine, Kiev, Ukraine, *lutmail@ukr.net*
[3] MNUTS IT and C, National Academy of Scinces and Ministry of Education and Science of Ukraine, Kiev, Ukraine
[4] Botanic garden National Academy of Scinces of Ukraine, Kiev, Ukraine
[5] Main Astronomical Observatory of National Academy of Sciences of Ukraine, Kiev, Ukraine, *shem@mao.kiev.ua*
[6] Main Astronomical Observatory of National Academy of Sciences of Ukraine, Kiev, Ukraine, *veles@mao.kiev.ua*

ABSTRACT. The study of total ozone over Kiev and its concentration changes with height in the troposphere has been made on the base of ground-based observations with the infrared Fourier-spectrometer in the Main Astronomical Observatory of National Academy of Sciences of Ukraine (MAO NASU) as part of ESA-NIVR-KNMI project no 2907 "OMI validation by ground based remote sensing: ozone columns and atmospheric profiles "(2005-2008) [1,2,4]. Ground-level ozone in Kiev for an episode of its high concentrations in August 2000 was also simulated with the model of urban air pollution UAM-V [5,6]. In 2008 the satellite data Aura-OMI on profiles of ozone in the atmosphere OMO3PR became available (*http://disc.sci.gsfc.nasa.gov/Aura/data-holdings/OMI/ omo3pr_v003.shtml*). They include ozone content in the lower layer of the atmosphere, beginning from 2005, which can be used to evaluate the ground-level ozone in all cities of Ukraine. The comparison of the data of ozone air pollution in Kiev (ozone - the pollutant of the first class of danger) and medical statistics data of of respiratory system (RS) diseases of the city population was carried out with the package "Statistica". A regression analysis, prognostic regression modelling, and retrospective prognosis of the epidemiological situation with respect to RS pathologies in Kiev in 2000-2006 were performed.

Key words: Stars: He-weak: magnetic field; stars: individual: HD182255, 3 Vul

Introduction

The study of total ozone over Kiev and changes of its concentrations with altitude in the troposphere has been made on the basis of ground-based observations of the infrared Fourier spectrometer of the Main Astronomical Observatory of National Academy of Sciences of Ukraine (MAO NASU) as part of ESA-NIVR-KNMI project no 2907 "OMI validation by ground based remote sensing: ozone columns and atmospheric profiles "(2005-2008 years) [1,2,4]. It was also modeled ground-level ozone in Kiev for an episode of its high content in August 2000 [5,6] using a model of urban air pollution UAM-V. Ground-level ozone is a secondary pollutant which is highly toxic to humans and all living matter. It is formed by photochemical reactions of precursor substances, emissions, mainly from vehicle exhausts and large technology companies, and, indeed, is an indicator of anthropogenic pollution of the studied areas. As chemical and toxic substance ozone has been well studied. As for its effect on human health, the residents of modern cities, then, unlike the U.S. and Europe, in Ukraine this question is only beginning to be studied. At the same time, it is here that this problem requires the most careful study: firstly, because of the complexities of economic, medical and environmental conditions prevailing in recent years, and secondly, because we observe an intense transformation of cities into a modern metropolis with a huge park of vehicles. This phenomenon, from many points of view, the new has not yet been studied, including in health and ecological aspects.

Aims and objectives

The main purpose of this study - to perform a retrospective study of the influence of ozone on the health of Kiev city population, from 2000 until the present time. It is known that the primary target of ozone impact on human health is the respiratory system (RS), as well as health in general. The aim of this work is to create a database on the problem of ozone in Kiev and to carry out on its basis the necessary epidemiological and theoretical studies to predict the ozone impact on the respiratory system of the city population. It is also expected to use the results of epidemiological studies to assess the risk of harmful effects of ozone on the health of the inhabitants of Kiev and other cities in Ukraine, both at the population and individual (personal) level.

Materials and methods

To carry out this work, we asked for medical statistics regarding the RS diseases of the population of 14 districts of Kyiv. We select 12 indicators for determining the general and primary morbidity of the population by ozone de-

pending RS pathologies for the period 2000-2006. The data obtained related to five socio-age groups of Kiev residents: children, adolescents, adults of working age and pensioners. Data of averaged maximum ozone pollution for 14 districts of Kiev, as well as in Kiev as a whole for the "ozone episode" in August 2000, calculated from the results of urban ozone modelling with UAM-V. for surface layer of the atmosphere over the city [5,6], Fig. 1. The model UAM-V takes into account the following factors: topography of the city, weather conditions, intensity of solar radiation, the number of point and area sources of industrial emissions to the atmosphere, the number of vehicles in the city, the speed and temporal loading of traffic. In 2008, the satellite data Aura-OMI on ozone profiles in the atmosphere OMO3PR (*http://disc.sci.gsfc.nasa.gov/Aura/data-holdings/OMI/ omo3pr_v003.shtml*), became available which include the ozone concentration in the lower layer of the atmosphere since 2005. We performed a comparison of these data with ozone profiles obtained by us from observations with the infrared Fourier spectrometer and the modelling with program MODTRAN4 [1,2]. The first comparison of our profile for the April 23, 2007 showed a significant difference with the profile of the Aura-OMI in the tropospheric part of the profile, Fig. 1a. However, the data OMI of version 2009 agree well with our profile for the same date, Fig.1b. This gives grounds for using OMI data in assessing the ground-level ozone concentrations in all major cities of Ukraine.

Epidemiological study of the SVD diseases for population of Kiev (2000)

The first epidemiological study on the problem of surface ozone in Ukraine was carried out by us with the modelling results of ozone episode of 2000 [3]. At that time the administrative structure of Kiev was comprised of 14 districts, each of which was served by a network of district clinics delivering statistics data to the Kiev centre for medical statistics "Medinstat". This made possible to carry out a full statistical comparison of district averaged RS indicators for city's population and averaged maximal district ozone concentrations calculated from ozone modelling (Fig. 2). The correlation study showed that the socio-aged group "adults", counting more than 70% of the Kiev population, has statistically significant relationships ($r > 55$) for indicators "respiratory diseases" and "pneumonia". Socio-aged group "children" shows statistically significant relationship in terms of "asthmatic bronchitis" ($r = 0,66$).

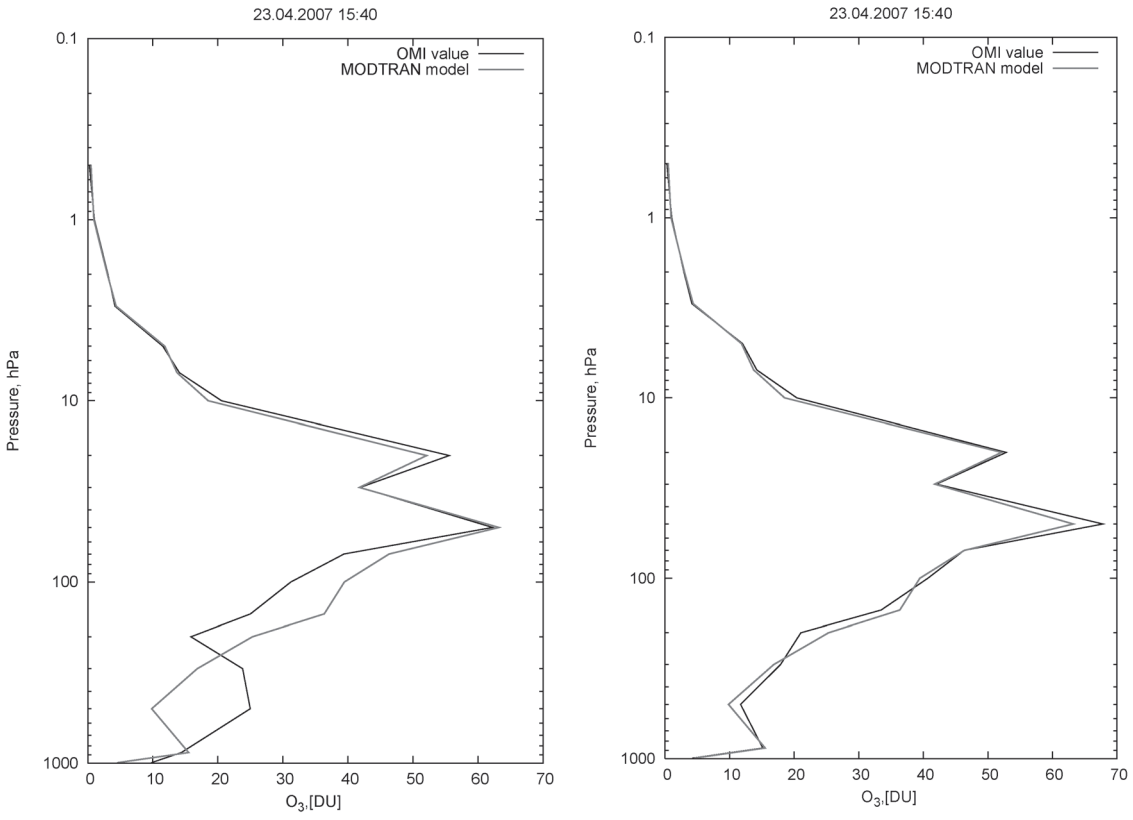

Figure 1: Comparison of our retrieved atmospheric ozone profile with the OMI data (OMO3PR): a) OMI data of version 2008, b) OMI data of version 2009

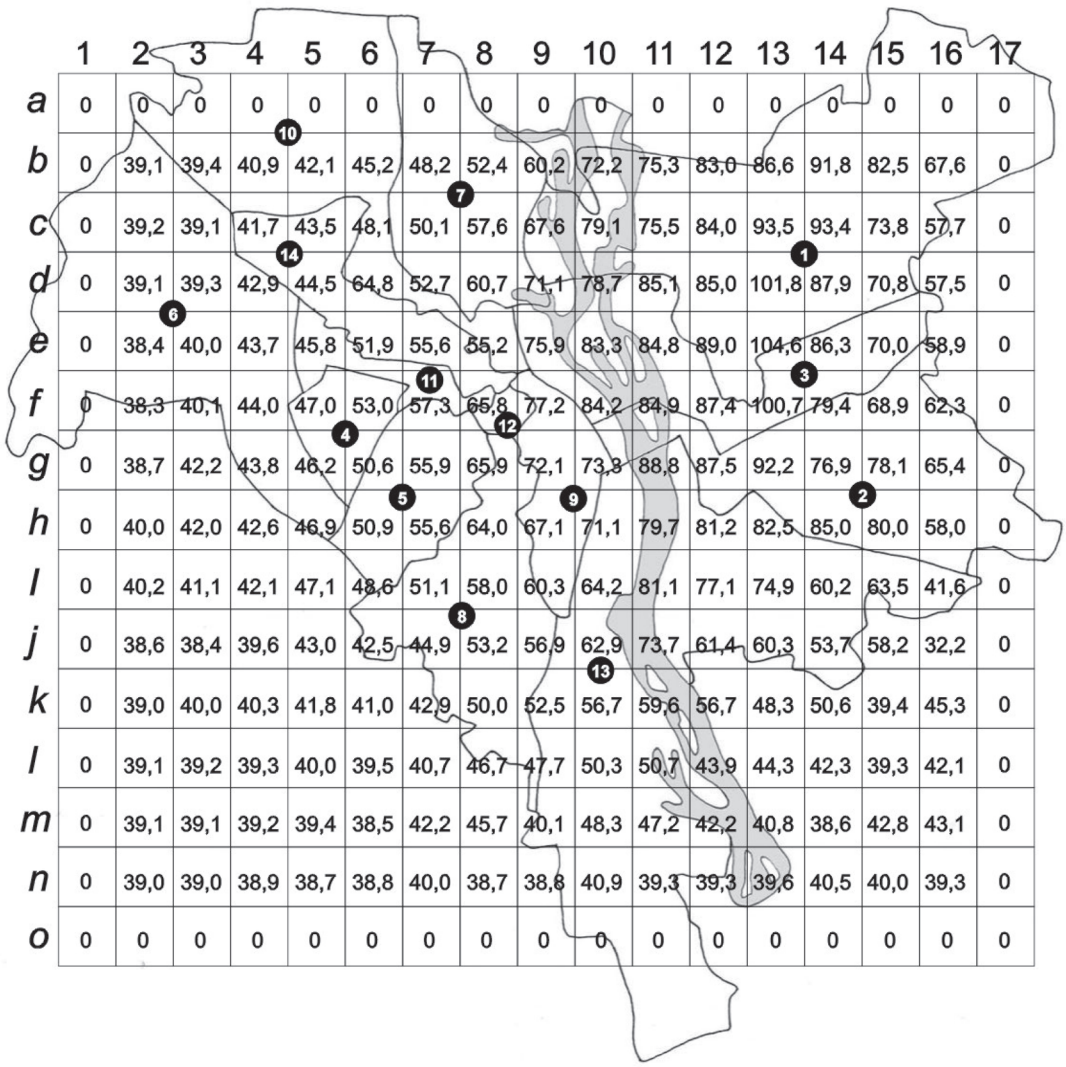

Figure 2: Mean maximal concentrations of ozone in the Kiev areas, calculated from the modelling: 1. Vatutinski district (76 ppb), 2. Darnitski district (71ppb), 3. Dneprovski district (73.3ppb), 4. Zhovtnevyi district (46.2 ppb), 5. Zaliznichnyi district (60 ppb), 6. Leningradski district (38.8 ppb), 7. Minski district (51.9 ppb), 8. Moskovski district (50.3 ppb), 9. Pecherski district (64.1 ppb), 10. Podolski district (46.2 ppb), 11. Radyanski district (52.5 ppb), 12. Starokievski district (61 ppb), 13. Kharkovski district (59.1 ppb), 14. Shevchenkovski district (46.4).

When we select for the study the areas of the city "sleeping" districts with their socio-economic and medico-ecological features, as well as the similar population density (5 000 inhabitants per 1 km^2.) We found in this case the high correlations between ozone cocentrations and RS indicators. For adults they reached values of r = 0,83, for children r = 0,8. Further, with the correlations obtained we carried out the regression analysis of the data and constructed linear regression equation that will predict the RS state for residents of Kiev. Indicators "Respiratory diseases" in adults and "asthmatic bronchitis" in children are based on summer peak concentrations of ozone in their areas. The prediction of the epidemiological situation with respect to RS diseases in Kiev in 2002-2006 was carried out using the data of measurements of the surface ozone at the Botanical Garden, satellite data Aura-OMI, as well as results of surface ozone concentrations modelling for Europe (including Ukraine) performed in the Rhenish Institute for Environment at the University of Cologne (*http://www.eurad.uni - koeln.de/index_e.html*). It was assumed that these data for Kiev characterize the city average concentration of ozone in 2000-2006. On their basis it was forecasted the total number of respiratory diseases (adults) and asthmatic bronchitis (children). The comparison of the results of prediction and health statistics for 2000-2006 (Kiev) showed that forecasts constructed on the modelling results are mainly confirmed. The discrepancy in the values of the indices studied does not exceed 26% (Table). The prognosis based on the satellite Aura-OMI (2005, 2006 years) for the same indicators was close enough to the statistics data.

Table. Surface ozone impact on respiratory diseases of Kiev city population. Comparison of predicted respiratory system diseases in Kiev with the data of medical statistics.

year	2000	2002	2003	2004	2005	2006
Concentr.3(ppb)						
Model O3	56.9	75.0	75.0	55.0	78.5	71.5
Aura-Omi					63.0	61.9
Ozonometer:						
Bot.Garden, GAO	56.9	75.5	71.1	67.9	84.2	77.0, 70.0
Respir. diseases (adults)						
Med.statistics data (100000 persons)	2996	3236	3534	3391	3561	3600
Prognosis:						
Model O3	2996	3886	3884	2902	3714	3714
deviation		20%	10%	14%	3%	3%
Aura-Omi					3295	3252
deviation					9%	9.6%
Ozonometer:						
Bot.Garden, GAO		3911	3694	3537	4339	3985
deviation		21%	4.5%	4.3%	22%	11%
Asthmatic bronchitis (children)						
Med.statistics data (1000 persons)		8.75	9.2	7.12	9.2	8.75
Prognosis:						
Model O3		9.7	9.7	9.3	10.1	9.0
deviation		11%	5.4%	24%	11%	3%
Ozonometer:						
Bot.Garden, GAO		11.	9.2	8.8	10.9	9.95
deviation		26%	0.1%	6%	18%	14%

Conclusion

Summing up the results of this work, we should say that the expansion of the database of ground-level ozone pollution for the other cities of Ukraine, as well as statistics on the health of the population of these cities is a necessary condition for the study and solving of the problem of ozone in the Ukraine. Note very high concentrations of ozone in the summer 2010 in Odessa (up to 200 ppb), given by the EURAD modelling in the Rhenish Institute for Environment at the University of Cologne. As a result of this work, it became apparent that the modelling of ground-level ozone in the city should be repeated at least every 3-4 years, taking into account the growth rate of the city, as well as changes in the quantitative characteristics of morbidity by ozone depending RS pathologies. Such studies, combined with satellite data (in particular the Aura-OMI) and modelling of ozone pollution for cities opens up the opportunities for predicting risks of ozone harmful effects on the health of the population of major cities in Ukraine.

Acknowledgements. This work was partially supported by the Space Agency of Ukraine.

Reference

1. Shavrina A.V, Pavlenko Ya.V, Veles, A.A et al.: 2008, *Kosmichna nauka i tehnologiya*, **14**, N 5 , 85.
2. Shavrina A.V Sheminova V.A, Pavlenko Ya.V. et al.: 2010, *Kosmichna nauka i tehnologiya*, **16**, N 4,3.
3. Mykulska I.A., Shavrina A.V., Kiforenko S.I.: 2008, *In Coll. Biomedical information technology in health care,* Kyiv, BMIT-2008, **BMP-2009**, 41.
4. Shavrina A.V., Pavlenko Ya. V., Veles A. et al.: 2007, *J. of Geophys. Res.*, **112**, D24S45.
5. Shavrina A.V., Sosonkin M.G., Veles A.A. et al.: 2008, *Simulation and Assessment of Chemical Processes in a Multiphase Environm.*, Barnes I., Kharytonov, M. M. (Eds.), NATO Science for Peace and Security Series C:Environmental Security. Springer, **XXV**, 345.
6. Shavrina A.V., Veles A.A., Nochvaj V. et al.: 2010, *NewsLetters of the FP7 EC MEGAPOLI Project*, N 8, 31.

INVESTIGATION OF CHEMICAL COMPOSITION OF GIANTS IN THE HYADES

Shereta E.P.

Astronomical Observatory of I.I.Mechnikov Odessa National University, Odessa, Ukraine

ABSTRACT. This paper has presented the results of abundance analysis of three giants in the Hyades. The study based on the spectra which were obtained on 1.93 telescope of the Haute-Provence Observatory (France) equipped ELODIE spectrometer, spectral resolution is 40 000, in the spectral range of 4400 – 6800 AA, the main parameters - the effective temperature $T_{\rm eff}$, the surface gravity $\lg g$, microturbulent velocity V_t and elemental abundances of Fe, Na, Mg, Al, Si, Ca, Ti, V, Cr, Co, Ni were determined. The determination errors were presented. The studied stars shown the homogeneity of chemical composition and Na overabundance.

1. Introduction

Hyades is a stellar open cluster, which located in Taurus. It has a mass of about 300-400 $M_\odot$ and the age of approximately 625 = ± 50 Myr, It's known the importance of the Hyades cluster in the study of Galactic structure and understanding the chemical evolution of the Galaxy (De Silva et al., 2006), and determining the distance scale that based on the distance of the Hyades, etc. However, there are some questions were connected with this cluster. So, photometric study shows higher metallicity of giants compared to the dwarfs, while the Hyades stars have the same origin and therefore should have similar chemical composition.

2. Observations

Spectra for the studied stars were obtained on 1.93 telescope of the Haute-Provence Observatory (France) equipped ELODIE spectrometer. Spectral resolution is 40 000, in the spectral range of 5100 – 6800 AA. Spectra processing (continuum level location, measured of equivalent widths etc). was performed using DECH 20 software (Galazudinov, 1992) Equivalent widths EWs of lines where measured by means of a Gaussian fitting.

3. Stellar parameters

The temperature was determined by the method. (Kovtyuh et al., 2003), which basic on different response of a line with different excitation potentials of the lower level to the temperature. The internal precision of this method is about 10 K.

Surface gravity g is defined using the star's parallax and the temperature by the standard formula:

$$\lg g = 4 \lg T_{\rm eff} + 0.4\, M_{\rm bol} + \lg (M/M_\odot) - 12.5.$$

The data on the parallax π", stellar magnitude V were taken from database SIMBAD, the bolomrtric correction BC was taken from paper Flower (1996).

Microturbulent velocity V_t was determined from the condition of independence of the abundance of iron obtained with of neutral iron, line from the equivalent width of this line. Table 1 shows the main parameters of the studied stars.

4. Abundance Analysis

The chemical composition was determined in the assumption of LTE. We used the model atmospheres of Kurucz (1993) . Determination of Fe, Na , Mg, Al , Si , Ca , Sc, Ti , V , Cr, Mn, Co, Ni of abundances was performed on the measured equivalent widths using solar oscillator strengths (Kovtyuh and Andrievsky, 1999), by Kurucz's WIDTH9 software. Error in determining the individual values of chemical elements (σ) does not exceed 0,1 dex - for Fe I, 0,14 dex - to Fe II, Na I, Mg I, Al I, Si I, Ca I, Ti I, VI, Cr I, Mn I, Co I, Ni I. Most of the elements shows a small overabundances, which corresponds to a given age of the cluster and the previously obtained data.

Figure 1 shows the contents of chemical elements for the cluster giant. In the figure 1 shows the average value of the content elements by the line. The figure demonstrats the relative uniformity of content of the elements in the atmospheres of giants.

Table 1: Main parameters of the studied giants.

HD	Sp	π"	V	T_{eff}	V_t	lg g	[Fe/H]	M_v	M_{bol}
27371	K0III	0,02117	3,654	4945	1,6	2,26	-0,04	-0,38	-0,05
28307	K0IIIb	0,02066	3,847	4946	1,4	2,32	0,03	-0,23	0,1
28305	G9.5III	0,02104	3,54	4912	1,6	2,19	-0,04	-0,53	-0,19

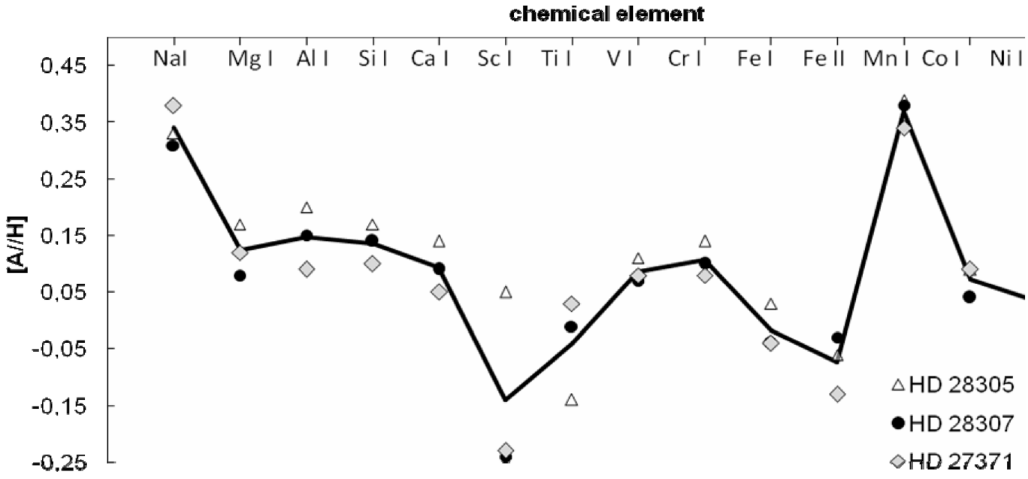

Figure 1: Chemical composition of te stellar atmosphere in giants of the Hyades.
A - Species

5. Error Analysis

Error in the determination of element content is due to errors in determining of the effective temperature, surface gravity, turbulent velocity, and choice of the models. In the approximation of local thermodynamic equilibrium, so there may be errors associated with deviation from LTE. NLTE effects are specific in relation to the atom and influence act on each element separately, so the error for different elements due to NLTE manifestation will be different. Error is also associated with the uncertainty of the oscillator strength and continum level location. Since giant stars are in almost identical conditions and have similar parameters, their errors of the chemical composition determination did not differ significantly. Table 2 shows the error for each of the chemical elements for the star HD28307.

Table 2: Error in the determination of chemical elements for the star HD28307.

Element	ΔT_{eff}	Δ lg g	ΔV_t	*Total*
Fe I	0,02	0,04	0,02	0,05
Fe II	0,01	0,03	0,01	0,03
Na I	0,28	0,03	0,23	0,36
Mg I	0,01	0,08	0,05	0,09
Al I	0,01	0,15	0,15	0,21
Si I	0,01	0,14	0,11	0,18
Ca I	0,01	0,09	0,08	0,12
Sc II	0,01	0,24	0,01	0,24
Ti I	0,01	0,01	0,19	0,19
V I	0,01	0,07	0,08	0,11
Cr I	0,01	0,10	0,1	0,14
Mn I	0,05	0,38	0,45	0,59
Co I	0,01	0,04	0,05	0,06
Ni I	0,01	0,01	0,02	0,02

6. Conclusions

The parameters of the atmospheres: the effective temperature T_{eff}, the surface gravity lg g, microturbulent velocity V_t and the metallicity [Fe / H] for the stars HD028305, HD28307, HD27371 were found. The following elements Fe, C, Na, Mg, Al, Si, Ca, Ti, V, Ni, Co show a small overabundances, which is close to that obtained previously for the stars of the Hyades cluster. Excess of sodium Na in the giants due to removal of material from deeper layers, formed in a chain of hydrogen burning NeNa-cycle was determined.

References

Castellani V., Degl'Innocenti S., Prada Moroni P.G.: 2001, *Mon. Not. R. Astron. Soc.*, **320**, p. 66–72

De Bruijne J.H.J., Hoogerwerf R. and de Zeeuw P.T.: 2001, *A&A*, **367**, 111-147.

Flower P.J.: 1996, AJ, **469**, 355.

Galazudinov G.A.: 1992, *Preprint Special Astrophysical Observatory*, **92**, 52.

De Silva G.M., Sneden C., Paulson D.B., Asplund M., Bland-Hawthorn J., Bessell M.S., Freeman K.C.: 2006, *A.J.*, **131**, 455-460.

Kovtyuh V.V., Andrievsky S.M.: 1999, *A&A*, **351**, 597-606.

Kovtyuh V.V., Soubiran C., Belic S.L., Gorlova N.I.: 2003, *A&A*, **411**, 559-564.

Kurucz R.L. *Atlas 9 stellar atmosphere programs and 2 km/s grid*: Cambrige, Smithsonian Astrophys. Observ., 1993 CD-ROM № 13.

Mishenina T.V., Gorbaneva T.I., Bienayme O., Soubiran C., Kovtyukh V.V., Orlova L.F.: 2007, *A.J.*, **84**, №5, 429-441.

Mishenina T.V., Gorbaneva T.I., Cancen L.E., Soubiran C.: 2002, *Kinematics and Physics celestial objects*, **18**, №4, 306-326.

ON THE ISSUE OF SEGMENTATION OF SPACE OBJECTS IMAGES AGAINST THE STARRY SKY BACKGROUND IN ASTRONOMICAL TELEVISION MEASURING SYSTEM FOR ARTIFICIAL SATELLITES OBSERVATION

N.Z.Strygin

Astronomical Observatory of I.I.Mechnikov Odessa National University, Odessa, Ukraine

Segmentation refers to the process of automatic partitioning of an image into meaningful regions, so the important part of it in applied respect is the extracting (detection) of objects that differ in their brightness and geometric characteristics, as well as in physical interpretation (Денисов Д.А., Низовкин В.А., 1985).

Segmentation of nontrivial images is one of the most difficult tasks in image processing (Гонсалес Р., Вудс Р., 2005).

The problem of segmentation is one of the most important tasks of image analysis (Tetsuo Asano and Naokazy Yokoya, 1981).

As far as the results of segmentation are the only to be further processed, segmentation is the major image processing operation in information extraction systems, which the examined astronomical television measuring system (ATVMS) belongs to (Стрыгин Н.З. и др., 2007); the place of segmentation in the production string of IPC operations in ATVMS is given in (Стрыгин Н.З. и др., 2007).

Ideally, the devising of segmentation methods for some image model (class) should rely on specific knowledge of the subject, of the equipment and of technical processes of the image-forming system (Розенфельд А., Дейвис Л.С., 1979). In television astronomy, the last includes natural factors, such as atmosphere and lighting. Atmosphere is a compound optical constantly moving medium, which is not homogeneous as the refractive index varies.

On traveling through the atmosphere, the light beams are randomly deflected, causing image tremor and spreading (Селиванов А.С., 1990); the above indicates that the image-forming system parameters vary haphazardly (Хант Б.Р., 1980); therefore, in the present case, the knowledge of influence of the atmosphere, of the conditions of observation and natural illumination is indispensable (Стрыгин Н.З. и др., 2007).

As a rule, segmentation algorithms for monochrome halftone images of scenes with compact objects are based on one of the two basic characteristics of the brightness signal B(x, y) – image function: discontinuity and homogeneity.

In the first case, the approach consists in image partitioning on the base of sharp changes of the signal – image brightness jumps B(x,y); that approach is called ‘edge detection’.

In the second case, the approach called ‘interest points detection’ is used; that means image decomposing into domains with features of the same preliminary given types (Гонсалес Р., Вудс Р., 2005; Денисов Д.А., Низовкин В.А., 1985).

A lot of segmentation procedures are worked out; however, there is neither any sufficiently strict and general solution of the problem nor even its definition that causes the heuristic and, sometimes, interactive nature of the devised procedures (Борисенко В.И. и др., 1987).

By analyzing of compound images, designing of efficient algorithms for segmentation “becomes a separate important task of principle. As a rule, the segmentation procedures are aimed at solution of specific applied problems, and the quality of the solution is estimated by an expert at that” (Борисенко В.И. и др., 1987).

Image segmentation methods are effective only for those image classes that they were devised for (Путятин Е.П., Аверин С.И., 1990). Hence, it is important to define a class of the processed image, as well as applicability of certain methods (algorithms) for segmentation of images of that class.

There is no complete classification of images from a position of their processing. With development of science, engineering and production, that is caused not only by ever-increasing diversity of objects, effects, events, as well as variety of subjects, their compositions, scenes, observation conditions and processing purposes, but also by the lack of formalized criteria of image quality and estimation of quality of image processing.

The peculiarities of observation conditions and segmentation of space objects images against the starry sky background are the following:

1. The conditions of observations are short-term and nonreproducible.

2. As space objects are moveable, it is necessary to analyze a sequence of images that is the subject of a specific field of image analysis.

3. Natural space objects can be either an interfering background for segmentation of artificial satellites images or attendant objects, recognition and definition of image numerical characteristics of which is necessary to specify the latter for the observed artificial satellites.

4. The background "breathes" (its brightness distribution and location on the image field change with time).

5. The foreground reduces the contrast of space object image.

6. The areas of the regions of space objects images can be from several pixels up to several tens and even hundreds of pixels depending on the conditions of observation and the photoelectric converter used; the areas of artificial satellites images can be from several units to several tens of pixels.

7. The space object image function B(x,y) is an upper convex (concave downwards), falling down from the maxima along x- and y- axes. Sometimes, on the down trend, there are hills and valleys up to 7% of the current value B(x,y) in 1,2,3,4 pixels either compactly connected or horizontally or vertically deployed. It is rare that B(x,y) is a convex (concave upwards) due to appearance of hills along the edges of a space object image.

8. There is an evolution of spatial variations of the background and space objects brightness.

In television astronomy, by analogy with the most advanced application of digital image processing – computer vision, segmentation can be reduced to π and π_1 imaging by methods of interest points detection and edge detection, respectively (Путятин Е.П., Аверин С.И., 1990).

The difficulty of π and π_1 imaging can be caused by the fact that such concepts as 'object', 'background', 'edge of an object' are rather relative, they are not accurately formalized in terms of digital image B[i,j]. The following considerations, which should be formalized of themselves, can serve as information for such imaging:

1. objects are detected against a background;

2. object regions are coherent;

3. absolute value of the brightness gradient for the edge points of objects exceeds its magnitudes for other image points;

4. since object regions do not intersect, then the region of each object is not contained in any larger related region that consists of the objects points.

The methods and algorithms for segmentation can be considered as formalization of the concept of ability of objects detection against a background or of the concepts related to the brightness gradients (Путятин Е.П., Аверин С.И., 1990). The reliability of algorithms for segmentation depends on the level of accuracy and completeness of taking into consideration additional information, which mainly consists of the following data:

- number of objects *K* and their density per unit of area of the starry sky image;

- some characteristics of brightness distribution within object regions and the background ones; for example, extreme brightness values, number of brightness drops;

- estimation of the brightness jumps when moving between the background region and the objects region;

- information about what part of the field of view is occupied by the merged object regions (Путятин Е.П., Аверин С.И., 1990).

Starry sky is taken as a light two-dimensional pulse parametric field that is observed against natural two-dimensional random dynamic fields (or jointly with them) and in presence of natural spatially distributed noise and disturbances, the level of which is rather low under normal conditions (Стрыгин Н.З. и др., 2007).

From a position of information content and structure, a starry sky image is referred to as a locally informative type, from which interpretation objects and background part can be extracted in accordance with the task meaning (Вальтерис С.Э., Ярославский Л.П, 1983); that is why its segmentation comes to space objects extraction from a certain background. To extract space objects (either natural or anthropogenic) by that way, the local thresholding algorithm is the only among known ones that can be used due to spatial nonhomogeneity and dynamicity of a background (Бакут П.А. и др., 1987).

The ideal conditions for such segmentation are the following: there is only one object in the scanning aperture; the object brightness and the background brightness are distributed evenly within the corresponding regions and the contrast between them is rather sharp. Uneven distribution of brightness over object and background regions, as well as low contrast between their brightness cause some errors similar to false positive ('false alarm') and false negative ('lapse in attention'); such errors imply that the background regions with brightness value greater than the local threshold are labeled as the object regions; and the object regions with the brightness value less than the local threshold are labeled as the background regions. Errors of both types lead to distortion of the segmented SO parameters: the object region area S_i, the total brightness of that area $B(S_i)$ and the position of centroids of optical emission by that region area $(x_0, y_0)_i$, $i = \overline{1,k}$. In so doing, the number of space objects segmented in the frame of the starry sky image – k, and their parameters depend on the scanning aperture size; thus, the last should be adjusted to the size of the segmented SO: the object image regions should be inscribed into the scanning aperture, and their areas must equal to 30-40% of the aperture area.

The above requirement can be met by multiple scanning of an image frame with apertures of different sizes or by one-time scanning using an adaptive aperture with the size that efficiently conforms to the size of the caught space object image.

In the first case, it is necessary to promptly determine what aperture was used when the SO true parameters were detected. In the second case, it is needed to efficiently detect the size of the SO image region (i.e. to conduct a sort of preliminary rough segmentation of the SO image region), and then to form the conformable aperture. In both cases, the segmentation process is considerably complicated and prolonged, so, as for now, it can be realized only in interactive mode.

A more efficient algorithm for segmentation of SO images against the starry sky background (Strygin N.Z. et al., 2009/2010) was developed at OAO with an allowance for

the considerations mentioned above. It has more fast-action and field of applicability and has better spatial resolution.

References

Денисов Д.А., Низовкин В. А.: 1985, *Зарубежная радиоэлектроника*, **10**, 5-30.

Гонсалес Р., Вудс Р. *Цифровая обработка изображений*: М., Техносфера, 2005.

Розенфельд А., Дейвис Л.С.: 1979, *ТИИЭР*, **67**, №5, 71.

Вальтерис С.Э. и др.: 1983, *Труды АН Литовской ССР*, *сер. Б*, **3(136),** Ч. I, 97-104.

Борисенко В.И., Златопольский А.А., Мучник И.Б.: 1987, *Автоматика и телемеханика*, **7**, 3-56.

Путятин Е.П., Аверин С.И. *Обработка изображений в робототехнике,* М., Машиностроение, 1990.

Бакут П.А., Колмогоров Г.С., Ворновицкий И.Э.: 1987, *Зарубежная радиоэлектроника*, **10**, 6-24.

Стрыгин Н.З., Прокофьева В.В., Сухов П.П., Карпенко Г.Ф.: 2007, *Odessa Astron. Publ.*, **20**, part 2, 118-130.

Хант Б.Р.: 1980, *Применение цифровой обработки сигналов* /ред. Э.Оппенгейм: М., Мир, 552.

Strygin N.Z., Sukhov P.P., Karpenko G.F.: 2009/2010, Odessa Astron. Publ., **22**, 52-54.

Селиванов А.С. *Космос – миру. Телевизионные системы для исследования планет*. М., Знание, 1990, 64. (сер. «Радиоэлектроника и связь», № 2).

Tetsuo Asano and Naokazy Yokoya: 1981, *Pattern Recognition*, **14**, N 1–6, 267–273.

COMPARISON OF EFFICIENCY OF LOCAL THRESHOLDING ALGORITHM AND THE PROPOSED ALGORITHM FOR SEGMENTATION OF SPACE OBJECTS' (SO) IMAGES AGAINST THE STARRY SKY BACKGROUND

N.Z.Strygin, P.P.Sukhov, G.F.Karpenko

Astronomical Observatory of I.I.Mechnikov Odessa National University, Odessa, Ukraine

ABSTRACT. In the article are presented comparative results of the space objects separation algorithms test on the television images of the sidereal sky regions – both the local thresholding method with the scanning apertures of various sizes and the new algorithm developed at the OAO. Advantages of the OAO algorithm are shown.

The problem of space objects (natural and artificial SO) image segmentation on the sidereal sky (SS) background is considered in respect of functional algorithmic support for astronomical television measuring system (ATVMS) to observe artificial satellites. The peculiarities of such observation conditions are edduced in the article (Strygin N.Z., 2010), and the place of SO separation operations in the technologic chain of digital image processing (DIP) operations when artificial satellites observating is given in [Strygin N.Z. et al., 2007]. The tests were carried out for several real television frames of the SS images obtained when geostationary satellites observating.

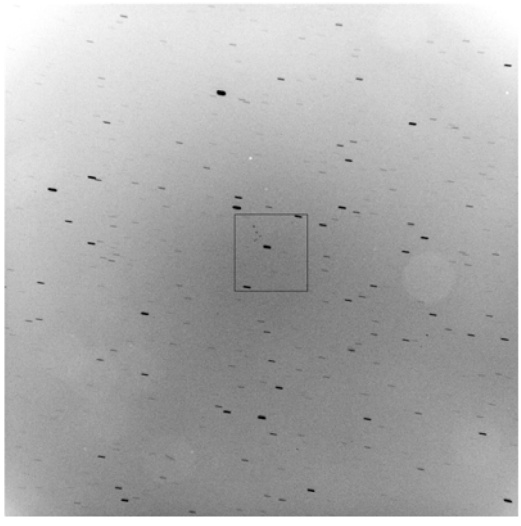

Figure 1. The SS region including geostationary satellites HotBird selected for the test. 28.11.2006. "Tair-19" lens. Field - 3° × 3°, CCD FLI 1024×1024 pixels. Processor INTEL Pentium–4, 1.6Ghz.

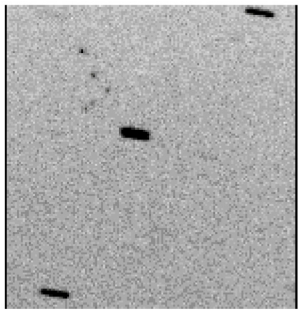

Figure 2. Fragment of the frame including 5 GSS Hot Bird and 3 reference stars. 150×150 pixels

The only feasible in our conditions (Бакут П.А. и др., 1987) the local thresholding algorithm for separation of compact low-sized objects on the complex dynamic background, was tested, as well as the the OAO algorithm. The local threshold (LT) in the scanning aperture (SA) was determined by the valley point of its pixel signals bimodal histogram formed with the algorithm given in (Стрыгин Н. З., 1987).

The peculiarities of separation of SO in the SS image using local threshold processing method – (Бакут П.А. и др., 1987); (Strygin N.Z., 2009/2010) are the following:

1) A local threshold can not be defined if there is only either SO or background in the SA.

2) Even distribution of SO and background brightnesses in the corresponding image regions, as well as a rather sharp contrast of SO against the background are the perfect conditions to select a local threshold. If the brightness of SO and the background vary within the corresponding image regions, or the contrast of SO against the background is not enough, some errors similar to false positive ('false alarm') and false negative ('target missing') occur. Such errors imply that the background image regions with brightness value equal or greater than the local threshold are labeled as the SO regions; and the SO regions with the brightness value less than the local threshold are labeled as the background regions.

3) A local threshold can be defined if there is only one SO against background in the SA.

4) To distinguish clearly two modes on the SA pixel signals histogram, it is necessary to match the SA sizes with

the segmented SO dimensions: the area of the mentioned SO image region must occupy 30-40% of the SA area.

5) The bigger SA size is, and the larger SO density per area unit of a frame is, the more probable is that more than one SO are to occur in the SA.

To illustrate the above, the processed television frame is shown in Fig. 1, and its fragment is shown in Fig. 2. The observed and computed data for GSS and reference stars are presented in Table 1, 2: optical brightness centroids - $(x, y)_i$, SO images areas - S_i, the total brightness of that area - $B(S_i)$, i = 1, …k, with k – the number of SO segmented in the image frame.

The local threshold processing was carried out for the following sizes of the SA (in pixels):19×19, 11×11, 9×9, 7×7 and 5×5.

Table 1. The comparative results of different algorithms for GSS segmentation on the fragment shown in Fig. 2

Algorithm / Object	LT 19×19	LT 11×11	LT 9×9	LT 7×7	LT 5×5	OAO algorithm
Satellite 1, pixels	0 186 0 145 216 140	0 186 0 145 216 140	0 186 0 145 216 140	0 186 0 145 216 140	0 186 0 145 216 140	133 186 0 145 216 140
$(x_c, y_c)_1$	495.99, 445.73	495.99, 445.73	495.99, 445.73	495.99, 445.73	495.99, 445.73	496.5, 445.5
S_1	4	4	4	4	4	5
$B(S_1)$	687	687	687	687	687	820
Satellite 2, pixels	161 153 137 176	161 153 137 176	161 153 137 176	161 153 137 176	161 153 137 176	161 153 0 137 176 0 0 121 121
$(x_c, y_c)_2$	501.52, 457.50	501.52, 457.50	501.52, 457.50	501.52, 457.50	501.52, 457.50	. 502.83, 458.00
S_2	4	4	4	4	4	6
$B(S_2)$	627	627	627	627	627	869
Satellite 3 pixels	0 133 134 167 0 125	0 133 134 167 0 125	0 133 134 167 0 125	0 133 134 167 0 125	0 133 134 167 0 125	123 133 134 167 0 125
$(x_c, y_c)_3$	508.76, 464.99	508.76, 464.99	508.76, 464.99	508.76, 464.99	508.76, 464.99	509.60, 464.80
S_3	4	4	4	4	4	5
$B(S_3)$	559	559	559	559	559	682
Satellite 4 pixels	–	0 133 127 120 139 0	0 133 127 120 139 0	0 133 127 120 139 0	0 133 127 120 139 0	133 127 139 0
$(x_c, y_c)_4$	–	502.00, 471.50	502.00, 471.50	502.00, 471.50	502.00, 471.50	502.33, 471.33
S_4	–	4	4	4	4	3
$B(S_4)$	–	519	519	519	519	399
Satellite 5 pixels	0 117 121 121 167 0 0 128 0 0 121 0	0 117 121 121 167 0 0 128 0 0 121 0	121 0 0 0 121 167 0 0 128	121 0 0 0 121 167 0 0 128	121 0 0 0 121 167 0 0 128	121 167 0 128 0 121
$(x_c, y_c)_5$	499.00, 474.17	499.00, 474.17	497.32, 474.01	497.32, 474.01	497.32, 474.01	498.75, 474.75
S_5	6	6	4	4	4	4
$B(S_5)$	775	775	537	537	537	537

Table 2. The comparative results of different stars segmentation algorithms

Object \ Algorithm		LT19×19	LT 11×11	LT 9×9	LT 7×7	LT 5×5	OAO Alg.
Ref. Star 1.	$x_{c,1}$	463.71	464.26	464.55	464.50	464.88	462.77
	$y_{c,1}$	409.36	409.42	409.36	409.38	409.80	408.94
	S_1	100	95	92	90	85	94
	$B(S_1)$	21102	19814	19366	19159	17994	20715
Ref. Star 2	$x_{c,2}$	523.70	524.27	524.30	524.32	524.79	522.60
	$y_{c,2}$	487.28	487.27	487.24	487.12	487.29	486.63
	S_2	87	79	78	66	59	90
	$B(S_2)$	17852	16827	16665	15068	13697	19018
Ref. Star 3	$x_{c,3}$	489.00	484.09	484.17	490.00	483.82	482.59
	$y_{c,3}$	566.00	566.29	566.36	566.00	566.53	566.15
	S_3	55	49	49	40	41	63
	$B(S_3)$	10981	10149	10149	8750	8804	12478
	$T_{el\ [sec]}$	48.5	28.7	23.8	18	14	12.81
	N_{SO}	48	48	47	47	52	63

Note: T_{el} – elapsed time of algorithms processing for the entire television frame;
N_{SO} – the number of objects separated in the entire frame shown in Fig. 1.

The following interim conclusions can be made on the grounds of the tests performed:

1. As the SA size decreases from 19x19 to 5x5, the elapsed time of LT processing of the entire television frame shortens from 48.5 s to 14 s respectively.

2. As the SA size decreases from 19x19 to 5x5 (in so doing the spatial resolution of LT algorithm increases), the number of segmented SO grows from 47 to 52 (Fig. 1) respectively.

3. The LT algorithm is inefficient against furrow-like backgrounds.

4. The OAO algorithm has:

a) higher efficiency – it takes 12.81 sec for frame processing shown in Fig.1.

b) better spatial resolution – 63 SO were separated in Fig.1.

References

Strygin N.Z.: 2009/2010, *Odessa Astron. Publ.*, **22**, 49-51.

Стрыгин Н.З.: *А.С. СССР № 1487069, кл. МПК G06 F 15/66, приоритет от 2.03.1987.*

Strygin N.Z., Prokof'eva V.V., Sukhov P.P., Karpenko G.F.: 2007, *Odessa Astron. Publ.,* **20**, P. 2, 118-130.

Бакут П.А., Колмогоров Г.С., Ворновицкий И.Э.: 1987, *Зарубежная Радиоэлектроника*, **10**, 6-24.

УДК 523.4

PHOTOMETRICAL RESEARCH OF GSS «INTELSAT 10-02»

Sukhov P.P.[1], Karpenko G.F.[1], Epishev V.P.[2], Motrunych I.I.[2]

[1] Astronomical Observatory of I.I.Mechnikov Odessa National University, Odessa, Ukraine
[2] Laboratory of Space Researches of the Uzhgorod National University, Uzhgorod, Ukraine
sppete@rambler.ru lkd.uzhgorod@gmail.com

ABSTRACT. On example of the studies the obtained coordinate and photometrical data GSS «Intelsat 10-02» is shown as possible surveillance with the help of ground-based optical facilities dynamic state satellite and his behaviors on orbit.

The analysis of variation character of the light curves in B,V,R filters, time intervals between the flashes, the color indexes variation shows that the systems of stabilization of the platform, the transceiving antennas and the solar panels worked in operating normal mode during the dates of observation. The solar panels orientation relative to the Sun maintains well enough, rotated practically along the equtor plane tracking the Sun's path (the Earth's rotation). Orientation to axis of the rotation of the platform practically remains to be unchanged to direction on the centre of the masses of the Earth.

Some photometric characteristics of active three-axis stabilized communicative geostationary satellite (GSS) "Intelsat 10-02" (28358/2004 022 A) were calculated on the basis of electrophotometrical observations that were carried out on the 6th, 7 th 12th, 13th and 14th of October, 2010 on its entry and exit from the Earth's shadow. The longitude of the sub point GSS was $359^0.0$ *E*, the inclination to the equator was $i=0^0.05$, the eccentricity was *e=0.00.* The following characteristics were computed: average effective reflecting areas $S\gamma_\lambda$ for the phase angle $\psi=0°$, spectral reflection coefficients γ_λ for the *B, V, R* filters for the phase angle $\psi=0^0$, the color index variation *(B-V), (V-R)* for the phase angle $\psi=25°$.

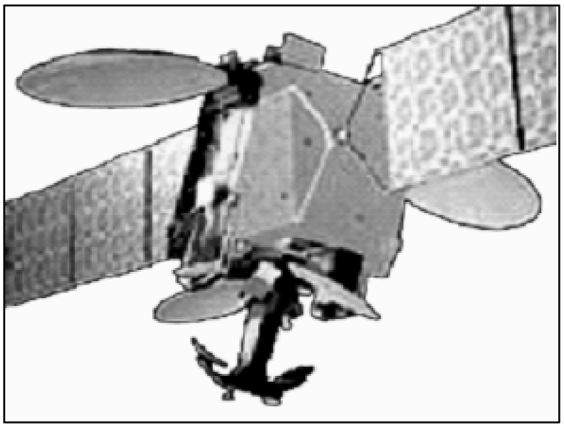

Figure 1

The appearance of satellite "Intelsat 10-02" is shown on the figure 1 alongside on the left [1], the total span of the solar batteries (SB) wings is 45m. "Eurostar-3000" platform is close to a parallelepiped, two of five sectional solar panels with independent orientation towards the Sun are mounted on its lateral surfaces. Two antennas of about 2m in diameter and two antennas of about 1m in diameter are mounted on the GSS platform. The GSS is stabilized and maintained in the given sub-satellite point according to its mission.

The observations were conducted suburban of Odessa in the *B, V, R* filters on 0.5m telescope using photomultiplier FEU-79. The electron signals passed through a wide-band amplifier and a pulse counter then were received on microcontroller ATMega16 and fed into the PC through serial port RS232. To reduce to the standard photometric system we used G2V stars, similar to the Sun, from the WBVR catalogue of the Sternberg State Astronomical Institute [2]. The mean quadratic error of magnitude for all dates was within the range of $0^m.02$ - $0^m.05$.

The analyzing of light curves of active stabilized satellites of certain form and dimensions allows determining of spectral reflection coefficients γ_λ for *B, V, R* filters close to their real values. The set of photometric characteristics of different types of the known active GSS is to facilitate interpretation of light curves of unknown satellites and as a consequence to accelerate satellite identification. The complex analysis the coordinate and photometric characteristics data makes it possible to checking the current state of a satellite (operating or normal mode, emergency state, ending of operational life, fragmentary state), and to reveal the source of a satellite's emergency state. As it was repeatedly noted [3, 4, 5], the observations carried out on the GSS entry and exit from the Earth's shadow allow to improve substantially the temporal resolution of photometrical observations and hence to make more precise the detailing of the field structure of reflective surface of satellites.

As per McCue et al. [6] the satellite magnitude m_{sat} can be equated as follows:

$$m_{sat} = - m_{sun} - 2.5 \lg [S\gamma F(\psi)/d^2]$$

with m_{sun} – the Sun's magnitude, S – an object's cross-sectional area, γ – reflection coefficient, d –topocentric distance to the satellite, $F(\psi)$ – phase function. This equation was used to calculate the GSS photometric character-

istics. For diffusing of the reflection of the light from flat surface phase function possible to present as:

$$F(\varepsilon,\theta) = \cos\varepsilon \cdot \cos\theta,$$

where ε and θ - corresponding to angles of the fall and reflections of the light to plane of the solar panels.

The analysis light curves the "Intelsat 10-02"

The phase light curves and color indexes of satellite "Intelsat 10-02" are presented below in Fig. 2-9. The computation of solar panels and platform angle of orientation with specular flashes at the light curves with vectors normal to the reflective surface was conducted in the satellite-centric equatorial coordinate system by applying the methods suggested by Yepishev V.P. and described in his work [9].

In row of the table, left to right, serial number and date of the observations, moments of the observations first and the second maximum of the light curves GSS in scale of universal time UT, time of stay of the satellite in shadowe of the Earth Δt minute, geocentric equatorial coordinates GSS α_{geoc} and δ_{geoc} in degres, value of the phase angle ψ and angle Q inclination of the panels SB to direction on Sun for moments of the observations, as well as minimum value of this angle Q_{min} on interval of the observation in the night (in degree).

Table 1. Results of the calculations of the position GSS and conditions of his illumination for moments fixing maximum light.

№ n/n	Data obser.	UT	Δt (min.)	α_{geoc}, °	δ_{geoc}, °	Ψ, °	Q, °	Q_{min}, °
1	06.10.2010	$1^h43^m54^s$	55	39.76	-0.01	27.36	13.63	9.55
		$2^h08^m13^s$		45.83	-0.01	32.76	16.37	
2	07.10.2010	$1^h43^m22^s$	52	40.60	-0.01	27.45	13.63	10.58
		$2^h06^m00^s$		46.63	-0.01	32.44	16.18	
3	12.10.2010	$1^h37^m55^s$	30	44.41	-0.01	27.43	13.72	7.98
		$2^h02^m24^s$		50.03	-0.01	32.63	16.30	
4	14.10.2010	$1^h59^m58^s$	20	51.17	-0.01	32.54	16.26	13.52

Table 2. Results of the determination to orientation of the solar batteries panels for moments of the GSS maximum light

№ n/n	Data obser.	UT	$\alpha_\odot$, °	$\delta_\odot$, °	α_{obser}, °	δ_{obser}, °	α_n, °	δ_n, °
1	06.10.2010	$1^h43^m54^s$	191.56	-5.02	216.37	6.82	204.01	0.92
		$2^h08^m13^s$	191.71	-5.03	222.44	6.82	207.05	0.92
2	07.10.2010	$1^h43^m22^s$	192.48	-5.40	217.21	6.82	204.89	0.72
		$2^h06^m00^s$	192.62	-5.40	222.81	6.82	207.72	0.72
3	12.10.2010	$1^h37^m55^s$	197.05	-7.30	220.76	6.82	208.97	-0.23
		$2^h02^m24^s$	197.20	-7.31	226.88	6.82	212.03	-0.23
4	14.10.2010	$1^h59^m58^s$	199.05	-8.05	228.28	6.82	213.68	-0.63

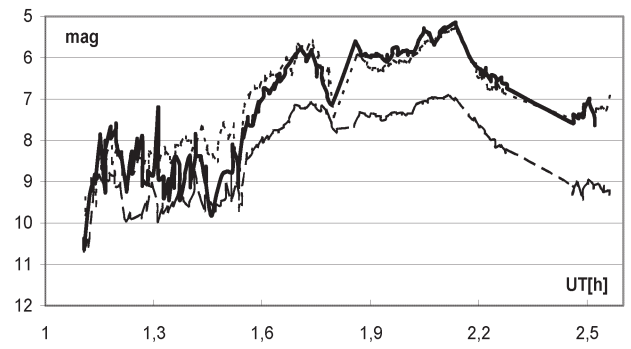

Figure 2. The light curves for "Intelsat 10-02" exited from shadow on 06.10.10. V – solid line, R ---, B – –.

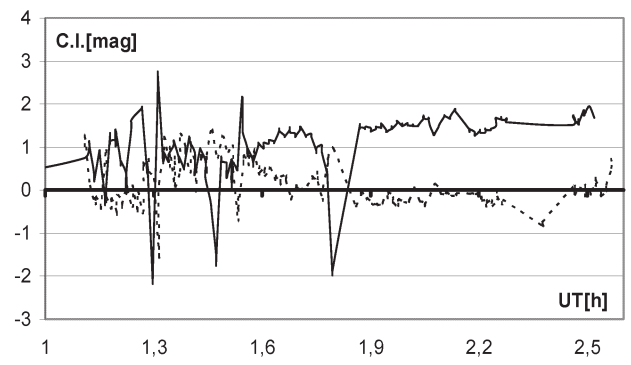

Figure 3. The color index variation for "Intelsat 10-02" exited from the shadow on 06.10.10. (B-V) solid line , (V-R) ---.

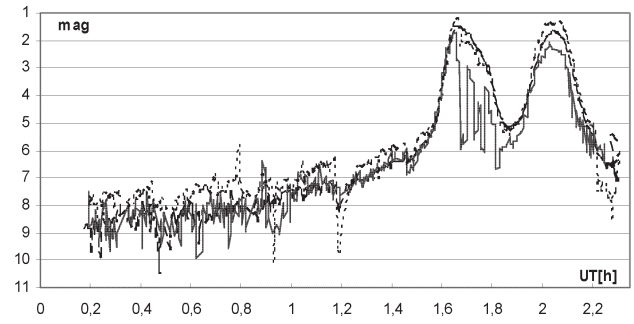

Figure 6. The light curves for "Intelsat 10-02" exited from shadow on 12.10.10. V – solid line, R ---, B – –.

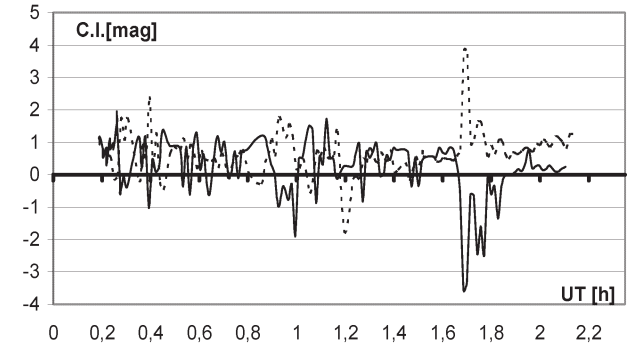

Figure 7. The color index variation for "Intelsat 10-02" exited from the shadow on 12.10.10. (B-V) solid line , (V-R) ---.

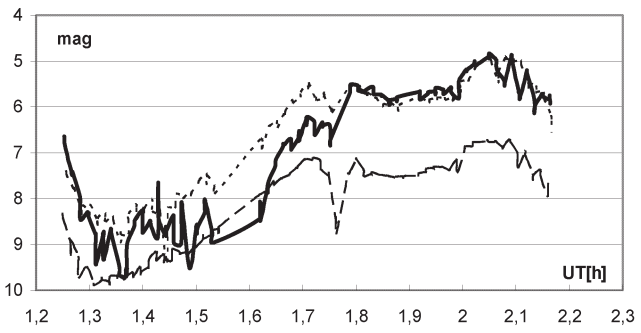

Figure 4. The light curves for "Intelsat 10-02" exited from shadow on 07.10.10. V – solid line, R ---, B – –.

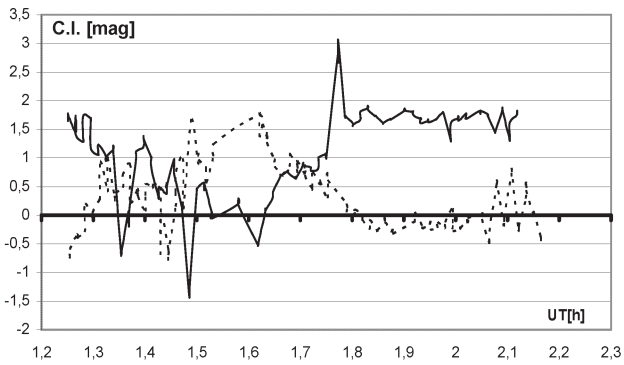

Figure 5. The color index variation for "Intelsat 10-02" exited from the shadow on 07.10.10. (B-V) solid line , (V-R) ---.

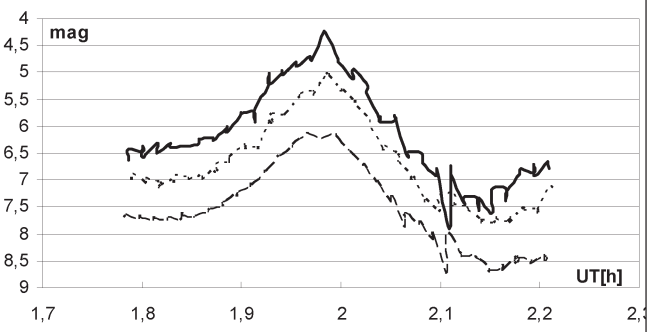

Figure 8. Second maximum of the the light curves for "Intelsat 10-02" exited from shadow on 14.10.10. V – solid line, R ---, B – –.

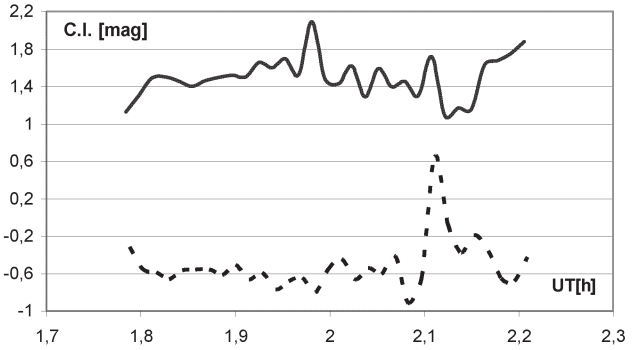

Figure 9. The color index variation for "Intelsat 10-02" exited from the shadow on 14.10.10. (B-V) solid line , (V-R) ---.

The first three rows of this table are identical the such of the table 1. Next, in row left to right, are shown Sun equatorial coordinates ($\alpha_\odot$, $\delta_\odot$) at the moments of the observations GSS, observer (α_{obser}, δ_{obser},) coordinates and directions normal to panel SB (α_n, δ_n) - in degree.

Only the second maximum of the light curve was recorded successfully in details on the night of 13/14.10.2010. Almost simultaneous brightness variation similar to the previous three light curves was observed in three filters. This is noted also for fixsed change the factors of the colour in all observant nights. Only October 12 2010 fixed mirror flashes reached maximum value before $m \approx 1^m$, but object was seen during half of the hour by naked eyes.

The obtained results interpretation

In the light flow, reflected from satellite "Intelsat 10-02", the main contribution give its solar battery panels (in all filter) in spite of the fact that factor of their reflection is less than 20%. There is one more additive of the light, reflected from antennas and lateral verges of the satellite's body in yellow and red area of the spectrum. It is conditioned by golden colour of the platform details and it is comparatively non-significant. After the GSS exits from the shadow, the Sun except panels well illuminated the lower part of the satellite's body where are placed various instruments, including smaller, than diameter of the antennas. In this time the light flow reflected to the observer's direction still is weak. Much weakly is illuminated also the front side of the satellite's body, which may be seen by observer. So on area of the light curve before first flash are observated of the light fluctuations practically in all filters with amplitude about 1^m.

While the Sun rises over horizon and its height increases, the lateral side of the satellite's body started to illuminate better, and while panel is turning, the angle of light reflection to observer's direction is decreasing. The satellite's light in all filters, fluctuating, grows before maximum with some additional jump in the yellow area of the spectrum. Greater values of the colour-index in these moments are conditioned not so much by optical features of the satellite's surface details, as by their mutual shadowing. The maximum of the light consists as if it were of two parts. At this moment the panels are most aptly oriented respectively the Sun and observer. But a part of remote panel is not seen by observer. It is overlapped by the body of the satellite.

Beginning since 6-th of October 2010, in maximum of the light GSS, into the observer's field of view gradually, from observation to observation was started to get the image of the Sun, solar glare, which was moving under some angle on the panel's surfaces. In the first night of observation the edge of glare has fallen in the observer's direction at the edge of one panel only, making insufficient increasing of GSS light at the end of the maximum. But in the 7-th of October 2010 the part of glare was seen along both panels. But, commencing its way from the end of panel which is remote from observer for a while it has fallen into shadow of the satellite's body and then was passing on lateral side of the satellite's body with antenna, oriented in the space otherwise than SB panels, that has brought about reduction of the light, and has finished its procession on the second panel nearest to observer, just once again increasing the GSS light.

To the night 12.10.2010 this glare was seen practically completely, having increased light of the GSS on 4^m, and has conditioned zero value of the colour-index (B-V). During shadowing by satellite's body and by nearest big antenna, it disappears from the observer's field of vision for 20 minutes, reducing the GSS light to accustomed 5^m, but then, passing on the second panel, it once again was increased. To the last night 14.10.2010, the conditions of the glare's visibility vastly grew worse that is confirming and the colour-index value (B-V). The GSS light is decreased, but value of the colour-index is increased.

From performed calculations it is seen that the most favorable observation of solar glare should be expected to 11.10.2010, when the declinations $\delta_\odot$ and $\delta_{obs.}$ on absolute value were equal. But, it is pity, in that night, because of bad conditions, observations were not conducted. Therefore, the maximum of the GSS light is closest to ideal "mirror" on the light curve for 12.10.2010. Thus and the obtained values of the satellite's orientation and its SB panels for this date are to be the most exact.

In the table 3 are shown calculated some photometric and optico-geometrical parameters of investigated GSS for the dates of observations.

In the table are given: spectral area of observation (filter), the star magnitudes M of GSS light reduced to the phase angles 25° and 0°, colour-indices (B-V) and (V-R) reduced to the phase angle 25°, and also geometric albedo A_{geom} and efficient reflection areas S_λ.

Table 3. The GSS «Intelsat 10-02» calculated photometric and optico-geometrical parameters.

Date, The Sun declination	Filter	M ψ =25°	M ψ = 0°	B-V ψ =25°	V-R ψ =25°	A_{geom}	S_λ, [м^2] ψ =0°
06.10.2010 $\delta_\odot$ = -04°58'	B	9.39	9.12	0.57	1.07	0.11	9.47
	V	8.82	8.54			0.15	13.45
	R	7.75	7.47			0.24	21.56
07.10.2010 $\delta_\odot$ = -05°21'	B	9.14	8.87	0.39	1.02	0.13	11.88
	V	8.75	8.48			0.16	14.30
	R	7.73	7.46			0.24	21.95
12.10.2010 $\delta_\odot$ = -07°14'	B	7.89	7.62	0.09	0.50	0.42	37.42
	V	7.80	7.53			0.38	34.14
	R	7.30	7.03			0.36	32.61

Remark: The spectral reflection factors are calculated for average efficient reflection area of diffusive plane reduced to zero phase angle. In our case they are coinciding with the values of geometric albedo A_{geom}, i.e., integral characteristics, averaged on the whole reflecting area, including various details of constructions with various optical properties.

From provided in the table 1-4 data and described above dynamics of the GSS "Intelsat 10-02" visible light change is clearly seen that the SB panels are rotating in the small time lag around only one axis, which is perpendicular to equatorial plane. But the normal vector to the SB panels lies in the equatorial plane, making full turn overnight, accompanying Sun. Herewith number of the panels periodic moving is completely includes into the satellite's rotation period on its orbit. Both maximums on the satellite's light curve, from observation to observation, happen to one and same phase angle value (tabl. 1.). Regrettably insufficient time duration of each observation doesn't provide enough safely to define the period one, apart taken, tumbling of the panels tracing visible moving of the Sun disk.

Conclusions

The analysis of the GSS light change in three filters, corresponding to its colour-indices (the Figs. 2-9) and the time-lag values between the flashes, shows; that the systems of platform stabilizations, receive- transmitting antennas and SB in our observation dates functioned in staff operating duty. On length of the observed nights orientation panels SB beside satellite "Intelsat 10-02" was fairly well saved for directions on Sun. The tumbling of the panels SB occurred, probable whole, around axis perpendicular to the equatorial plane, tracing visible motion of the Sun (caused by rotation of the Earth and GSS, accordingly). The orientation to main axis of the platform, within error of the calculations, remained to be unchangeable to direction on the Earth masses centre.

The obtained coordinate and photometric information on GSS shows that using the ground-based optical facilities is possible effective control of the satellite dynamic condition [10], and estimation of the its visible surfaces details optical features and behavior the satellite on its orbit.

Table 4. Calculation results of the directing cosine (X_n,Y_n, Z_n) of normal vector to the surface of solar batteries (SB) and platform (P) for the chosen moments of the time.

	Satellite element	Date	UT	X_n	Y_n	Z_n	ψ, °	F_n, °
1	SB	6.10.2010	$2^h07^m03^s$	-0.8994	-0.4366	0.0210	33.42	1.2031
2	SB	7.10.2010	$1^h42^m15^s$	-0.8963	-0.4432	0.0175	27.97	1.0026
3	SB	12.10.2010	$1^h39^m21^s$	-0.8817	-0.4717	0.0003	27.66	0.0172
4	SB	14.10.2010	$1^h57^m58^s$	-0.8442	-0.5359	-0.0065	31.88	-0.3724
5	P	6.10.2010	$2^h08^m07^s$	-0.8984	-0.4387	0.0210	33.66	1.2031
6	P	7.10.2010	$2^h03^m00^s$	-0.8960	-0.4436	0.0175	32.57	1.0026
7	P	12.10.2010	$1^h39^m33^s$	-0.9289	-0.3703	0.0004	27.70	0.0229
8	P	14.10.2010	$1^h58^m58^s$	-0.8431	-0.5378	-0.0066	32.11	-0.3781

Where: ψ is phase angle; F_n is geodesic latitude of normal vector to the surface of SB.

References:

1. *http://www.skyrocket.de/space.*
2. Корнилов В.Г., Волков И.М. и др. Каталог WBVR - величин ярких звезд северного неба/Под ред. Корнилова В.Г.: 1991, *Труды ГАИШ,* **63**, М., Изд-во Московского ун-та, 400 с.
3. Диденко А.В., Усольцева Л.А.: 2002, *Космические исследования в Казахстане*, *Алматы, КазГосИНТИ,* 355-373.
4. Диденко А.В., Усольцева Л.А.: 2005, *Современная астрофизика: традиции и перспективы, Алматы,* с. 75-76.
5. Багров А.В. Диссертация на соискание ученой степени доктора физико-математических наук: М., 2002, с. 44.
6. McCue et al.: 1971, *Planet And Space Sci.*, **19**, 851-868.
7. Ерпылёв Н.П., Смирнов М.А.: 1983, *Письма в АЖ*, **9**, N 3, 181.
8. Багров А.В., Павленко Е.П., Прокофьева В.В., Смирнов М.А. Наблюдение зеркального отражения от геостационарного спутника: *АЦ 1286*, 1993, окт. 28, с. 3.
9. Епишев В.П.: 1983, *Астрометрия и астрофизика АН УССР*, 89-93.
10. Диденко А.В., Усольцева Л.А.: 2009, *Известия НАН РК, Серия физико-математическая,* № **4**.

ODESSA TELEVISION METEOR PATROL

Y.M. Gorbanev

Astronomical Observatory of I.I.Mechnikov Odessa National University
Odessa, Ukraine
skydust@rambler.ru

ABSTRACT. The historical information on the photographic meteor studies in Odessa is given. A modern observational complex – television meteor patrol for recording the meteor events occurred in the Earth's atmosphere is presented. The meteor patrol instruments available and the observation methods are specified. The meteor database structure is analyzed; the statistics of meteor observations conducted from June, 2003, to December, 2010, is reported. The total number of meteor events recorded by television method using various instruments is 4276. The software package is developed including 12 programs that enable to carry out the whole cycle of processing the observation data: from preprocessing to obtaining of the orbital elements of the recorded meteor particles. The programs on the basic and non-basic observations made in Odessa and at the observation stations in Kryzhanovka village and on Snake Island are presented. We also discuss the principal tendencies in the meteor studies conducted at Odessa astronomical observatory on the basis of observation results obtained by the meteor patrol using the television method.

Key words: meteor, meteor shower, television observations, the meteoroid monitoring.

1. Introduction

The first photographic meteor patrol was assembled at Odessa astronomical observatory by E.N. Kramer and engineer N.I. Timchenko in 1953. It consisted of four surveying cameras with F-24 lenses (with the focal length of 200 mm; the lens speed of 1:2.9; the angle of view of 48 degrees). A rotary disc shutter rotated in from of the lenses with the angular velocity of 24 tps. It is then that the first pictures of meteor events were made. Odessa observatory participated in the International Geophysical Year (IGY) program. The workgroup of the Committee on comets and meteors under the Astronomical council of the Academy of Science of the USSR approved Odessa astronomical observatory as the leading institution on the "Meteor studies" issue (section "Ionosphere"). The meteor patrol has been conducted in Odessa for over 40 years, from 1953 to 1993. More than 600 pictures of basic meteors and several thousands of those of non-basic meteors have been recorded. The data received by Odessa meteor patrols underlay several hundreds of scientific publications.

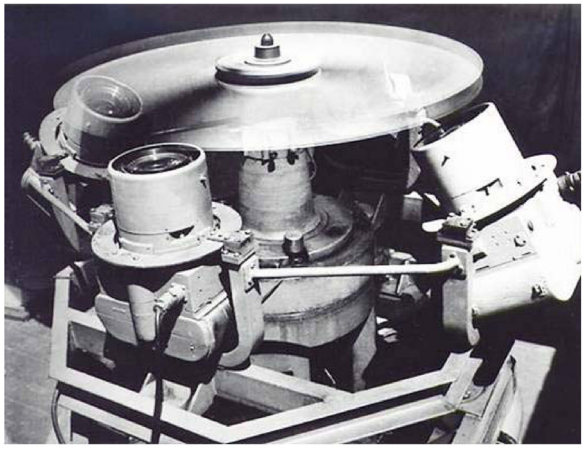

Figure 1. The photographic meteor patrol at Odessa astronomical observatory

The photographic meteor patrol consisting of four cameras HAFA-3C/25 and the rotary disc shutter system to determine the time marks is shown in Fig.1. Unfortunately, the outdated meteor patrol instruments became obsolete and required cardinal modernization. Thus, as per [1], a new ideology and new technical means were indispensable to continue carrying out the effective meteor patrol.

As the range of speeds, masses of meteor dust particles and conditions of their meeting the Earth's atmosphere is rather wide, there can be no all-purpose method of meteor astronomy.

The comparative scheme for peculiarities of different observational methods in meteor astronomy is shown in Fig. 2. None of those methods, except the telescopic one, can cover the full meteor event brightness range; besides, the time, position and photometric accuracies differ by a factor of a hundred. However, in the previous century, the telescopic method, on being visual, suffered from a number of shortcomings, such as, in particular, a narrow field of view when patrolling and impossibility to reliably record a meteor event. That is why the telescopic method was used just to solve purely specific problems concerned with the weakest meteors.

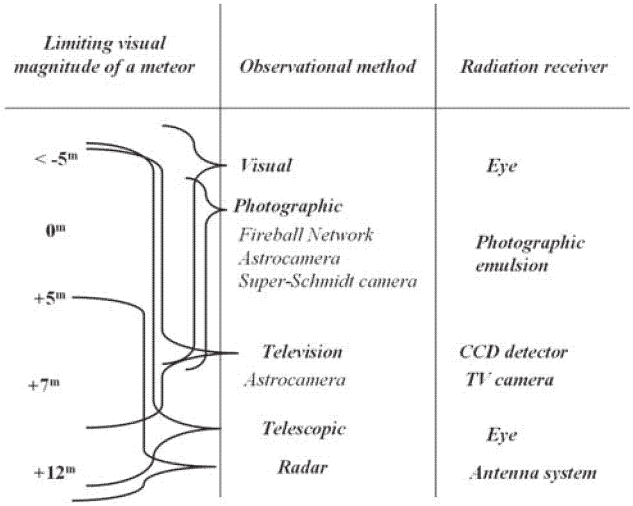

Figure 2. Facilities of the observational methods in meteor astronomy

The main problem, which arose when passing from the photographic methods of recording the meteor events to the recording by solid-state photoelectric detectors, was that of small sizes of the recording effective areas of those detectors. There is no photoelectric analog of the photographic emulsion for such cameras as HAFA-3C/25 (the field of view of tens of degrees with a spatial resolution of seconds) yet. That is why there were two alternatives for the panoramic patrol systems to pass to new detectors without loss of spatial resolution. The first option was to enlarge the sizes of the solid-state photoelectric detectors; the second – to narrow the effective fields of view of the meteor patrol. The reduction of the fields of view for the meteor patrolling leads to a decrease in the number of records of the meteor events. When the new highly sensitive solid-state photoelectric detectors had been applied, it became possible to combine the telescopic method with the television equipment for recording the meteor events. A new chance to reject complex and barely reliable rotary disc shutter systems to receive the temporal resolution appeared. The television method copes with that task: the meteor event image is recorded in separated frames.

2. The television meteor patrol and the methods of observations

Through objective and subjective reasons, it managed to renew the outdated meteor patrol at Odessa astronomical observatory only by June, 2003. When combining telescopic and television methods, the Schmidt telescope (see Fig. 3) was chosen certainly owing to its lens speed and comparatively wider field of view as the linear dimension of the recording surface of the detector – WATEC LCL902 camera – is just of ½ inches.

Figure 3. The meteor patrol on the base of the Schmidt telescope and the detector – WATEC camera

The details of the initial stage of the television telescopic method implementation in the meteor patrolling practice are given in [2].

There was just one telescope at that time; at present, the meteor patrol complex contains a set of various instruments; however, the choice of the detector model has not changed: WATEC LCL902K, WATEC LCL902H and WATEC LCL902H2 cameras proved to be the best among all tested ones. The implementation of new optical schemes in the meteor patrolling practice was caused, firstly, by new tasks on the meteor studying area and, secondly, by the shortcomings of the pair 'the Schmidt telescope – WATEC camera'. One peculiarity of the new television patrol should be noted. The old photographic patrol with wide-angle cameras allowed of using fixed mounts. The increase of the focal length up to 50 cm caused the necessity of using guiding mounts as a shift of the images of stars and meteors can be observed in the television frame even with exposure of 20 ms. That is why, we install the instruments on parallactic mounts and carry out the meteor patrol near the radiant points of the meteor showers.

At the initial stages of research, the observations were conducted only at one station and using the only instrument – the Schmidt telescope.

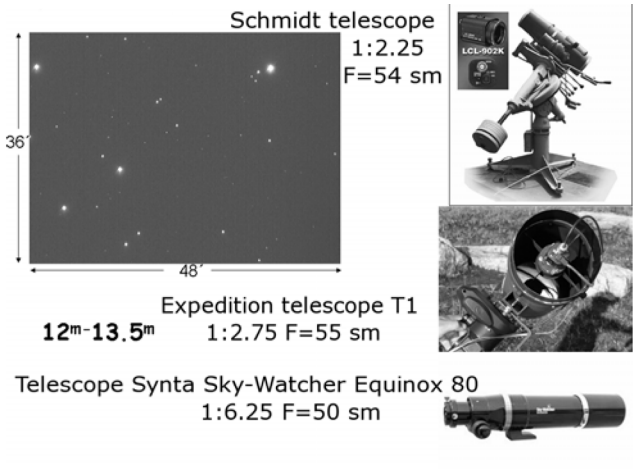

Figure 4. The telescopic systems of the meteor patrol

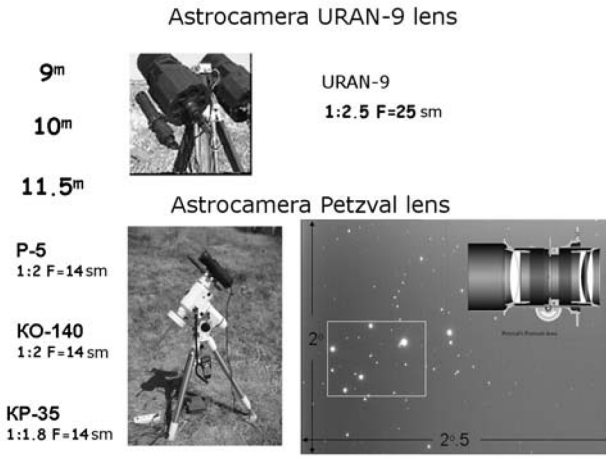

Figure 5. The astronomical cameras of the meteor patrol

Except the main observation station in Kryzhanovka village, located near Odessa, the basic observation stations in Odessa (at Odessa astronomical observatory in the T.G. Shevchenko Park), the observation station in Mayaki village and the expeditionary observation station on Snake Island were operated. The basic distances and the execution periods of the observational programs are presented in Fig. 7.

Except the main Schmidt telescope, modified in 2008 (a new corrector plate was installed), the telescopic systems that had been tested during expeditions to Snake Island were applied. Those were small telescopes (see Fig. 4) that allowed of reliably recording of faint meteors on even being inferior to the main telescope.

At the subsequent stages of modernization, in order to expand possibilities of the meteor patrol, the astronomical cameras with different performance characteristics, but with detectors of the same type were operated. The astronomical cameras with Uran-9 lenses from old cameras HAFA-3C/25 were created and used for observations; however, they had to refuse using them due to the narrow field of view (of about 1 arc degree) and low penetration power (9^m).

The cameras with the Petzval lenses P5, KO-140, KP-35 with fields of view of 2 by 2.5 arc degrees (see Fig. 5) showed themselves to considerable advantage. Although those astronomical cameras yielded to the Schmidt telescope in the resolution (3-5 arc seconds to 1 arc second for the Schmidt telescope) and in the penetration power (11.5^m to 13.5^m for the telescope), they performed a number of associated patrolling tasks due to their wider field of view. Except the Petzval lenses, other lenses have also been used, such as Sigma AF 70-200 f/2.8 EX F=13.5 cm.

That lens enabled to change the focal length of the astronomical camera from 7 cm to 20 cm and accordingly to select the field of view depending on the observational task. The astronomical cameras with Nikon lens 85 mm f/1.8D AF Nikkor F=8.5 cm allow of the meteor patrolling with the field of view of 4 by 4.5 arc degrees and the penetration power of 11.5^m.

The astronomical cameras with Samsung and Sony lenses with the focal length of just 8 mm and the field of view of 36 by 49 arc degrees have been used for the meteor patrol of the fireballs.

The penetration power of such systems reaches the value of 7^m.

The so-called synchronous observations – observations using three-four polytypic instruments, installed on the same parallactic mount, proved themselves to be especially efficient. The application of the synchronous method permits to take advantage of different optical systems in full measure. Depending on the observation task, there is a possibility to widen the field of view or to record the meteor event with a high resolution using different systems.

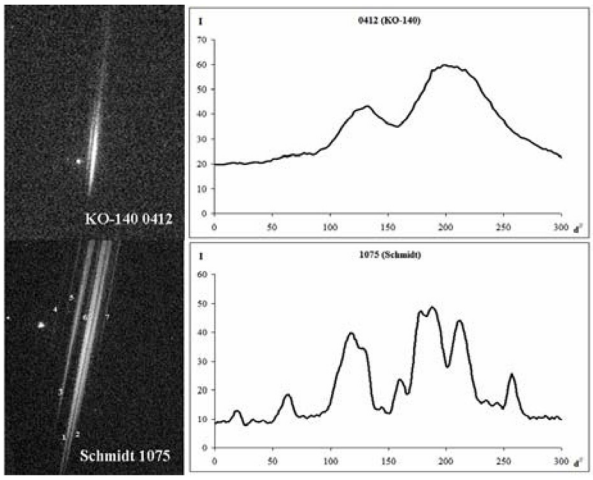

Figure 6. The comparison of the meteor TV images recorded with the Schmidt telescope and astronomical camera KO-140

Figure 6 presents the results of such synchronous observations when the meteor event is recorded by different instruments, namely using astronomical camera with the Petzval lens KO-140 (meteor 0412 in the database) and the Schmidt telescope (meteor 1075). The indicated figure shows the meteor event frames (with the time resolution of 20 ms) as well as the cross-scans of the meteor path

images in relative intensity units (in arc seconds). It is easy to see in the image recorded with the astronomical camera that only two fragments of the broken meteoroid can be identified. At the same time, the image recorded with the Schmidt telescope shows that there are at least seven such fragments. Therefore, the astronomical camera enabled to record the meteor path almost entirely, and the telescopic system resolved the event details. That is why in the meteor patrolling practice we keep using the method of synchronous observations. The methods of selection of the celestial sphere regions for the meteor patrol consist in the preliminary analyzing of the ephemerides of the meteor showers for the current observation night. The area of the meteor patrolling should be close to the radiant point of the meteor shower at some distance; then, the probability of entirely recording the meteor path rather than in fragments is getting higher. The angular distance from the radiant point (elongation) depends on the altitude and also on the linear velocity of the meteor. Sometimes, an observer selects the region of the patrolling empirically; especially if it is not possible to preliminary identify the recorded meteors as components of some meteor shower. There is a practice of analyzing the observation data of the past years and nights to detect the areas of activity of different meteor showers and to conduct the patrol in those areas. The time reference is carried out with Trimble's module ACE III GPS.

3. The meteor patrol database and statistics

According to the generally accepted definitions, the created meteor database (MDB) can be characterized as a distributed database – a set of logically interconnected databases, distributed in the computer network [5]. The MDB consists of a set of individual databases. An individual database is created for each new instrument or new observation point. Besides, with large information content, it is possible to stop the receiving new observation material to the current database and to continue the receipt to a new one. The structure of all databases is absolutely analogous, that is why there is a possibility to connect a new database to the network of the available ones. To connect a new database, it is enough to make necessary records to the configuration (profile) files, and then to copy new observation material. The creation of individual profile files allows of working with both the whole of databases network and the selected databases. The observation materials – the recorded meteors – are objects for individual and complex investigation from the viewpoint of studying of their belonging to the same meteor shower. That is why such structure of database makes it possible not only to conduct measurements and computations for each meteor event individually, but also to analyze spatial and temporal characteristics of the meteor showers in whole.

Table 1: Television meteor patrol statistic data

Database name	Observation point	Focal length	Field of view	Observation period	Quantity of meteors
Schmidt	Kryzhanovka village	540 mm	36 x 48 arc minutes	28.06.03-15.06.09	1173
Uran-9	Kryzhanovka village	250 mm	1 x 1.5 arc degrees	05.11.05-10.03.06	18
Uran-9 Island2005	Snake Island	250 mm	1 x 1.5 arc degrees	08.12.05-27.08.05	29
P-5	Kryzhanovka village	140 mm	2 x 2.5 arc degrees	18.07.06-10.10.07	125
P-5 Island2006	Snake Island	140 mm	2 x 2.5 arc degrees	05.08.06-24.08.06	84
T-1 Island2006	Snake Island	550 mm	32 x 45 arc minutes	05.08.06-24.08.06	20
KO-140	Kryzhanovka village	140 mm	2 x 2.5 arc degrees	05.12.06-17.06.09	604
KO-140 Island2006	Snake Island	140 mm	2 x 2.5 arc degrees	08.07.07-01.08.07	119
T-1 Island2007	Snake Island	550 mm	32 x 45 arc minutes	08.07.07-01.08.07	45
KO-140 Island2008	Snake Island	140 mm	2 x 2.5 arc degrees	16.06.08-03.07.08	14
EQ Island2009	Snake Island	500 mm	52 x 60 arc minutes	21.07.09-03.08.09	4
NK Island2009	Snake Island	85 mm	4 x 4.5 arc degrees	21.07.09-03.08.09	100
SG Island2009	Snake Island	85 mm	4 x 4.5 arc degrees	21.07.09-03.08.09	20
SM Island2009	Snake Island	8 mm	36 x 49 arc degrees	21.07.09-03.08.09	46
SM Odessa	Odessa	8 mm	36 x 49 arc degrees	18.11.09-18.11.09	19
SchmidtII	Kryzhanovka village	540 mm	36 x 48 arc minutes	21.06.10-31.12.10	279
KO-140IIa	Kryzhanovka village	140 mm	2 x 2.5 arc degrees	21.06.10-31.12.10	549
KP-35	Kryzhanovka village	140 mm	2 x 2.5 arc degrees	22.06.10-31.12.10	814
KO-140 Island2010	Snake Island	140 mm	2 x 2.5 arc degrees	08.08.10-24.08.10	73
NK Island2010	Snake Island	85 mm	4 x 4.5 arc degrees	08.08.10-24.08.10	100
Kryzhanovka NKb	Kryzhanovka village	85 mm	4 x 4.5 arc degrees	25.11.10-07.01.11	41
Total: 4276					

Moreover, the work with the MDB allows of remote placing of users. The astronomical observatory and observation stations or different observatories are located far from each other, but the MDB structure makes possible both to ensure the receipt of new observation data and to simultaneously process the interconnected databases.

The main work unit of the MDB is an AVI-film with the recorded meteor event. Each film is rigidly assigned with an identifier – the number of the meteor in the database, the observation date and time, information on the instrument used, the guiding star, the timing of the television frame with the meteor image. When it is necessary, it is possible to revert to the initial material any moment, and then, on having the preprocessing repeated, to rectify any errors, which could arise on different stages of measurements and computations. The total content of AVI-films has been enlarging with the lapse of time, and that hampers the work with the MDB; that is why the following approach is used: the inquiry of the lists of the films' names, but not the films themselves is made, that permits to store the films in archives on separate carriers. The structural object DATA exists to store the data of the preprocessing of the television image of each meteor event. Physically, there is a separate corresponding folder in the database for each meteor. It is filled in with information as the observation data are received, and the measurements and computations are made. Besides, separate television frames of the meteor event, the combined pictures of the meteor path, the aggregate pictures for positioning with the reference stars images, the files with the data of the preprocessing of the picture background, etc. are stored in that folder. As the further processing is made, the files with parameters of the meteor event are added. For instance, COMBO objects are the combined pictures of meteors; PRO are the files with the longitudinal scanning data of the meteor picture. Such independent structure enables to connect new processing modules as the new software is developed and also to add new object types for the results of processing or any other information without any additional structural changes.

There is a possibility to store the parameters of profiles, procedures of measurements and computations for each database in object Common Meteor Files. If the profile is global in respect of all databases, object Common Meteor Files.MDB is used. The mentioned objects allow to take into account peculiarities of each working database separately and all databases in whole. The FTP (File Transfer Protocol) is supported that permit to save the measurements to a remote server.

Some features of the object-oriented database (OODB) are used in the MDB, namely control of parallelism (a property of systems to make computations simultaneously or concurrently), restoration of data and the associated queries.

The statistics of the meteor patrolling at Odessa astronomical observatory is shown in Table 1 in chronological order. The names of individual databases and the corresponding observation points, the focal lengths of optical systems of instruments, the working fields of view, the time periods of the meteor patrolling and the quantity of the recorded meteors are indicated. Totally, 4276 meteor events have been recorded from June, 2003 to December, 2010. To process the observation material, it became necessary to devise methods and to develop a series of programs, combined to the program package.

4. Software

The Program package *Odessa Meteor* is intended for processing the results of the television meteor patrolling and was created by the workers of the Department of Small Solar System bodies department at Odessa astronomical observatory using the license version of programming language Visual Basic 6.0, which is a part of Microsoft Visual Studio 6.0. The working out of methods of processing the meteor observations and the development of the programming code were made as the observation material had been received and the observational equipment and the methods of the meteor patrolling had been improved. For some programs the algorithm was corrected on the testing stage as the computation errors had been revealed.

Some methods of processing are similar to those used when the photographic observations had been carried out; but in most cases, the computation algorithms had to be adapted to the television method of observation.

Here below, we give the list of software (SW) that is used at present.

1. *AVICutter* program is intended to carry out the preprocessing of the initial AVI-films with duration of 4 seconds. During the processing, the working folders of the numbered meteors are created, and the procedures of creation of separate and combined frames of the meteor event, and the file of the background values are conducted. The demand for such program is caused by the large content of the observation material and the necessity to promptly fill the MDB. Thanks to *AVICutter*, the preprocessing takes an observer just up to one minute. Besides, the archiving of the primary AVI-film and its conversion to the 8-bit format is made at the same stage.

2. *AVIStar* program is intended to carry out the preprocessing of the observation material to determine the parameters of scintillation of the star images. Due to the atmospheric conditions, not all the nights were favourable to conduct observations. That is caused mainly by the meteorological factors and the condition of the upper layers of the atmosphere. With the strong turbulence there are random non-uniformities in the atmosphere that refract the light rays, arousing the scintillation of stars. When observing, they become apparent in variations of brightness, scintillation of the star images and unsharpness of the meteor trails. *AVIStar* makes possible to estimate the sky quality for each observation using the initial AVI-film. The data obtained permit to classify the conditions of the meteor recording and to take into account the selectivity of observations caused by the condition of the Earth's atmosphere at those points at the coelosphere where the meteor patrolling is carried out.

3. *DubleCutter* is a graphics editor to work with the digitized data of the meteor image that enables to form the image of components of the trajectories of double and multiple meteors and to create the longitudinal and cross-section profiles of the meteor trajectories at the specified point with the predetermined step. The necessity of devel-

opment of such editor program was dictated by the research of the processes of fragmentation of the meteor particles during its flight.

4. *Meteor Manager* is a program to conduct the further integration of the observation material into the meteor database with the possibility of timing. It enables to work with both a separate database and all databases simultaneously. It consists of a number of files and editors that permit to work with AVI-films, to adjust the positioning and timing of separate frames of the film, to structure the list of the guiding stars, and, using the FTP protocol, to compile the results of measurements and computations, made by different users on the remote computers. It permits to create the total tables on the results of observations and to select samples for different databases by basic and synchronous observations. The demand for such program has arisen with the enlargement of the observation material content and appearance of the synchronous and basic methods of observation.

5. *Combo* is special software that enables to create a combined image of the meteor path using separate frames of the meteor event. With the television method of observation the image of the meteor trajectory is recorded frame-by-frame with exposure of 20 ms. The set of frames is enough to see the process dynamics; however, to measure the whole meteor path, it is necessary to combine all separate frames of the meteor event into the single image. To carry out such procedure correctly, the mentioned program was developed. The software allows of combining pictures both in manual and semiautomatic modes.

6. *PicScan* allows of conducting the high-accuracy measurements of the meteor path image in the rectangular coordinate system of the picture. The program is adjusted to work with both poor and diffuse, and bright overexposed images of meteors. When processing, the meteor image signal is selected and the meteor path pixel array is formed. There are several methods of scanning of the meteor path image used that enables to select the most appropriate one for each specific meteor. The methods of measurements using SW *PicScan* are stated in detail in study [3]. A user can analyze the results of the measurements by deviations of coordinates of the points of the meteor path. In the end of measurements made, a separate file of processing data is formed for each measuring instrument; the analysis of such files enables to eliminate distinct errors.

7. *PSF* is software to promptly identify and automatically measure the rectangular coordinate system of the picture, and to reduce the rectangular coordinates by the equatorial ones by Turner's method. The measurement of star images on the picture is carried out, and the coordinating of six or twelve constants is determined by Turner's method. The methods of measurements are based on the principles of the aperture CCD-photometry. To identify stars, one of the compilation star catalogues, created on the base of SAO, Tycho2, USNO-A2, etc., with a restriction by magnitude in V-filter up to 13.5^m, is used.

8. *MeFoMer* is software that enables to conduct the photometric measurements of the meteor image, using the results of processing with *PSF* and *PicScan* SW and the meteor image itself, based on the principles of the aperture photometry.

There are two such methods of photometric measurements: for the stars images and for the meteor trails. The transition to the magnitude scale is made by the calibrating dependencies derived by the photometric measurements of the star images. That is why when carrying out the photometric measurements of the long-duration meteor trails, the circumference-type aperture is used, the same way as for the stars. The star and meteor profiles are presented in the Gaussian fixed model function.

9. *Meteor Control Data* enables to analyze the measurements of the rectangular coordinates, obtained with various measuring instruments, using SW *PicScan*. It permits to analyze the photometric measurements of the star images, made with SW *MeFoMer*, and to derive the characteristic dependencies, and then to study them. It analyzes the results of processing the scintillation of the star images, made using SW *AVIStar*.

10. *Meteor Pole* is a program to compute the equatorial coordinates of the polar point of the wide circle of the meteor path, taking into account the flight direction. It takes into account the interlace television effect correction for the meteor path image. It enables to analyze the pole coordinates and to identify the recorded meteor's belonging to the known meteor showers.

11. *Meteor Explorer* is software to arrange and conduct the basic television observations. It is intended for the telescopic meteor patrol observations, as well as for the observations with the astronomical cameras with narrow field of view. On the grounds of coordinates of two observation points and the known guiding star at the first patrol station, the program allows of compute the area of the meteor patrolling for the second station, orientating by the meteor zone in 80-100 km of the Earth's atmosphere. The application of that SW for the base "Snake Island – Kryzhanovka village observation station" (150 km of distance) enabled to record basic meteors when the basic television patrolling was carried out.

12. *Meteor Card File* is an electronic file of the recorded meteor events. Such file permits to store information on all meteor events, recorded by the meteor patrolling, on the measurements and computations, made with the program package *Odessa Meteor*. In particular, that is the archive name of the film with the recorded meteor event, the time of recording, the name of the observer, the observation data and time, the equatorial and horizontal coordinates of the meteor, the arc length and the angular velocity of the meteor. There is a possibility to view the combined and single pictures of the meteor event. Using that SW, it is possible to search the synchronous and basic meteors in different databases, to make computations by the Stanyukovich method. SW *Meteor Card File* has been constantly improving and makes possible to connect new modules to determine the kinematic and physical characteristics of the meteor particles. A separate module permits to work with the compilation catalogue of the coordinates of the radiants of the meteor showers and also those of individual meteors, recorded by the meteor patrolling.

5. Basic and non-basic observation programs

According to the practice of the meteor patrol, when the basic observations are carried out, the percentage of non-basic meteors is very high. There are several explanations of such situation:

1) The probability of favourable weather conditions at two and more stations simultaneously depends on many factors, especially if those stations are located at tens of kilometers away from each other.

2) Some technical problems, which can be caused by the equipment work, reduce the time of simultaneous work of basic stations.

3) The limited field of view of the astronomical cameras and telescopes, as well as spatial position of the meteor event trajectory, can cause the meteor is out of the field of view of one of the basic stations.

4) The essential difference in distances to the meteor from the basic stations can cause the meteor becoming not available for recording for one of the stations due to the absorption of the meteor radiation by the atmosphere.

5) If two basic stations and the recorded meteor are on the base line, then the angle of approach does not matters a lot that causes very poor accuracy in determination of kinematic characteristics of the meteor, and sometimes, it is absolutely impossible to process the observation material.

The indicated problems cause a great number of non-basic meteors that do not give full information on the meteor events as opposed to the basic ones.

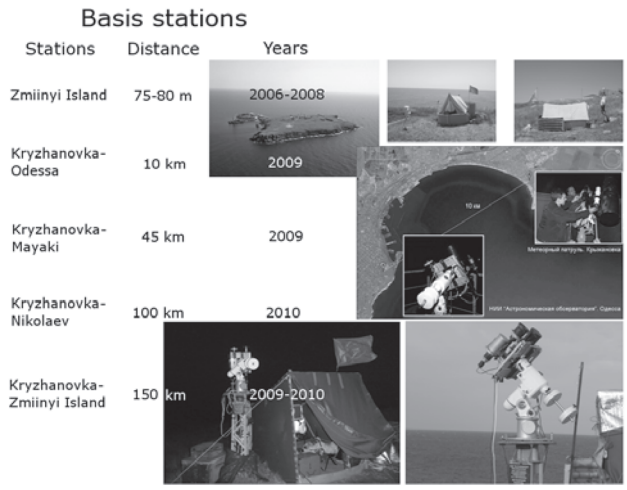

Figure 7. The basic stations of the meteor patrolling

When the methods of processing of our meteor observations were created, we addressed to those methods that had not been developed earlier due to the poor technical base. One of such methods was developed by Stanyukovich. In study [3], we present the results of application of the Stanyukovich method to the modern television methods of the meteor observations. To adjust the methods of processing of the non-basic meteors, it is necessary to conduct independent control of the results obtained. Independent usage of the non-basic methods of computation of the meteor parameters and classical basic methods of processing allows of receipt of reliable criteria of accuracy of the processing methods. That is why the basic meteor observations become more and more customary in the practice of our patrolling stations.

The information on the basic observations is presented in Fig. 7. Except the stationary mounts that conduct regular patrolling at the observation station in Kryzhanovka village, there is an expeditionary meteor patrol (EMP). As a rule, EMP is used on Snake Island during the activity of the Perseid meteor shower in August. In 2005, the first EMP, consisting of one station and non-guiding mount, was tested on Snake Island. In 2006, to conduct the basic meteor patrolling two observation stations started working on the island. Each station was equipped with a tent for the receivers (computer, TV-tuner, camera Watec-LCL-902K operating in the television mode). The distance between two observation stations was 75 meters. One of the stations used a telescope with the focus length of 55 cm and the field of view of 45 by 32 arc minutes (the maximum magnitude up to 11.5^m); an astronomical camera with the focal length of 14 cm and the field of view of 2 by 2.5 arc degrees and the penetration power up to 10^m was installed at another station. Both stations were equipped with the parallactic guiding mounts with the remote control. To synchronize the timing of the patrols the computer network was set, and one of the stations was equipped with a GPS-receiver. To synchronize the work of the observers the intercoms were used. The basic stations demonstrated high performance facilities of the observation complex.

Figure 8. The coordination of work of the basic patrol stations for the meteor observation

In 2007, similar observations were conducted on Snake Island using the modernized facility to study the July meteor showers.

Each year since 2005, when the next meteor expedition to Snake Island was prepared, the EMP is modernized on having taken into account its exploitation during the previous expeditions and in accordance with the given observational tasks. The observations with a large base demanded to develop specific software *Meteor Explorer* to

arrange and conduct the basic television observations, as well as to provide the continuous tracking the area of patrolling at the one of the stations. The synchronization of the work of two basic stations demanded to set an Internet connection and to provide a reliable work of the mobile communication in the expeditionary conditions on the island. The brief list of the basic observations is presented below:

From 2006 to 2008, the basic observations (3 expeditions) were conducted on Snake Island using two stations located at the distance of 75-80 meters from each other. The similar observations are presented in study [6], where the basic distance was 105.2 m and even 27.5 m. The precondition of such basic observations is the usage of the long-focus instruments.

The observations of the Leonid meteor shower were carried out on the base of 10 km Odessa-Kryzhanovka village in 2009.

In the same year, the basic observations at the observation stations in Mayaki and Kryzhanovka villages, the distance between which is 45 km, were conducted.

In July-August of 2009 and 2010, the basic observations (2 expeditions) were carried out on Snake Island and at the observation station in Kryzhanovka village, the distance between them was 150 km.

At present, the testing of observations at the observation stations in Kryzhanovka village and Mykolaiv is conducted.

As a result, about 50 basic meteors were obtained during the television meteor patrolling with the super short basic distances (75-80 m) and super long distances (150 km).

References

1. Kramer E.N. *History pages of astronomy in Odessa,* Part **4**: Odessa, 1997, 26-33.
2. Gorbanev Yu.M., Golubaev A.V., Zhukov V.V., Kimakovskaya I.I., Kimakovsky S.R., Knyazkova E. F., Podlesnyak S.V., Sarest L.A., Stogneeva I.A., Shestopalov V.A.: 2006, *Solar System Research,* **40**, 5.
3. Gorbanev Yu.M., Golubaev A.V., Zhukov V.V., Kimakovskaya I.I., Kimakovsky S.R., Knyazkova E. F., Podlesnyak S.V., Sarest L.A., Stogneeva I.A., Shestopalov V.A.: 2008, *Solar System Research,* **42**, 1.
4. Gorbanev Yu.M., Shestopalov V.A., Sarest L.A., Golubaev A.V. *Zmiinyi island Scientic project Abiotic Characteristics*: Astronomical studies, Part **6**, 138-154.
5. Date C.J. *An Introduction to Database Systems*: 8/E Addison-Wesley, 2004, 1024 p.
6. Kaiser N., Brown P., Hawkes R.L.: 2004, *Optical Trail Width Measurements of Faint Meteors Earth, Moon and Planets*, **95**, Issue 1-4, 579-586.

THE CONDITIONS FOR APOPHIS 99942 APPROACHING EARTH IN 2029

A.A.Tokovenko [1], A.A.Bazey [2]

[1] Odessa Astronomical Observatory of I.I.Mechnikov Odessa National University
[2] Department of Astronomy of I.I.Mechnikov Odessa National University
Odessa, Ukraine
astro@paco.odessa.ua

ABSTRACT. The discovery of Apophis 99942 asteroid in 2004 raised a number of questions in the sphere of the asteroid threatening. On April 13, 2029, the asteroid is to pass at a close distance from Earth. The study of the path of that asteroid both before and after such close approaching showed that the repeated passing by Earth and even its collision with Earth is possible in April, 2036.

In the present work, the area of the resonant return of asteroid Apophis, the Moon influence to its shape and position are considered.

Asteroid Apophis 99942 was discovered on June 19, 2004, at Kitt Peak National Observatory. The computed parameters of the asteroid orbit allowed of assigning it to the class of Near-Earth asteroids (NEA). Its orbital plane is inclined 3^0 to the ecliptic plane, and the semi-major axis is 0,9233 AU [1]. Therefore, the asteroid orbit is close to the Earth's orbit, but its passing is far from the higher-order resonance [2]. The first evaluations of the orbital elements showed that the collision of the asteroid with Earth is probable on April 13, 2029. On having additional radar observations carried out and more accurate definition of the orbital elements made, the probability of the impact was ruled out. The asteroid is to approach Earth up to 37600 km; then, it is to pass the Moon at a distance of 97000 km and move away along the orbit disturbed by Earth [3, 4, 5]. However, due to the inaccuracy of the initial data, there is a probability of collision of that object to the Planet in 2036 and the future years. Different researchers estimate the mathematical probability of the collision as $2{,}2 \times 10^{-5}$ [5] and $2{,}5 \times 10^{-5}$ [6]. Besides, there is a theoretical possibility of such collision later in the future; but it is much lower than the probability in 2036.

The study of the evolution of the orbit of Apophis asteroid has been conducted within the bounds of the problem of 14 bodies in the rectangular heliocentric coordinate system relative to the equator and the equinox 2000.0. In the model, the disturbances of the major planets of the solar system, Pluto, the Moon, the largest three asteroids (Ceres, Pallas and Vesta), the light pressure and the Earth oblateness were taken into account. The positions of the major planets, Pluto and the Moon were adopted from the numerical theory DE405/LE405 [7, 8]. The coordinates of Ceres, Pallas and Vesta were determined by the numerical integration of the equations of their movement, the initial conditions for which were taken from the E. Bowell catalogue [9]. When taking into account the influence of the light pressure, the albedo of the asteroid was considered to be equal to 0.3, and the diameter - to 260 m. At the time of the present article has been written, the error of the above mentioned parameters was equal to ±0.08 and ±60 m, respectively.

The combined differential equations of the system bodies' movement were solved by the numerical integration method by Everhart of the 15^{th} order [10] with the possibility to control the accuracy. In the present study, the accuracy of 0.01 mm was maintained at each integration step; and during the computations, the integration step has been changed from 4 days at the moment of the asteroid's maximum moving away from Earth to 6 minutes at the moments of the minimum approaching at that.

Using the derived system, we studied the evolution of the asteroid orbit during the period of 2004-2036. The following state vector was taken as the nominal initial condition for the asteroid at the moment JD = 2453360.5:

$$\begin{cases} X = 0.08942742963075248 \\ Y = 0.89794430458694535 \\ Z = 0.33638610886252548 \\ Vx = -0.0164623245524509 \\ Vy = 0.00458223264966611 \\ Vz = 0.00128067462049327 \end{cases}$$

the error in component coordinates was 5 km, and in component velocity was 0,0022 m/s. [11]

In the result of the integration of the initial conditions, without taking into account the error, we received the

nominal orbit of the asteroid. However, such an orbit do not enable to make any conclusions about the probable area of the asteroid passing as, during the integration, the error in definition of the path is growing. To estimate the error value, we applied the following method.

We considered the distribution of the probability density of the error of each coordinate and the Gaussian component of the velocity vector. Let ξ be one of the parameters (coordinate or the velocity component); then, if $\Delta\xi$ is the error in definition of that parameter (coordinate or the velocity component) ($\xi \pm \Delta\xi$), the standard deviation is $\sigma(\xi) = \frac{\Delta\xi}{\sqrt{3}}$.

By means of such a simple algorithm, we received the group of 250 thousands possible initial conditions. By integrating that bunch in the interval of 2004-2036, we obtained N (250 thousands) of probable orbits of the asteroid, enveloping the nominal orbit. Such approach enabled to study the evolution of the orbit of Apophis asteroid, taking into account the errors in the initial value of the state vector.

It took 6-7 seconds to integrate a separate initial condition. However, by the specificity of the integration algorithm, we could parallelize the computations that allowed of cutting the time of computations by 2-3 times. Hence, it took 5-6 days to carry out all computations with the 4-kernels processor Core Quad of 3 KHz and 8 GB of the on-line storage.

In accordance with the results of the numerical integration, the asteroid is to closely approach to Earth two times: on April 13, 2029, and on April 13, 2036. The dependency of the distance of the asteroid to Earth from time is still almost constant for all 250 thousands of the initial conditions up to the moment of the first approaching.

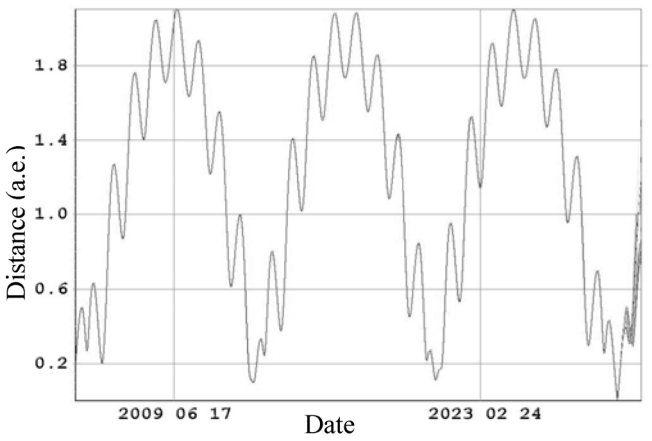

Figure 1. The distance between the asteroid and Earth.

After the first approaching, the error of definition of the position of the studied object is growing that enables to more accurately determine its position. It is possible to say that April 13, 2029 is the key moment which determines the conditions for Apophis approaching to Earth in 2036.

From the whole group of the possible initial conditions, only 40382 orbits are approaching to Earth in 2036 closer than 40000 km. Among them, 28 orbits intersect the Earth's surface. The estimation of probability of such events as approaching and collision of the asteroid with Earth in 2036 give the following values: 0,16% – the probability of the asteroid pass around Earth in 2036 closer than 40000 km and 0,00011% – the probability of the asteroid impact with Earth in 2036.

Among the whole bunch of the initial conditions, the most interesting for the studying are those that cause the collision of the asteroid with Earth in 2036.

As the conditions of the approaching on April 13, 2029 are to determine the further evolution of the asteroid orbit, we tried to define the area of the near-Earth space-time where the asteroid, on having entering that area, is to approach the trajectory to impact with Earth in 2036. Due to the narrow dimensions of that area, it is called the "keyhole" [12].

It is obvious that the precise position and dimensions of the "keyhole" are of great interest. To determine those in 6-dimensional phase space of coordinates-velocities near 28 state vectors that lead to the collision of the asteroid with Earth in 2036, we generated additional 60 thousands of possible trajectories. Those were obtained by variation of each coordinate and velocity component of the asteroid as of April 13, 2029. The integrating of the group of trajectories, received by that way, up to April, 2036, showed that 6.5 thousands of trajectories intersect the Earth's surface at that moment. Thus, the position of those trajectories as of April, 2029, is to give a view of the "keyhole".

The possible positions of the asteroid during its approaching Earth in 2036 are shown in Fig. 2. 6.5 thousands of positions that lead to the collision are marked as circles; the orbits that approach to the center of Earth at the minimal distance of 7000-10000 km are marked as crosses.

The same possible positions of the asteroid at the maximum approaching on April 13, 2029 are presented in Fig. 3. At that moment, the positions on the trajectories that lead to the collision in the future (marked as circles) and the positions on the trajectories that do not cause the catastrophe (marked as crosses) and that to be away from the center of Earth at the distance of 7000-10000 km in 2036 occupy the same area in space. We did not succeed in determination of the shape of the "keyhole" and in separation of two types of the trajectories.

The numerical modeling shows that on having approached Earth, Apophis is to fly by the Moon 24 hours later. The distance between the celestial bodies will diminish to 95876 km. The change in distance between them from April 13 to April 16, 2029, is shown in Fig. 4.

When the asteroid passes the point of the minimal approaching to the Moon, the probable orbits are divided in two separate groups. Apparently, the Moon's gravitational field disturbs the asteroid's movement by the diluting of the "keyhole" near Earth.

To check such an assumption, we carried out the modeling of the asteroid's movement with the same group of the possible trajectories, but not taking into account the Moon's gravity. Some numerical criterion of the display of the lunar disturbances was demanded. We chose the average square of distances between the momentary positions of the asteroid that lead to the collision with Earth in 2036 (x_i, y_i, z_i), and that do not cause such an impact (ξ_j, η_j, ζ_j):

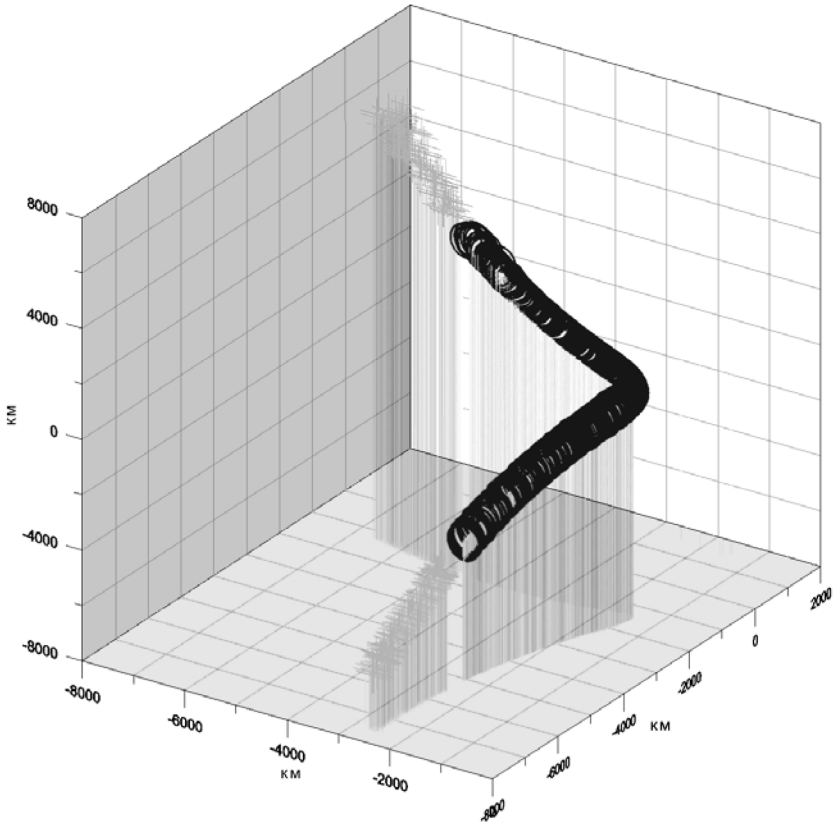

Figure 2. The asteroid's position relative to Earth as of April 13, 2036.

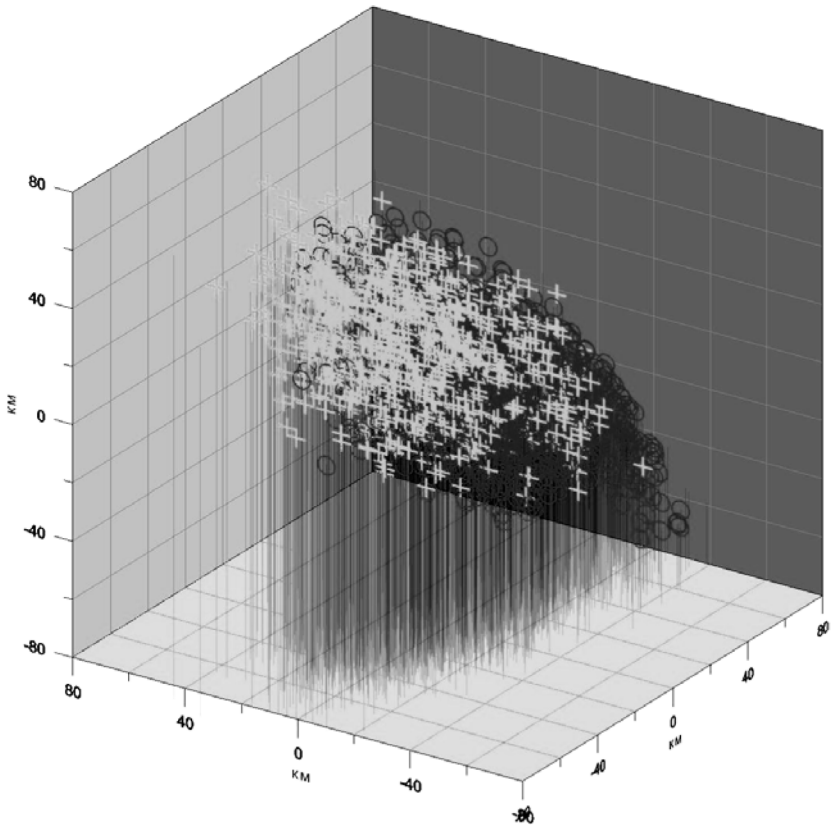

Figure 3. The same possible positions of the asteroid at the maximum approaching on April 13, 2029

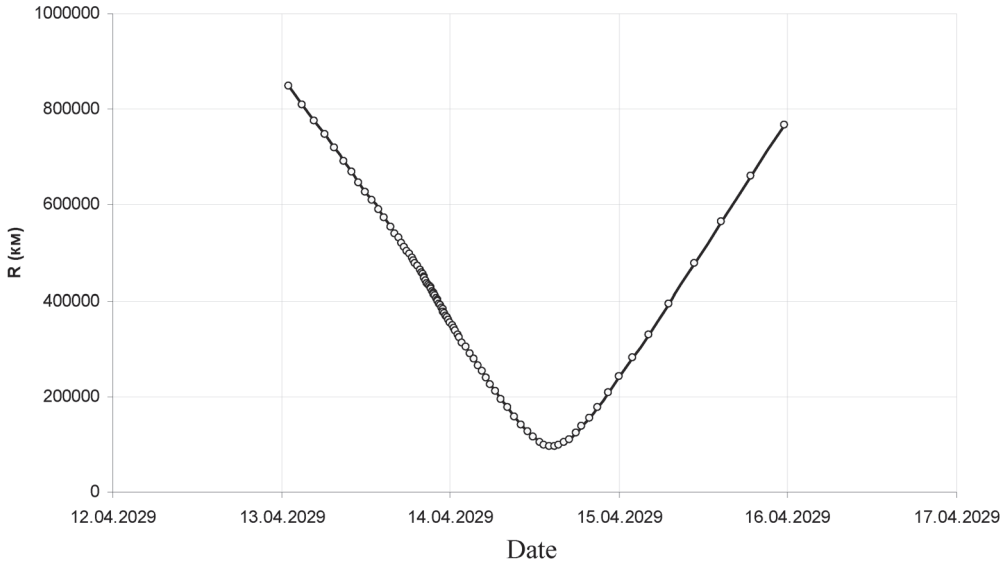

Figure 4. The distance between the asteroid and the Moon.

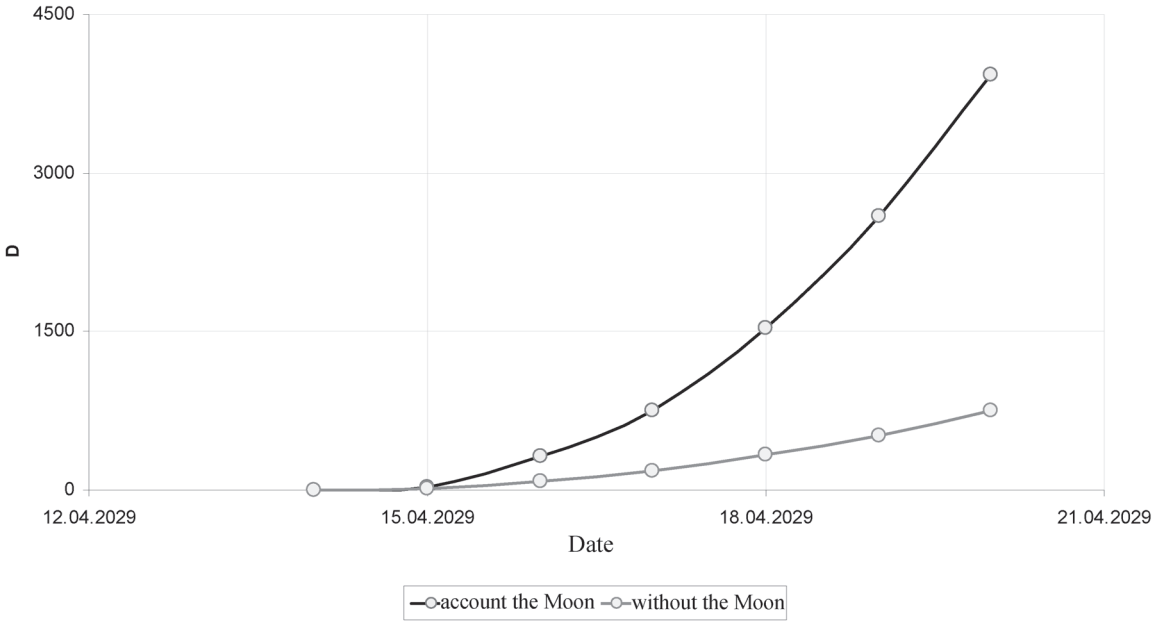

Figure 5. Parameter D

$$D = \sum_{i=1}^{n}\sum_{j=1}^{m}\left((x_i-\xi_j)^2+(y_i-\eta_j)^2+(z_i-\zeta_j)^2\right).$$

The value of D parameter is considered to be 1 at the moment of the maximum approaching to Earth. The variation in value D, taking into account the lunar disturbances and without doing that, is shown in Fig. 5. The lunar disturbances monotonously increase value D. That confirms the assumption that the Moon has a "diluting" influence on the "keyhole" near Earth.

Thus, after the close approaching to Earth on April 13, 2029, asteroid Apophis is to approach the Moon on April 14 at 14:47 UT at the distance of 95876 км. That approaching is to influence also on the growth of the uncertainty of the asteroid's movement in future. It is possible that the position of the "keyhole" should be found in the group of its possible trajectories not near Earth, but near the Moon.

References

Заботин А.С., Кочетова О.М., Шор В.А.: 2005, *Всероссийская конф. "Астероидно-кометная опасность-2005", С.-Пб.,* 134-137.

Быкова Л.Е., Галушина Т.Ю., Тимошенко Л.В.: 1998, *Фундаментальные и прикладные проблемы современной механики*, *Томск,* ТГУ, 163-164.

Токовенко А.А.: 2007, *Труды 36-й Международной студенческой научной конференции «ФИЗИКА КОСМОСА»*, 240.

Токовенко А.А.: 2007, *Изучение объектов околоземного пространства и малых тел Солнечной системы. Междунар. научная конф.,* Николаев, 116.

Базей А.А., Токовенко А.А.: 2007, *Материалы Научной конференции «Ломоносовские чтения»* и *Международной научной конференции студентов, аспирантов и молодых ученых «Ломоносов-2007»*, 143.

Смирнов Е.А.: 2007, *Материалы международной конференции «Околоземная астрономия-2007»*, 54.

http://neo.jpl.nasa.gov/risk/a99942.html

Токовенко А.А.: 2006, *Труды 35-й Международной студенческой научной конференции «ФИЗИКА КОСМОСА»*, 257.

http://ssd.jpl.nasa.gov/?sb_elem

Базей А.А., Кара И.В.: 2007, *Изучение объектов околоземного пространства и малых тел Солнечной системы,* Николаев, 109-116.

Быкова Л.Е., Галушина Т.Ю.: 2010, *Космические исследования*, **48**, № 5, 419–426.

Potential Impact Detection for Near-Earth Asteroids: 2005, *The Case of 99942 Apophis (2004 MN4), Steve Chesley, Asteroids, Comets, Meteor Proceedings, IAU Symposium* **229**, (See #11 в http://www.b612foundation.org/press/press.html)

CHEMICAL COMPOSITION OF PECULIAR STAR HD91375 – THE MEMBER OF SIRIUS MOVING GROUP

V. Yushchenko

Department of Astronomy of I.I.Mechnikov Odessa National University
Odessa, Ukraine

ABSTRACT. We present the results of determinations of the abundances of chemical elements in the atmosphere of hot chemically peculiar star HD91375 - member of Sirius moving group. We used the observations made at 8.2 meter ESO telescope. The abundance pattern of HD91375 is found for the first time, the comparison with the abundances of Sirius A is made. The abundance patterns of Sirius and HD91375 are clearly different. It confirms the possibility of recent accretion event in the Sirius binary system.
Key words: stars: abundances; stars: individual (HD91375, Sirius).

1. Introduction

Stars of the upper main sequence show a variety of abundance patterns, it is still impossible to point the reason of peculiarities - it is hard to find the star with standard solar composition in this region of HR diagram. High resolution spectra allow to investigate the magnetic fields, the stratification of chemical elements, the spots, the unidentified lines, the radial and nonradial pulsations in the atmospheres of these stars. The interplay of above mentioned and other effects, first of all the radiative diffusion and the accretion of interstellar matter results in a variety of different anomalies.

In this paper we show the results of the determination of atmospheric chemical composition of HD91375. This star is a member of Sirius moving group, that is why we will show the results of comparison of its chemical composition with the chemical composition of Sirius.

2. Observations

We used the spectra observed by S. Hubrig at 8.2 meter ESO telescope. The wavelength coverage is from λ=3060 Å to λ=9460 Å, spectral resolving power is R=80000, signal to noise ratio S/N is near 500 in the wavelength region between λ=5000 Å and λ=6000 Å.

The spectra were obtained during ten minutes, but the variability of profiles and the asymmetry of spectral lines were clearly observed. That is why to measure the equivalent widths of absorption lines the red and the blue wings of the line profiles were fitted by different Gauss profiles.

It should be noted that the asymmetry is the same for all clean lines in the whole observed spectral range. It can be the sign of nonradial pulsations of the star.

3. Chemical composition

Yushchenko et al. (2008) made the review of previous observations of HD91375 and found the following atmosphere parameters: the effective temperature $T_{\rm eff}$=9100 K, the surface gravity – $\log g$=3.8, the microturbulent velocity – $v_{\rm micro}$=2.12 km s^{-1}, and the iron abundance – logN(Fe)=7.66.

Using these values the synthetic spectrum was calculated for the whole observed region. It helps to make the reliable identification of spectral lines. Abundances were found using model atmosphere method. The full description of used methodic can be found in Yushchenko et al. (2005)

Table 1 contains the results of determination of chemical composition of the atmosphere of HD91375. The columns are the atomic numbers, the designations of the elements, the numbers of used lines, the derived mean abundances and its errors, the relative abundances with respect to the Sun.

4. Discussion

The chemical composition of HD91375 is typical for Am stars but the existence of magnetic field can be the reason of the classification of the star as a member of Ap group.

HD91375 is a member of Sirius group (Palous & Hauck 1986), so it will be very interesting to compare the chemical composition of HD91375 and the chemical composition of Sirius A. The temperature of Sirius A is only 700 K higher than the that of HD91375, but no detectable magnetic field was found for Sirius A.

Fig. 1 shows the comparison of chemical composi-

Table 1: Chemical composition of HD91375

Z	Element	n	logN	Error	Star-$\odot$
4	Be II	1	1.18		0.03
6	C I	3	8.30	0.20	-0.25
7	N I	5	7.63	0.13	-0.34
8	O I	5	8.63	0.15	-0.24
11	Na I	2	6.39	0.03	0.06
12	Mg I	2	7.25	0.31	-0.33
	Mg II	1	7.31		-0.27
13	Al I	2	6.58	0.08	0.11
	Al II	1	6.77		0.30
14	Si II	2	7.39	0.10	-0.16
16	S I	3	7.54	0.10	0.21
18	Ar I	1	6.77		0.25
20	Ca I	7	6.50	0.05	0.14
	Ca II	1	6.44		0.08
21	Sc II	13	3.13	0.24	-0.04
22	Ti II	23	5.51	0.27	0.49
23	V II	2	4.83	0.37	0.83
24	Cr II	4	5.71	0.06	0.04
25	Mn II	8	6.30	0.07	0.91
26	Fe I	25	7.63	0.06	0.13
	Fe II	34	7.68	0.14	0.18
27	Co II	1	5.71		0.79
28	Ni I	3	6.63	0.13	0.38
29	Cu I	1	5.12		0.91
30	Zn I	2	5.17	0.25	0.57
38	Sr II	3	3.56	0.08	0.59
39	Y II	11	3.21	0.23	0.97
40	Zr II	18	3.67	0.17	1.07
41	Nb II	2	2.18	0.06	0.76
44	Ru II	1	2.47		0.63
56	Ba II	3	3.09	0.11	0.96
57	La II	4	2.03	0.10	0.86
60	Nd III	4	2.39	0.22	0.89
64	Gd II	1	3.26		2.14
66	Dy II	2	2.13	0.06	0.99
68	Er II	2	2.46	0.22	1.52
70	Yb II	1	1.54		0.46
72	Hf II	2	2.25	0.36	1.37

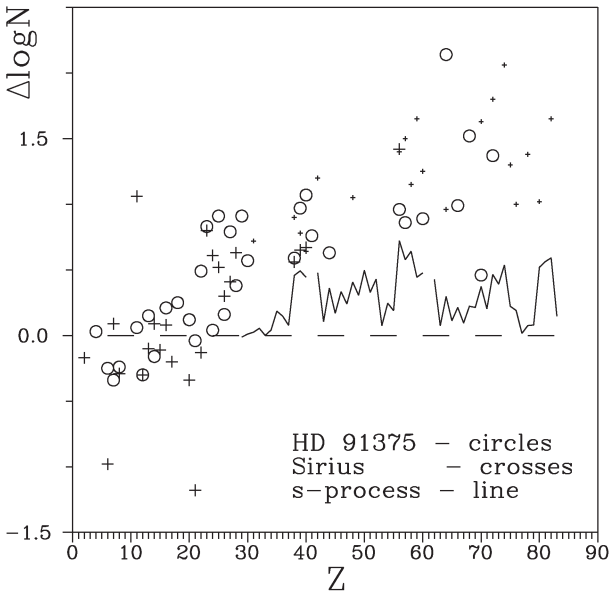

Figure 1: Chemical composition of HD91375 (open circles) in comparison with Sirius A (big crosses – Landstreet, 2011; small crosses - Yushchenko et al., 2007) and *s*-process enriched pattern (line, Yushchenko et al. 2004). The axes are the atomic numbers of the elements and the abundances with respect to the Sun

tion of HD91375 with the abundance pattern of Sirius A (Landstreet 2011, and our preliminary results on the abundances of heavy elements) and with typical s-process enriched pattern. It is obvious that the distribution of abundances in HD91375 is different from that of the Sirius A.

It is worth to note that the abundance pattern of Sirius A (maybe) was influenced by accretion of s-process enriched matter from its binary companion, now it is white dwarf Sirius B. The differences in chemical composition of HD91375 and Sirius A permit to confirm the possibility of accretion event in the Sirius binary system.

Recently Landstreet (2011) found that at least 0.5 solar mass of the matter of AGB star (white dwarf now) were accreted to Sirius A. It confirms the contamination of the atmosphere of Sirius A by *s*-process enriched matter found by Yushchenko & Gopka (2006) and Yushchenko et al. (2007).

Note that the mass of Sirius A now is close to 2 solar masses, that is why the star increased its mass at least by one third. It means that the comparison of chemical compositions of Sirius A and other members of Sirius moving group is not correct. Other members of Sirius moving group maybe were not affected by strong accretion in the past. That is why it is necessary to make independent analysis of the abundance pattern of HD91375.

Fig. 2 compares the abundances in HD91375 with classical *r*-, and *s*-processes abundance distributions.

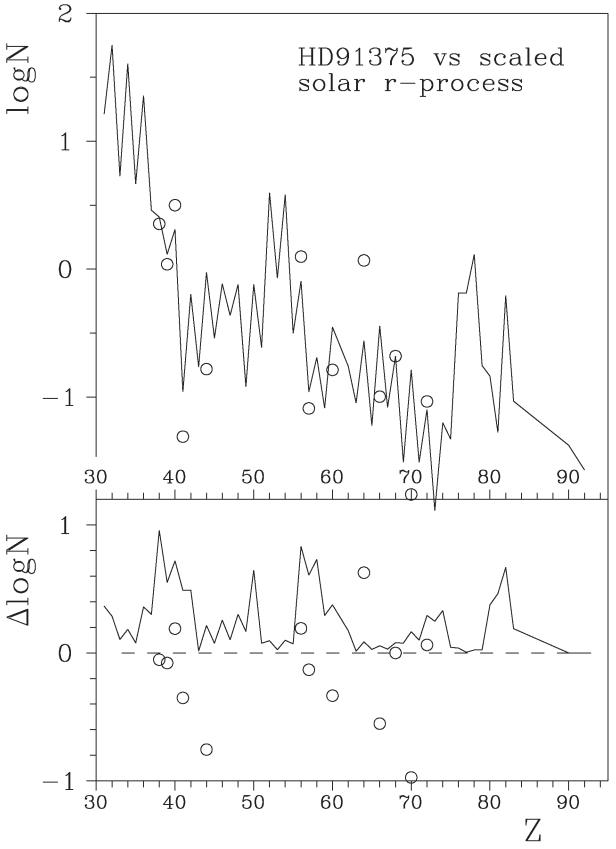

Figure 2: Upper panel compares the surface abundances in HD91375 (circles) with the solar system $r-$process abundance distribution scaled at the observed Dy abundance (line). The solar system $r-$process abundances are taken from Simmerer et al. (2004). The bottom panel shows the deviations of the observed abundances in HD91375 from scaled solar system $r-$abundances. The line is the deviations of solar photosphere abundances from solar $r-$process abundance distribution. The maximums of this curve correspond to the elements with the highest relative $s-$process contributions.

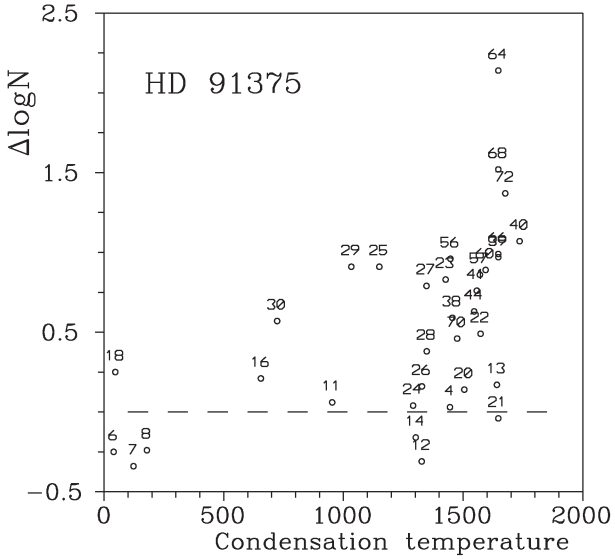

Figure 3: The plot of the relative surface abundances of chemical elements in HD91375 as a function of the condensation temperature of these elements. The values of condensation temperatures for a solar-photosphere composition gas are taken from Lodders (2003) calculations. The atomic numbers of the elements are marked.

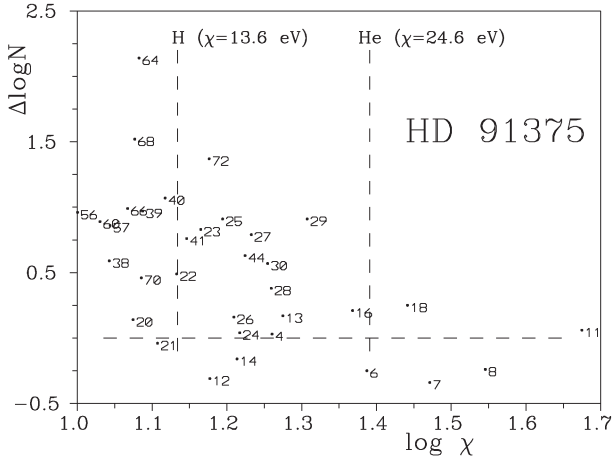

Figure 4: The plot of the relative surface abundances of chemical elements in HD91375 as a function of the second ionization potential (log χ) of these elements. The positions of the ionizations energies of hydrogen and helium are marked by vertical dotted lines. The atomic numbers of the elements are marked near the corresponding points.

The examination of this plot allow to conclude that the distribution of abundances of heavy elements is quit close to r-process, but the deviations are as high as 1.0 dex. These discrepancies can not be described as the influence of s-process.

Fig. 3 shows the distribution of abundances of chemical elements in the atmosphere of HD91375 as a function of condensation temperatures of these elements. Venn & Lambert (1990, 2008) found that the existence of dust envelope in λ Boo type stars (the effective temperatures of these stars are close to that of HD91375) results in the anticorrelation of relative abundance vs the condensation temperatures. We found nothing like this in HD91375, that is why it is possible to conclude that the dust is absent in the environment of HD91375.

Fig. 4 is the plot of relative abundances in the atmosphere of HD91375 with respect to the second ionization potentials of these elements. As it was shown in papers from Greenstein (1949) to Bohm-Vityense (2006) the accretion of interstellar gas by stars with radiative atmospheres results in charge-exchange reactions of the hydrogen and helium atoms which are the main components of interstellar medium with the atoms in the stellar photosphere. The result of these reactions is the understandable of the elements with ionization potentials close to those of hydrogen and helium atoms, namely 13.6 and 24.6 eva.

These underabundances, first of all the underubundances of Ca and Sc are clearly observed in Sirius A and other Am type stars, but it is not detected in the atmosphere of HD91375. As it was pointed here before, the temperatures and the gravities of HD91375 and Sirius A are not very distinct, that is why the reason of different chemical composition can be the existence of magnetic field in HD91375 or different evolutionary status of these stars.

Landstreet (2011) pointed that the accretion in the Sirius binary system took place 50-100 millions years before. This time was sufficient for charge-exchange reactions to set the main features of Am type stars abundance pattern. The absence of these features in the atmosphere of HD91375 may be the result of low density of interstellar medium along the path of the star in Galaxy, or the magnetic field. Maybe the second case is more important as the difference in the paths of Sirius moving group members can not be very distinct.

5. Conclusion

The detailed abundance pattern of HD91375 is found for the first time. The abundances of 34 chemical elements allow to claim the significant difference between the chemical composition of the members of Sirius moving group - Sirius and HD91375. It is obviously explained by the binarity of Sirius. The single star approximation can not be used for explanation of Sirius evolutionary path.

The distribution of abundances of heavy elements in HD91375 can be roughly fitted by r-process, but the deviations are as high as 1.0 dex. Maybe no signs of s-process are present in the atmosphere of HD91375.

The chemical composition of HD91375 was not influenced by dust or gas accretion, but the accretion was very important in the case of Sirius. It seems reasonable that the presence of weak magnetic field in the case of HD91375 can be responsable for the absence of accretion.

The signs of possible nonradial pulsations of HD91375 were found, but the used spectra were observed during 10 minutes only, that is why we can say nothing about the mode of pulsation.

This paper was supported by the Swiss National Science Foundation (SCOPES project No. IZ73Z0 -128180/1).

References

Bohm-Vityense E., 2006, *PASP*, **118**, 419
Greenstein J.L., 1949, *ApJ*, **109**, 121
Landstreet J.D., 2011, *A&A*, **528**, A132
Lodders K., 2003, *ApJ*, **591**, 1220
Palous J., Hauck B.: 1986, *A&A*, **162**, 54
Simmerer J., Sneden C., Cowan J.J., Collier J., Woolf V.M., Lawler J.E., 2004, *ApJ*, **617**, 1091
Venn K.A., Lambert D.L., 1990, *ApJ*, **363**, 234
Venn K.A., Lambert D.L., 2008, *ApJ*, **677**, 572
Yushchenko A.V., Gopka V.F., Kim C., Liang Y.C., Musaev F.A., Galazutdinov G.A. 2004, *A&A*, **413**, 1105
Yushchenko A., Gopka V., Goriely S., Musaev F., Shavrina A., Kim C., Kang Y.-W., Kuznietsova J., Yushchenko V.: 2005, *A&A*, **430**, 255
Yushchenko A., Gopka V. 2006, *AIPC*, **847**, 503
Yushchenko A., Gopka V., Goriely S., Lambert D., Shavrina A., Kang Y.-W., Rostopchin S., Valyavin G., Lee B.-C., Kim C. 2007, *ASPC*, **362**, 46
Yushchenko V., Gopka V., Yushchenko A., Shavrina A., Hubrig S., Musaev F., 2008, *OAP*, **21**, 151